Unstructured Adiabatic Quantum Optimization

Thesis submitted in partial fulfillment
of the requirements for the degree of

Master of Science in Computer Science and Engineering by Research

by

Alapan Chaudhuri
2019111023
alapan.chaudhuri@research.iiit.ac.in

Centre for Quantum Science and Technology (CQST)
International Institute of Information Technology (IIIT)
Hyderabad - 500032, India
February 2026

International Institute of Information Technology
Hyderabad, India

CERTIFICATE

It is certified that the work contained in this thesis, titled "Unstructured Adiabatic Quantum Optimization" by Alapan Chaudhuri, has been carried out under my supervision and is not submitted elsewhere for a degree.

_____ _____

Date Adviser: Prof. Indranil Chakrabarty

_____ _____

Date Co-Adviser: Prof. Shantanav Chakraborty

To a world that feels like it's splitting apart.
May we keep repairing what we can.

“Computers are more forgiving than bare-bone nature or mathematics
— both of which are infinitely more forgiving than academia."

Abstract

[TODO]

Acknowledgement

Contents

List of Theorems

List of Algorithms

List of Figures

Chapter 1

Introduction

Chapter 2

Physics and Computation

Three people walk into a room with the same problem. A logistics manager needs the shortest route through a hundred cities. A physicist needs the lowest energy state of a hundred interacting spins. A computer scientist needs to prove that no algorithm can find the answer faster than brute search. They are all navigating the same exponentially large space of configurations, and they will all get stuck in the same ways. But they will formalize the problem differently, and that difference will determine what each of them can prove.

This chapter builds the vocabulary that makes that claim precise. The path runs from physics through complexity theory to the adiabatic mechanism, and each piece earns its place by answering a question the previous piece leaves open.

2.1 Reality

What does it mean to choose a formalization? It means committing to which aspects of physical reality the mathematics captures. This thesis needs one such commitment: mathematics models regularities in the physical world but does not replace the world itself.

The consequence is immediate. A complexity claim is meaningful only after the computational model and the resource accounting are fixed. If access to the input changes, if precision demands change, or if the available control primitives change, the same task can move from easy to hard. Hardness is not an intrinsic property of a problem. It is a joint property of the problem, the model, and the resources being counted.

A concrete example makes this vivid. Finding the minimum of a function $f : \{0,1\}^n \to \mathbb{R}$ with no promise about its structure requires checking nearly every input in the worst case. In a classical query model this costs $\Theta(2^n)$ evaluations. In a quantum query model the same task costs $\Theta(2^{n/2})$ evaluations [1, 2]. The function did not change. The counting of resources did not change. Only the model of computation changed, and with it the sharp boundary between efficient and inefficient.

The dependence on model choice will recur throughout this thesis, and it helps to have a picture for it. Physical assumptions determine a computational model. The model determines a resource accounting. And

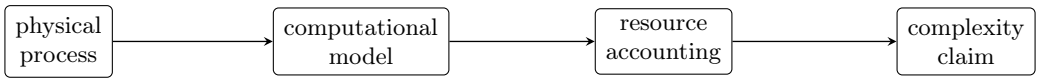

Figure 2.1: The modeling chain: physical assumptions determine the computational model, which determines resource accounting, which supports or refutes complexity claims.

the resource accounting supports, or fails to support, a complexity claim. Chapters 3 and 4 will put this chain under pressure: the optimization objective stays fixed while the computational model shifts from query circuits to continuous Hamiltonian evolution.

2.2 Physics

The modeling chain begins with physics, and physics contributes a single object that will persist through every chapter of this thesis: the Hamiltonian. Energy plays a double role. It generates the dynamics of a system, and it simultaneously defines what it means for a configuration to be preferred. This double role is what connects physics to optimization.

In classical mechanics, a system with f degrees of freedom lives in a phase space of generalized coordinates $q_1, \ldots, q_f$ and conjugate momenta $p_1, \ldots, p_f$. The Hamiltonian $H_{\mathrm{cl}}(q, p)$ determines the full time evolution through Hamilton's equations

$$\dot{q}_j = \frac{\partial H_{\mathrm{cl}}}{\partial p_j}, \qquad \dot{p}_j = -\frac{\partial H_{\mathrm{cl}}}{\partial q_j}. \tag{2.2.1}$$

The rate of change of each variable is set by how the energy depends on its conjugate. The Hamiltonian does not merely label states by their energy. It generates the flow that carries one state to the next.

Statistical mechanics introduces the second role. When a system is coupled to a heat bath at temperature T, the probability of finding it in configuration z is not uniform. Low-energy configurations are exponentially preferred. For a cost profile $C(z)$ and inverse temperature $\beta = 1/(k_B T)$, the Gibbs distribution assigns probabilities

$$\pi_\beta(z) = \frac{e^{-\beta C(z)}}{Z_\beta}, \qquad Z_\beta = \sum_z e^{-\beta C(z)}. \tag{2.2.2}$$

As $\beta \to \infty$, mass concentrates on the minimizers of C. The mechanism is direct: for any non-optimal configuration z, the ratio $\pi_\beta(z)/\pi_\beta(z^*) = e^{-\beta(C(z)-C_{\min})}$ vanishes exponentially as β grows. Finding the ground state is what thermal equilibrium does at zero temperature. The partition function Z_β encodes the full thermodynamic content of the system, and evaluating it turns out to be, in general, computationally hard. Section 2.4 will make that precise.

Quantum mechanics preserves the Hamiltonian as generator but changes the arena. The state is now a unit vector $|\psi\rangle$ in a Hilbert space, the Hamiltonian is a Hermitian operator, and with $\hbar = 1$ the evolution law is

$$i\frac{d}{dt}|\psi(t)\rangle = H(t)\,|\psi(t)\rangle\,. \tag{2.2.3}$$

The ground state of H is its minimum-energy eigenstate, and finding it is the quantum analogue of minimizing a cost function. The eigenvalue structure of the Hamiltonian, specifically the spectral gap between the ground state and the first excited state, will turn out to control how long an adiabatic algorithm must run. Sections 2.5 and 2.7 develop this connection.

2.3 Computation

The spectral gap determines how long the adiabatic algorithm runs. But "long" needs a yardstick, and that yardstick comes from complexity theory: a precise framework for measuring hardness across computational models. Without it, saying that an adiabatic algorithm is fast or slow would be meaningless.

The baseline model is the Turing machine [3]. A language $L \subseteq \{0,1\}^*$ is decidable if some Turing machine halts on every input and accepts exactly the strings in L. Decidability separates what can be computed from what cannot. The Church–Turing thesis asserts that every physically realizable computation can be performed by a Turing machine. The extended Church–Turing thesis goes further, adding an efficiency claim: every physically realizable computation can be simulated by a probabilistic classical machine with at most polynomial overhead [3]. Quantum computation challenges this efficiency claim while leaving computability untouched [4, 5]. Whether the challenge succeeds is the question this thesis addresses in the setting of unstructured optimization.

With the model fixed, "efficient" means polynomial time.

Definition 2.3.1 (Class P)**.** *A decision problem is in* P *if a deterministic Turing machine solves it in time polynomial in input length.*

Evaluating a cost function $C(z)$ at a given z is typically in P: substitute values and compute. But minimizing C over all of $\{0,1\}^n$ appears to require searching an exponentially large space. Boolean satisfiability makes the difficulty concrete. A 3-SAT formula has the form

$$F(x_1, \ldots, x_n) = \bigwedge_{j=1}^{m} (\ell_{j,1} \vee \ell_{j,2} \vee \ell_{j,3}), \tag{2.3.1}$$

with each literal $\ell_{j,k}$ being either x_i or $\overline{x}_i$. Given a candidate assignment x, checking whether $F(x) = 1$ takes time linear in the formula: evaluate each clause and confirm all are satisfied. A first-year student can verify a solution. But finding a satisfying assignment from scratch, or proving that none exists, appears to require effort that grows exponentially with n. This asymmetry between finding and checking is not an accident of 3-SAT. It is the heart of the P versus NP question.

Definition 2.3.2 (Class NP)**.** *A decision problem is in* NP *if every yes-instance has a certificate of length polynomial in the input that can be verified in polynomial time by a deterministic Turing machine.*

Every problem in P is also in NP, since an efficient algorithm can serve as its own verifier. The converse, whether P = NP, is the most famous open problem in theoretical computer science. The strong consensus is that P $\neq$ NP, but this remains unproved after more than fifty years.

What makes 3-SAT remarkable is not just that it appears hard, but that it captures the full difficulty of NP. Cook proved that every efficiently verifiable problem can be translated into an instance of SAT through a polynomial-time computable function that preserves yes and no answers [6]. Such a function is called a reduction: it converts one problem into another while preserving the answer.

Definition 2.3.3 (Polynomial-time many-one reduction)**.** *For decision problems A and B, write $A \leq_p B$ if there exists a polynomial-time computable function r such that*

$$x \in A \iff r(x) \in B. \tag{2.3.2}$$

A reduction from A to B means that B is at least as hard as A: any algorithm for B immediately yields one for A by composing with r, so hardness flows upward through a hierarchy of problems. A problem to which all of NP reduces is NP-hard; if it also lies in NP, it is NP-complete. Cook proved that SAT is NP-complete; Karp then showed that many combinatorial problems, including 3-SAT, are NP-complete through polynomial reductions [7]. Solving any one of them in polynomial time would collapse the entire class. The hardness reductions in Chapter 8 of this thesis begin from exactly this problem.

The point of contact with optimization is threshold decision. Given a cost function C and a threshold τ, ask whether there exists z with $C(z) \leq \tau$. For 3-SAT, this asks whether the minimum number of violated clauses is at most τ. If this threshold language is NP-hard, no generic polynomial-time algorithm can minimize C over all instances, unless P = NP. The adiabatic algorithm's task is precisely this minimization. The complexity classes just defined measure how hard that task is.

2.4 The #P Complexity Class

There is a subtlety the decision framework misses. The spectral parameters that control adiabatic runtime in Chapters 5 through 8 depend on the degeneracies $\{d_k\}$ and energy gaps $\{E_k - E_0\}$ of the problem Hamiltonian. Computing these parameters to the precision the algorithm requires can be #P-hard (Chapter 8). The issue is not just whether a solution exists, but how many solutions exist. For the spectral quantities that govern this thesis, counting is the operative difficulty.

Two Boolean formulas might both be satisfiable, but one could have a single satisfying assignment while the other has exponentially many. A decision algorithm cannot distinguish the two cases. A counting algorithm must, and counting turns out to be a fundamentally harder task.

Definition 2.4.1 (Class #P)**.** *A function $f : \{0,1\}^* \to \mathbb{N}$ is in* #P *if there exists a nondeterministic polynomial-time Turing machine M such that $f(x)$ equals the number of accepting branches of M on input x.*

Valiant introduced #P and established the hardness of canonical counting problems [8]. The standard example is

$$\#\mathrm{SAT}(F) = |\{x \in \{0,1\}^n : F(x) = 1\}|\,. \tag{2.4.1}$$

Decision SAT asks whether this count is nonzero. But computing the exact count is far harder. #P is at least as hard as every class in the polynomial hierarchy [9, 3], placing counting strictly above NP-hard decision problems in a strong structural sense. The permanent of a 0-1 matrix provides a vivid example: computing it is #P-complete [8], yet the closely related determinant is computable in polynomial time. A single sign change in the summation separates efficient computation from intractability.

The ground-state degeneracy $d_0 = |\{z : C(z) = C_{\min}\}|$ is exactly such a counting object. Adiabatic runtime depends on the full degeneracy spectrum through spectral parameters defined in Chapter 5. Chapter 8 proves that approximating the key parameter A_1 to additive precision $\varepsilon < 1/(72(n-1))$ is NP-hard. The #P-hardness result is stronger: $O(\mathrm{poly}(n))$ exact oracle queries to the spectral parameter suffice to extract the degeneracy d_0 by polynomial interpolation, and computing d_0 is #P-hard. Near-exact estimation at precision $\varepsilon \in O(2^{-\mathrm{poly}(n)})$ therefore inherits #P-hardness [10].

2.5 Spectral Complexity

Where does counting complexity meet quantum dynamics? In the eigenvalue structure of the Hamiltonian. The Schrödinger equation (2.2.3) is linear in the state vector, without approximation. For a time-independent Hamiltonian it has the explicit solution $|\psi(t)\rangle = e^{-iHt}|\psi(0)\rangle$, and even for time-dependent Hamiltonians the evolution remains a linear map on $\mathcal{H}$. One might expect that linearity implies computational simplicity. It does not.

The difficulty resides not in the evolution equation but in the spectrum. Consider an interpolation $H(s) = (1-s)H_0 + sH_z$ between an initial Hamiltonian H_0 (whose ground state is easy to prepare; Chapter 4 specifies the concrete choice) and a problem Hamiltonian H_z diagonal in the computational basis, with s ranging from 0 to 1. As s varies, the eigenvalues of $H(s)$ trace curves. When two of these curves approach each other, they generically do not cross. Instead they undergo an avoided crossing: the curves repel, reaching a minimum separation before diverging again (Figure 2.2). The width of this avoided crossing and the value of s at which it occurs depend on the global structure of both Hamiltonians. For an n-qubit problem Hamiltonian with up to 2^n eigenvalues, the crossing geometry is determined by the full set of energies and degeneracies.

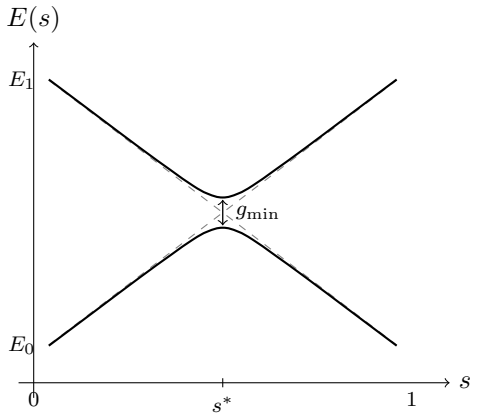

Figure 2.2: Avoided crossing in the spectrum of $H(s) = (1-s)H_0 + sH_z$. Dashed lines show the eigenvalues that would result if the two Hamiltonians did not couple; they cross at $s = s^*$. Solid curves show the actual eigenvalues, which repel near the would-be crossing. The minimum gap $g_{\min}$ sets the internal timescale of the quantum system: Section 2.7 makes precise how it controls runtime.

This is where computational hardness enters. Small perturbations to a Hamiltonian can rearrange its eigenvalue structure entirely: spectral gaps can close exponentially, avoided crossings can narrow or widen, degenerate subspaces can split. These spectral rearrangements control algorithmic runtime, and predicting them is NP-hard in general (Chapter 8). The interpolation between two Hamiltonians can be written in a single line. The location and width of the avoided crossing that controls the adiabatic algorithm's runtime depends on the full eigenvalue structure of the problem Hamiltonian, a structure that can itself be computationally hard to characterize. The evolution is simple. The geometry it must navigate is not.

2.6 Optimization

How does a combinatorial cost function become an energy spectrum? The translation is exact, requires no relaxation or rounding, and preserves every feature that makes the problem hard.

Write the optimization objective as

$$\min_{z\in\{0,1\}^n} C(z), \tag{2.6.1}$$

and define the diagonal Hamiltonian

$$H_z = \sum_{z\in\{0,1\}^n} C(z)\,|z\rangle\langle z|\,. \tag{2.6.2}$$

The ground states of H_z are exactly the minimizers of C. The combinatorial objective has become an energy spectrum, and finding the optimum has become finding the ground state.

For SAT, the encoding is explicit. Let $\chi_j(x) \in \{0,1\}$ indicate whether assignment x satisfies clause j, and define the penalty function

$$C_F(x) = \sum_{j=1}^{m} \big(1 - \chi_j(x)\big). \tag{2.6.3}$$

Then F is satisfiable if and only if $\min_x C_F(x) = 0$. Each unsatisfied clause contributes a unit penalty, so C_F counts the number of violations.

Counting resurfaces at the optimum. If $C_{\min}$ denotes the minimum cost, the ground-state degeneracy is

$$d_0 = \left|\{z \in \{0,1\}^n : C(z) = C_{\min}\}\right|. \tag{2.6.4}$$

Even an algorithm that outputs a single optimizer has runtime that depends, through the spectral structure of H_z, on how many optimizers exist. The spectral parameters controlling adiabatic runtime (defined in Chapter 5) are functions of the complete set of degeneracies $\{d_k\}$ and energy gaps $\{E_k - E_0\}$. A single-solution algorithm cannot escape the influence of a counting object.

A canonical hard family illustrating the encoding is the Ising model on a graph $G = (V, E)$

$$H_\sigma = \sum_{(i,j)\in E} J_{ij}\sigma_z^i\sigma_z^j + \sum_{j=1}^{n} h_j\sigma_z^j, \tag{2.6.5}$$

where σ_z^j is the Pauli-Z operator on site j (Chapter 3 develops the formalism), the first sum runs over edges of G with couplings J_{ij}, and the second sum includes local fields h_j. Many NP-hard combinatorial objectives map directly to this form [11, 12]. Weighted MaxCut provides a transparent example. For $x_i \in \{0,1\}$, the cut value is

$$C_{\text{cut}}(x) = \sum_{(i,j)\in E} w_{ij}(x_i \oplus x_j), \tag{2.6.6}$$

and under the spin substitution $\sigma_i = (-1)^{x_i}$ this becomes

$$C_{\text{cut}}(\sigma) = \frac{1}{2}\sum_{(i,j)\in E} w_{ij}(1 - \sigma_i\sigma_j). \tag{2.6.7}$$

The correspondence is $J_{ij} = -w_{ij}/2$ and $h_j = 0$: the total weight of edges crossing the cut is an antiferromagnetic Ising interaction energy. Any graph optimization objective expressible as pairwise interactions maps to an Ising model with no auxiliary variables, making the spectral analysis of Chapter 5 directly applicable. Combinatorial objectives and spin Hamiltonians are the same mathematical object. The encoding was introduced in the adiabatic context by Farhi et al. [13, 14], and it means that any NP-hard optimization objective can be attacked with Hamiltonian methods. Runtime analysis then reduces entirely to the spectral analysis of H_z, which is the subject of Sections 2.7 and 2.8.

2.7 Adiabaticity

The Hamiltonian H_z encodes the cost function. What remains is a mechanism for finding its ground state without knowing the answer in advance. The mechanism this thesis studies is adiabatic evolution, and understanding it requires understanding what "slow" means in quantum mechanics.

The word adiabatic comes from the Greek *adiabatos*, meaning "impassable," and entered physics through Clausius for processes with no heat exchange across system boundaries. The meaning in quantum mechanics differs from the thermodynamic original, but both rest on a shared structure: two competing timescales. Every adiabatic process has an external timescale, set by how rapidly conditions change, and an internal timescale, set by how rapidly the system can respond. Adiabaticity holds when external change is slow relative to internal response. In thermodynamics, the internal timescale is the relaxation time to local equilibrium: compress a gas slowly enough and it remains in equilibrium throughout. In quantum mechanics, the internal timescale is the inverse spectral gap. There is no absolute meaning of "slow." Slow is always slow compared to something.

For a quantum system governed by a time-dependent Hamiltonian $H(t)$, the internal timescale is set by the energy gap between eigenstates. At each instant, $H(t)$ has a spectrum of eigenstates and eigenvalues. If the system begins in an eigenstate and the Hamiltonian changes slowly enough, the state tracks the instantaneous eigenstate. It remains an eigenstate of $H(t)$ at every moment, even as the eigenstate itself changes character. If the Hamiltonian changes too rapidly, the state develops overlap with other eigenstates and the system has made a transition [15, 16]. In the context of an algorithm, this transition is a failure.

Why does the gap control transitions? The physical mechanism comes from first-order time-dependent perturbation theory. When the Hamiltonian changes, the amplitude for transitioning from the instantaneous ground state $|e_0(t)\rangle$ to an excited state $|e_n(t)\rangle$ acquires a factor

$$\frac{\langle e_n(t)|\,\dot{H}(t)\,|e_0(t)\rangle}{E_n(t) - E_0(t)}. \tag{2.7.1}$$

The energy denominator tells the story. Transitions to nearby energy levels are enhanced while transitions to distant levels are suppressed. The dominant leakage channel is the nearest excited state, and the gap $g(t) = E_1(t) - E_0(t)$ sets the relevant scale. The inverse gap $1/g(t)$ is the internal response timescale: the natural oscillation period between the two lowest eigenstates. For the Hamiltonian to change negligibly over this period, the fractional change per oscillation must be small compared to the gap itself.

This reasoning yields the adiabatic heuristic condition [17]

$$\frac{\|\dot{H}(t)\|}{g(t)^2} \ll 1, \tag{2.7.2}$$

where $\|\cdot\|$ denotes the spectral norm. This is the physical motivation behind every runtime bound in this thesis. Total evolution time T must be large enough that the sweep rate $\|\dot{H}(t)\|$ remains small relative to $g(t)^2$ at every point along the Hamiltonian path, requiring at minimum $T = \Omega(1/g_{\min}^2)$. The minimum gap along the path is the bottleneck. Small gaps force slowness, and that forced slowness is the computational cost. The heuristic captures the right qualitative scaling, but the rigorous version of the adiabatic theorem [17, 18] involves additional terms: the degeneracy of the ground state, norms of higher derivatives of $H(s)$, and an integral bound rather than a pointwise one. Chapter 4 states the precise result and derives the runtime from it.

The Landau–Zener formula makes the cost quantitative. For a two-level system with a linearly varying energy splitting near an avoided crossing, the probability of a diabatic transition is

$$P_{\mathrm{LZ}} \approx \exp\left(-\frac{\pi g_{\min}^2}{2v}\right), \tag{2.7.3}$$

where $g_{\min}$ is the minimum gap and v is the effective sweep rate [19, 20]. The formula is exact for an isolated two-level system with linear sweep and serves as the leading approximation whenever a crossing is traversed at approximately constant speed. A fast sweep through a narrow gap gives transition probability close to 1: the system jumps levels and the algorithm fails. A slow sweep gives exponentially suppressed transition probability: the system tracks the ground state and the algorithm succeeds.

One caveat belongs here, and it is not minor. For generic families of local Hamiltonians, even the ground-energy promise problem is QMA-complete [21]. The adiabatic quantum optimization regime studied in later chapters restricts to a rank-one driver Hamiltonian, a diagonal problem Hamiltonian, and a spectral condition on gaps and degeneracies (Chapter 4 specifies all three). The restriction is not a weakness of the analysis. It is what makes the analysis possible at all.

The deliverables of this section are the adiabatic heuristic condition (2.7.2) and the Landau–Zener formula (2.7.3). Together they determine how long any adiabatic algorithm must run as a function of the spectral gap profile along the interpolation path.

2.8 Energy Landscapes

Encoding a cost function into a Hamiltonian is exact, but the encoding does not solve the problem. What makes optimization hard is the geometry of the energy landscape, and the nature of that geometry differs between classical and quantum algorithms in a revealing way.

A classical landscape is rugged when it has many local minima separated by energy barriers. Escaping a local basin to explore deeper ones requires crossing the intervening barrier. At inverse temperature β, a barrier of height E_b costs time scaling like $\exp(\beta E_b)$: the Arrhenius bottleneck [22]. Simulated annealing navigates this landscape by cooling. The Metropolis acceptance rule [23] for moving from configuration z to z' is

$$P_{\mathrm{accept}}(z \to z') = \min\{1, e^{-\beta(C(z') - C(z))}\}. \tag{2.8.1}$$

At high temperature the walk moves freely but does not concentrate on the minimum. At low temperature it concentrates near low-energy configurations but takes exponentially long to cross barriers. In worst cases no polynomial cooling schedule suffices [22].

For an adiabatic quantum algorithm, the bottleneck is different. The system does not hop over barriers. It follows a continuous eigenstate trajectory through Hilbert space, and the obstacle is an avoided crossing where the spectral gap narrows. At the crossing, the ground state changes character rapidly over a small interval of the interpolation parameter: the eigenstate that was spread uniformly must concentrate on a small set of computational basis states, and the gap measures how abruptly this rearrangement occurs. The barrier height that governs classical runtime is replaced by the minimum gap that governs quantum runtime through condition (2.7.2). The two bottlenecks are structurally analogous but physically distinct, and instances where one is severe while the other is mild do exist [24].

Unstructured search calibrates the stakes. Among $N = 2^n$ configurations with a single marked item, classical query complexity is $\Theta(N)$: essentially no shortcut beyond exhaustive evaluation. Quantum query complexity is $\Theta(\sqrt{N})$ [1, 2]. This quadratic gap is the benchmark. The question is not whether quantum methods outperform all classical heuristics on all instances, but whether they achieve better worst-case scaling on specific, well-defined families. For unstructured optimization, the quadratic gap is the target against which everything in this thesis is measured.

2.9 Bridge to Quantum Computation

The vocabulary is now in place. The modeling chain (Figure 2.1) makes explicit that complexity claims depend on the computational model. Energy plays a double role as generator of dynamics and as optimization objective, and the diagonal Hamiltonian H_z encodes any combinatorial cost function exactly. The complexity classes P, NP, and #P measure the difficulty of deciding, verifying, and counting, and the spectral parameters that control adiabatic runtime live in the counting regime. The spectral gap is the computational resource: it sets the internal timescale of the quantum system and determines, through condition (2.7.2), how long the algorithm must run.

Writing down the Hamiltonian, however, does not reveal its ground state. A computational model must specify how the ground state is found, and a resource accounting must determine how long it takes.

Chapter 3 fixes the circuit and query baseline. It develops the quantum formalism, defines BQP, and establishes the unstructured frontier through Grover's algorithm and the BBBV lower bound. Chapter 4 holds the optimization objective fixed and changes the model from discrete oracle calls to continuous Hamiltonian evolution. Whether these two models achieve the same scaling for unstructured optimization, and what spectral information the adiabatic model demands, is the question that drives the remainder of this thesis.

Chapter 3

Quantum Computation

Chapter 2 established the pressure point. Hard optimization can be encoded in energy language, but encoding does not by itself produce an algorithm. To say anything precise, one must fix a computational model and a resource measure.

This chapter fixes that baseline in the circuit and query setting. It develops the finite-dimensional quantum formalism used throughout the thesis, defines the computational model, and establishes the unstructured-search frontier that later chapters must match or explain. The route is deliberate. First come states, measurement, and Hamiltonian dynamics. Then come circuits, oracles, and BQP. Then comes Grover's algorithm as geometry in a two-dimensional subspace, followed by the BBBV lower bound that proves the quadratic speedup is optimal. Only after this baseline is closed does it make sense to turn to adiabatic computation.

3.1 Quantum Mechanics Essentials

The modern theory of quantum computation begins with a modeling tension. Feynman argued that generic quantum dynamics appears classically expensive to simulate [25]. Deutsch then gave a universal model of quantum computation [4]. Shor and Grover later turned that modeling claim into explicit complexity separations [26, 1].

For this thesis, the operational lesson is simple. Any complexity claim is meaningful only after the computational model and its counted resources are fixed. Changing the model changes which lower bounds are provable.

A pure state of a finite-dimensional closed quantum system is a unit vector $|\psi\rangle$ in a complex Hilbert space $\mathcal{H}$ [27, 28]. A single qubit uses

$$\mathcal{H}_1 = \mathbb{C}^2 = \mathrm{span}\{|0\rangle, |1\rangle\}. \tag{3.1.1}$$

For n qubits,

$$\mathcal{H}_n = (\mathbb{C}^2)^{\otimes n}, \qquad \dim \mathcal{H}_n = N = 2^n. \tag{3.1.2}$$

The computational basis is $\{|x\rangle : x \in \{0,1\}^n\}$, and every pure state has an amplitude expansion

$$|\psi\rangle = \sum_{x\in\{0,1\}^n} \alpha_x |x\rangle, \qquad \sum_x |\alpha_x|^2 = 1. \tag{3.1.3}$$

Dirac and von Neumann gave the canonical operator-state formalism used here [29, 30].

Composite systems introduce non-factorizable states. A bipartite state $|\psi_{AB}\rangle$ is entangled if no pair $(|\psi_A\rangle, |\psi_B\rangle)$ exists with

$$|\psi_{AB}\rangle = |\psi_A\rangle \otimes |\psi_B\rangle. \tag{3.1.4}$$

Entanglement by itself is not a speedup theorem, but it expands the reachable space of correlations and therefore the algorithmic design space.

Global phase is physically irrelevant:

$$|\psi\rangle \equiv e^{i\phi} |\psi\rangle. \tag{3.1.5}$$

Relative phase is not. Interference depends on relative phase, and interference is where quantum algorithms get non-classical behavior.

Measurement is represented by orthogonal projectors $\{P_m\}$ with $P_m P_{m'} = \delta_{m,m'} P_m$ and $\sum_m P_m = I$. The Born rule gives

$$\Pr[m] = \langle\psi| P_m |\psi\rangle. \tag{3.1.6}$$

For rank-one measurement onto $|\phi\rangle$,

$$\Pr[\phi] = |\langle\phi|\psi\rangle|^2. \tag{3.1.7}$$

The post-measurement state for outcome m is $P_m |\psi\rangle / \sqrt{\Pr[m]}$, when $\Pr[m] > 0$.

Mixed states are represented by density operators

$$\rho = \sum_j p_j |\psi_j\rangle \langle\psi_j|, \qquad p_j \geq 0, \quad \sum_j p_j = 1, \tag{3.1.8}$$

with measurement rule

$$\Pr[m] = \mathrm{Tr}(P_m \rho). \tag{3.1.9}$$

The thesis mostly analyzes pure-state dynamics, but later adiabatic error bounds are naturally expressed on $\rho(s)$.

Eqs. (3.1.3)–(3.1.7) already expose a critical computational constraint. Amplitudes are not directly readable classical data. A measurement returns one sampled outcome, not the full amplitude table. Algorithmic advantage therefore requires controlled interference before measurement.

3.2 Hamiltonians and Time Evolution

A Hamiltonian H is Hermitian. Hermiticity guarantees real eigenvalues and an orthogonal eigenspace decomposition. In non-degenerate form,

$$H = \sum_j \lambda_j |\phi_j\rangle \langle\phi_j|, \tag{3.2.1}$$

where each eigenpair satisfies

$$H |\phi_j\rangle = \lambda_j |\phi_j\rangle, \tag{3.2.2}$$

and in projector form,

$$H = \sum_k E_k P_k, \tag{3.2.3}$$

where P_k projects onto the eigenspace at energy E_k. The expected energy in state $|\psi\rangle$ is

$$\langle H\rangle_\psi = \langle\psi| H |\psi\rangle. \tag{3.2.4}$$

For any sufficiently regular scalar function f, spectral calculus gives

$$f(H) = \sum_k f(E_k) P_k, \tag{3.2.5}$$

which yields $e^{-itH} = \sum_k e^{-itE_k} P_k$ as the time-evolution operator in the eigenbasis.

For optimization language, order distinct energies as $E_0 < E_1 < \cdots$. The ground energy is E_0, and the first spectral gap is

$$\Delta = E_1 - E_0. \tag{3.2.6}$$

If ground space is degenerate with dimension d_0, write its projector as

$$P_0 = \sum_{j=1}^{d_0} |\phi_{0,j}\rangle \langle\phi_{0,j}|. \tag{3.2.7}$$

Later adiabatic success statements are naturally written as overlap with P_0, not with a single selected vector.

Closed-system dynamics follows the Schrodinger equation (units $\hbar = 1$). For constant H,

$$i\frac{d}{dt} |\psi(t)\rangle = H |\psi(t)\rangle, \tag{3.2.8}$$

with solution

$$|\psi(t)\rangle = U(t) |\psi(0)\rangle, \qquad U(t) = e^{-itH}. \tag{3.2.9}$$

Unitarity,

$$U^\dagger U = I, \tag{3.2.10}$$

is exactly the algebraic statement that total probability is preserved during closed-system evolution. For time-dependent $H(t)$,

$$i\frac{d}{dt}|\psi(t)\rangle = H(t)|\psi(t)\rangle\,, \tag{3.2.11}$$

with formal propagator

$$|\psi(t)\rangle = \mathcal{T}\exp\left(-i\int_0^t H(\tau)\,d\tau\right)|\psi(0)\rangle\,. \tag{3.2.12}$$

Two remarks now prevent confusion later. First, adding cI to H shifts all energies but does not change eigenvectors. Second, this shift contributes only a global phase under unitary evolution. Measured probabilities are unchanged. Normalization choices such as setting a ground energy to zero are therefore computationally harmless.

Finally, distinguish static and path-dependent gaps carefully. Eq. (3.2.6) defines a static spectral gap of one Hamiltonian. In adiabatic evolution, $H = H(s)$ varies with schedule parameter s, and the relevant quantity becomes $g(s) = \lambda_1(s) - \lambda_0(s)$ along the full path.

3.3 Why Quantum Helps

At this point, the right question is not whether quantum mechanics is "powerful" in general. The right question is which mechanism a specific algorithm exploits and how that mechanism is certified by a complexity bound. For unstructured search, the mechanism is constructive interference in a two-dimensional invariant subspace. For Shor's algorithm, it is Fourier structure over periodicity. Different speedups come from different structures.

Superposition alone is not a speedup theorem. Entanglement alone is not a speedup theorem. Both enlarge state geometry, but complexity gains still require a unitary process that maps problem structure to measurable amplitude separation. This is why query lower bounds are indispensable. They separate what is physically expressible from what is information-theoretically learnable with bounded resources.

Tunneling is often discussed in optimization contexts, especially for adiabatic and annealing dynamics. It can help in specific barrier profiles, but broad claims of generic optimization advantage from tunneling alone are not proved. This thesis therefore tracks only quantities that support explicit theorems: oracle/query complexity in this chapter, then spectral gaps, schedules, and adiabatic error bounds in Chapters 4–9.

3.4 Circuits and Query Complexity

In the gate model, an algorithm is a uniform family of circuits over a universal gate set. Barenco et al. established standard finite universal gate constructions [31], and Bernstein-Vazirani formalized complexity in terms of uniform circuit families [5]. Uniformity means there is a classical polynomial-time procedure that outputs the circuit for input length n. Complexity is then measured by resources such as size, depth, and ancilla count as functions of n.

The choice of finite universal gate set does not change the complexity class. Solovay-Kitaev type compilation guarantees polylogarithmic overhead in target precision for approximating unitaries, so BQP is robust under standard gate-set choices [32, 33].

A schematic T-query quantum algorithm for oracle f has the interleaved form

$$|\psi^{(T)}\rangle = U_T O_f U_{T-1} O_f \cdots O_f U_1 O_f U_0 |0^m\rangle\,, \tag{3.4.1}$$

where U_j are input-independent unitaries and O_f carries the instance information. This is the fixed-oracle primitive. Optimization algorithms that use threshold updates run this primitive repeatedly with different oracles O_{f_τ} across outer-loop iterations.

For a function family f_n, bounded-error quantum query complexity $Q_2(f_n)$ is the minimum number of oracle calls in any algorithm of the form Eq. (3.4.1) that succeeds with probability at least $2/3$ on every valid input of size n. Classical randomized query complexity $R_2(f_n)$ is defined analogously with randomized decision trees [3, 27].

This separation is deliberate. Query complexity isolates information acquisition. Gate complexity measures full implementation cost. The thesis uses this query frontier as a baseline because Chapter 5 opens with unstructured optimization in that exact black-box sense.

The complexity class BQP contains promise problems solvable by uniform polynomial-size quantum circuits with bounded two-sided error. This definition is due to Bernstein-Vazirani [5]; Watrous and Arora-Barak provide standard modern treatments [34, 3]. A promise problem is a pair $(L_{\text{yes}}, L_{\text{no}})$ with $L_{\text{yes}} \cap L_{\text{no}} = \varnothing$. A BQP

algorithm must accept $x \in L_{\text{yes}}$ with probability at least 2/3 and reject $x \in L_{\text{no}}$ with probability at least 2/3. Standard repetition and majority vote reduce error exponentially, so the constant 2/3 is conventional. Promise formulations are not a technicality. They let us state complexity on the physically relevant input domain while leaving behavior unconstrained off-promise.

For orientation in the complexity landscape, P $\subseteq$ BQP $\subseteq$ PSPACE, with a standard route through BQP $\subseteq$ PP $\subseteq$ PSPACE [5, 34]. These inclusions are known; strictness relations remain open.

One distinction is worth fixing now. BQP is a decision-class notion for promise problems. Minimum finding is an optimization task. The bridge is threshold reduction: optimization is solved by repeated decision queries of the form "is there any item with cost at most τ?" This reduction is the reason query-optimal search bounds transfer directly to unstructured minimum finding. Operationally, the decision primitive is

$$D_\tau(C) = \mathbf{1}[\exists x,\ C(x) \le \tau]\,.$$

Optimization then becomes threshold management plus calls to D_τ.

3.5 Unstructured Optimization in the Oracle Model

For a Boolean oracle $f : \{0,1\}^n \to \{0,1\}$, the standard query action is

$$O_f\,|x, y\rangle = |x, y \oplus f(x)\rangle\,. \tag{3.5.1}$$

An equivalent phase-oracle form is

$$O_f\,|x\rangle = (-1)^{f(x)}\,|x\rangle\,. \tag{3.5.2}$$

These forms are interconvertible with one ancilla, so lower and upper bounds transfer between them.

Unstructured search asks for a marked input in a set $W \subseteq \{0,1\}^n$ of size $d_0 \ge 1$, given only oracle access. Unstructured minimum finding asks for $x^\star \in \arg\min_x C(x)$ for a black-box cost function $C : \{0,1\}^n \to \mathbb{R}$ with no promised exploitable structure. By contrast, structured optimization provides additional representation-level regularity, such as locality, sparsity, algebraic constraints, or graph symmetry, that can be exploited algorithmically. The unstructured model used for Grover and BBBV deliberately removes that advantage.

The word "unstructured" names the information model, not the computational paradigm. In the circuit model, one accesses the instance through oracle queries. In adiabatic optimization, one accesses it through the diagonal energy map $z \mapsto E_z$ of H_z, with no additional promised regularity such as locality, sparsity, or exploitable algebraic pattern. The two models therefore enforce the same absence of exploitable structure through different physical primitives. In worst-case formulations, no generic advantage can rely on basis labels themselves. Only permutation-invariant summaries, such as the number of marked states, are available to all algorithms [2].

The reductions between these tasks are explicit. Search reduces to optimization by

$$C_f(x) = 1 - f(x), \tag{3.5.3}$$

so minimizers are exactly marked items. Optimization reduces to threshold search with

$$f_\tau(x) = \mathbf{1}[C(x) \le \tau]. \tag{3.5.4}$$

Durr and Hoyer use this threshold view with Grover subroutines to obtain minimum finding in

$$\Theta\left(\sqrt{\frac{N}{d_0}}\right) \tag{3.5.5}$$

queries up to failure-amplification factors [35, 36, 37].

This is the baseline Chapter 5 invokes. In the circuit-query model, unstructured optimization already has a sharp exponent.

3.6 Grover as Geometry

Let W be the marked set with size d_0. Define normalized marked and unmarked superpositions

$$|w\rangle = \frac{1}{\sqrt{d_0}} \sum_{x \in W} |x\rangle\,, \qquad |r\rangle = \frac{1}{\sqrt{N - d_0}} \sum_{x \notin W} |x\rangle\,. \tag{3.6.1}$$

The uniform superposition is

$$|s\rangle = \frac{1}{\sqrt{N}} \sum_x |x\rangle = \sin\theta \; |w\rangle + \cos\theta \; |r\rangle \,, \qquad \sin\theta = \sqrt{\frac{d_0}{N}}. \tag{3.6.2}$$

The dynamics closes on $\mathrm{span}\{|w\rangle \,, |r\rangle\}$.

Grover's iterate is a product of two reflections,

$$G = (2\,|s\rangle\,\langle s| - I)(I - 2\,|w\rangle\,\langle w|), \tag{3.6.3}$$

which is a rotation by angle 2θ in that plane. In basis $(|w\rangle \,, |r\rangle)$,

$$G = \begin{pmatrix} \cos 2\theta & \sin 2\theta \\ -\sin 2\theta & \cos 2\theta \end{pmatrix}. \tag{3.6.4}$$

Hence

$$G^k \,|s\rangle = \sin((2k+1)\theta)\,|w\rangle + \cos((2k+1)\theta)\,|r\rangle \,, \tag{3.6.5}$$

so success probability is $\sin^2((2k+1)\theta)$.

The same operation has a circuit decomposition: one oracle reflection and one diffusion reflection per iteration. Writing

$$O_w = I - 2\,|w\rangle\,\langle w| \,, \qquad D = 2\,|s\rangle\,\langle s| - I, \tag{3.6.6}$$

the iterate is $G = DO_w$. The algorithm is therefore a repeated application of a fixed two-block circuit. The diffusion operator itself can be written as

$$D = H^{\otimes n}\,(2\,|0^n\rangle\,\langle 0^n| - I)\,H^{\otimes n}, \tag{3.6.7}$$

which is the form implemented in gate-level circuits.

Choosing

$$k^* \approx \left\lfloor \frac{\pi}{4\theta} - \frac{1}{2} \right\rfloor \tag{3.6.8}$$

maximizes success. For $d_0 \ll N$, $\theta \sim \sqrt{d_0/N}$, giving

$$Q_{\mathrm{Grover}} = \Theta\left(\sqrt{\frac{N}{d_0}}\right) \tag{3.6.9}$$

queries [1, 36, 37]. When d_0 is unknown, BBHT-style randomized iteration schedules retain the same asymptotic scaling in expectation while preserving bounded-error success [36]. For the one-solution case $d_0 = 1$, this reduces to $k^* = \lfloor (\pi/4)\sqrt{N} \rfloor + O(1)$ queries.

The geometric point matters for this thesis beyond Chapter 3. A large Hilbert space can still reduce to an effective two-level dynamics controlling runtime. Chapter 5 uses the same structural motif at the avoided crossing of adiabatic interpolation.

3.7 Why Grover Is Optimal

The query lower bound of Bennett, Bernstein, Brassard, and Vazirani (BBBV) states that unstructured search requires

$$\Omega\left(\sqrt{\frac{N}{d_0}}\right) \tag{3.7.1}$$

queries for bounded-error success [2]. For $d_0 = 1$, this is $\Omega(\sqrt{N})$.

A useful proof intuition is hybrid distinguishability growth. Compare final states under nearby oracles. Let $|\psi_T^{(w)}\rangle$ be the final state when the marked set is $\{w\}$, and let $|\psi_T^{(0)}\rangle$ be the final state for the null oracle (no marked item). One query changes average distinguishability by at most a controlled amount, so after T queries,

$$\frac{1}{N} \sum_{w \in [N]} \left\| |\psi_T^{(w)}\rangle - |\psi_T^{(0)}\rangle \right\|_2 \leq \frac{2T}{\sqrt{N}}. \tag{3.7.2}$$

When $T \ll \sqrt{N}$, the average distance remains $o(1)$, so the final states do not separate enough for any measurement to identify the marked oracle with constant bias. Constant success therefore needs $T = \Omega(\sqrt{N})$. The same argument with d_0 marked items yields $\Omega(\sqrt{N/d_0})$ up to constants. Nayak and Wu provide a complementary polynomial-method perspective on related bounds [38].

Combining Eq. (3.6.9) with Eq. (3.7.1) gives the exact frontier in the unstructured query model:

$$Q_{\text{search}} = \Theta\left(\sqrt{\frac{N}{d_0}}\right). \tag{3.7.3}$$

This is not merely a known algorithm. It is a closed asymptotic frontier.

The same exponent appears in continuous-time query models. Farhi, Goldstone, and Gutmann proved an $\Omega(\sqrt{N/d_0})$ lower bound for unstructured adiabatic search with a rank-one projector driver [39]. This is the formal bridge to Chapter 4. Changing the implementation from discrete queries to Hamiltonian evolution does not remove the unstructured lower-bound barrier.

3.8 Scope and Transition

This chapter worked in an ideal closed-system complexity model. Real devices are open systems and suffer decoherence and control noise [40]. Fault-tolerant frameworks address this in principle through encoding and active correction [41, 27]. Those engineering layers matter in practice, but they are not the analytical target of Chapters 4–9.

The next step keeps the optimization objective fixed and changes only the model. In the circuit-query setting, unstructured optimization is already pinned down by Eq. (3.7.3). In adiabatic computation, the same objective is pursued by continuous Hamiltonian evolution, and runtime is governed by pathwise spectral geometry rather than query count alone. Chapter 4 asks what this model shift buys and what it demands, once schedule design and gap control become algorithmic resources in their own right. That is the precise sense in which Chapter 5 can open by saying that, in the circuit model, unstructured optimization is already understood.

Chapter 4

Adiabatic Quantum Computation

Chapter 3 closed one model cleanly. In the circuit-query setting, unstructured optimization is characterized by a sharp frontier, $\Theta(\sqrt{N/d_0})$. The next question is not whether quantum mechanics helps in principle. The next question is what happens when the same objective is implemented by continuous Hamiltonian evolution instead of discrete oracle calls.

Adiabatic quantum computation answers that question in a physically direct way. Prepare a ground state that is easy to initialize, deform the Hamiltonian, and try to stay in the instantaneous ground space until the final Hamiltonian encodes the solution. This sounds conceptually simple, and that simplicity is exactly why it is so attractive. The technical reality is sharper. "Slowly" is not a vague instruction. It is the runtime law, and the spectral gap along the interpolation path is the central resource.

This chapter builds that framework from first principles and then narrows to the AQO regime used in Chapters 5–8. The story has four steps. Define the model. State the quantitative adiabatic control law. Understand avoided crossings and the Roland-Cerf benchmark. Then confront the central tension: universality of model power does not remove information bottlenecks in schedule design.

4.1 Model

An adiabatic algorithm is specified by a Hamiltonian path and a monotone schedule. The standard interpolation is

$$H(s) = (1-s)H_0 + sH_P, \qquad s \in [0,1], \tag{4.1.1}$$

where physical time $t \in [0,T]$ is mapped to s by increasing function $s(t)$ [13, 14]. In normalized time,

$$\frac{i}{T}\frac{d}{ds}\left|\psi(s)\right\rangle = H(s)\left|\psi(s)\right\rangle. \tag{4.1.2}$$

The algorithm starts in a ground state of H_0 and attempts to end with large overlap on the ground space of H_P.

Adiabatic quantum optimization is the special case where H_P is a classical cost Hamiltonian diagonal in the computational basis:

$$H(s) = (1-s)H_0 + sH_z. \tag{4.1.3}$$

This is the regime analyzed in Chapters 5 through 9.

The word "unstructured" must be pinned down before proceeding. In the circuit model, unstructured search means black-box oracle access with no exploitable regularity promised in labels. In this thesis, "unstructured adiabatic" refers to a Grover-type driver design: a uniform initial state, rank-one driver, and no instance-specific structure injected into H_0 [42, 39, 10]. It does not mean that the problem Hamiltonian H_z itself lacks combinatorial structure.

The concrete family used later is

$$H_0 = -\left|\psi_0\right\rangle\left\langle\psi_0\right|, \qquad \left|\psi_0\right\rangle = \left|+\right\rangle^{\otimes n} = \frac{1}{\sqrt{N}}\sum_{z\in\{0,1\}^n}\left|z\right\rangle. \tag{4.1.4}$$

This choice is mathematically consequential. With diagonal H_z, rank-one H_0 creates a single dominant low-energy avoided crossing that can be analyzed explicitly [10]. By contrast, transverse-field drivers can produce many narrow crossings and localization effects that obstruct generic runtime control [43, 44].

4.2 Gap and Schedules

The adiabatic theorem began with Born and Fock and was formalized in modern operator form by Kato [15, 16]. For algorithms, qualitative statements are insufficient. One needs explicit error scaling with runtime and gap profile.

The finite-dimensional quantitative form used in our work [10] follows Jansen, Ruskai, and Seiler [17]. Let $P(s)$ project onto the followed eigenspace of dimension d, let $g(s)$ be the spectral gap from that eigenspace to the rest of the spectrum, and assume H is twice differentiable. Then

$$|1 - \langle\psi(s)|\, P(s)\, |\psi(s)\rangle| \leq \nu^2(s), \tag{4.2.1}$$

with

$$\nu(s) = C\left\{\frac{1}{T}\frac{d\|H'(0)\|}{g(0)^2} + \frac{1}{T}\frac{d\|H'(s)\|}{g(s)^2} + \frac{1}{T}\int_0^s \left(\frac{d\|H''(s')\|}{g(s')^2} + \frac{d^{3/2}\|H'(s')\|}{g(s')^3}\right) ds'\right\}, \tag{4.2.2}$$

where C is an s-independent constant fixed by theorem conventions.

The constants are less important here than the structure. Small gaps amplify adiabatic error. Therefore, for fixed target accuracy, runtime must be concentrated near small-gap regions. This is the first place where spectral gap becomes a computational resource rather than a descriptive statistic.

Schedule design makes that resource explicit:

$$T = \int_0^1 \frac{ds}{ds/dt}. \tag{4.2.3}$$

A linear schedule spends equal time per unit s, regardless of gap profile. Local schedules spend time where it is needed. In a two-level reduction, the standard local control law is

$$\left|\frac{ds}{dt}\right| \lesssim \frac{\varepsilon\, g(s)^2}{\chi(s)}, \qquad \chi(s) = \left|\langle e_1(s)|\, \frac{dH}{ds}\, |e_0(s)\rangle\right|, \tag{4.2.4}$$

so the evolution slows near bottlenecks and accelerates where the path is safe [45, 42].

This local-gap logic now has broader scheduling theory behind it. Guo and An analyze power-law families $u'(s) \propto g(u(s))^p$ with $p \in (1, 2)$ and show, under a measure condition on small-gap regions, improvement from inverse-square to inverse-linear gap dependence [46]. Their framework is complementary to ours. It explains structurally why nonlinear schedules help. Our later chapters instead exploit explicit spectral formulas for a specific rank-one AQO family.

One warning belongs here. Gap-aware schedules require gap information. In general local-Hamiltonian settings, low-energy estimation is QMA-hard [21]. Schedule design and spectral inference are therefore not separate subproblems in general.

4.3 Avoided Crossings and Roland-Cerf

For AQO, runtime is usually controlled by an avoided crossing between the lowest two levels. Near that region, dynamics is effectively two-level. Landau-Zener analysis gives the right physical picture. For a linear sweep through an anticrossing,

$$P_{\text{dia}} \approx \exp\left(-\frac{\pi g_{\min}^2}{2v}\right), \tag{4.3.1}$$

where v is effective sweep rate and $g_{\min}$ is minimum gap [19, 20]. Passing too fast through the pinch creates leakage.

Roland and Cerf converted this physical intuition into the first adiabatic search construction matching Grover scaling [42]. For one marked state $|w\rangle$ among $N = 2^n$ basis states,

$$H_{\text{RC}}(s) = -(1-s)\, |\psi_0\rangle\langle\psi_0| + s\,(I - |w\rangle\langle w|), \qquad |\psi_0\rangle = \frac{1}{\sqrt{N}}\sum_x |x\rangle. \tag{4.3.2}$$

The evolution lives in a two-dimensional invariant subspace, mirroring the geometric simplification behind Grover in Chapter 3.

The spectral gap is

$$g(s) = \sqrt{(2s-1)^2 + \frac{4s(1-s)}{N}}, \tag{4.3.3}$$

so $g_{\min} = 1/\sqrt{N}$ near $s = 1/2$. With local schedule $\dot{s} = \varepsilon g(s)^2$,

$$T = \frac{1}{\varepsilon}\int_0^1 \frac{ds}{g(s)^2} = \frac{N}{\varepsilon\sqrt{N-1}}\arctan\sqrt{N-1} = \Theta\left(\frac{\sqrt{N}}{\varepsilon}\right). \tag{4.3.4}$$

So adiabatic evolution can match the quadratic circuit speedup in this one-marked-item setting.

The qualifier is crucial. The success relies on explicit knowledge of where the gap pinches and how sharply. In the same rank-one unstructured setting, Farhi et al. showed no adiabatic schedule can asymptotically beat this scaling [39]. So the Roland-Cerf runtime is optimal within that model.

This benchmark also reveals the generalization challenge. In Grover, crossing location and width are fixed by N. In general diagonal H_z, both depend on the full spectral profile.

4.4 Universality, Restrictions, and Information Cost

AQC is polynomially equivalent to the circuit model [47]. This resolves a model-power question. It says each model can simulate the other with polynomial overhead. It does not resolve the algorithm-design question relevant here: for a fixed interpolation family, can one realize the target speedup with feasible spectral information?

That distinction is visible across the literature. One line of work uses adiabatic evolution for tasks beyond optimization, including state generation, Markov-chain speedups, and ranking [48, 49, 50, 51]. A second line shows how adiabatic reasoning interfaces with gate-model primitives through Hamiltonian simulation and discretization [52, 53, 54].

The same literature also shows why universality is not a runtime guarantee. Filtering and endpoint strategies can outperform strictly gap-limited adiabatic paths in some settings [55, 56, 57]. Hard instances can exhibit localization and path obstructions that destroy naive adiabatic optimism [58, 43]. Practical annealing studies point to the same conclusion: path design and spectral structure dominate performance [59, 60, 61, 62, 63, 64].

Our AQO family is deliberately narrower:

$$H(s) = -(1-s)\left|\psi_0\right\rangle\left\langle\psi_0\right| + sH_z, \qquad H_z \text{ diagonal in the computational basis.} \tag{4.4.1}$$

This restriction is natural for classical cost functions and analytically sharp enough for explicit runtime and hardness theorems [10]. It is narrower than general AQC, and this tradeoff is intentional.

For the rank-one diagonal AQO family satisfying the spectral regularity condition used in [10],

$$\frac{1}{\Delta}\sqrt{\frac{d_0}{A_2 N}} < c$$

for sufficiently small constant c, write distinct eigenvalues of H_z as $E_0 < E_1 < \cdots < E_{M-1}$ with degeneracies d_k, let $N = 2^n$, and define

$$A_p = \frac{1}{N}\sum_{k=1}^{M-1}\frac{d_k}{(E_k - E_0)^p}, \qquad p \in \mathbb{N}. \tag{4.4.2}$$

Then d_0 is ground-state degeneracy, and the crossing geometry is governed by [10]

$$s^* = \frac{A_1}{A_1 + 1}, \tag{4.4.3}$$

$$\delta_s = \frac{2}{(A_1+1)^2}\sqrt{\frac{d_0 A_2}{N}}, \tag{4.4.4}$$

$$g_{\min} = \frac{2A_1}{A_1+1}\sqrt{\frac{d_0}{A_2 N}}. \tag{4.4.5}$$

These are crossing location, crossing width scale, and minimum-gap scale. Increasing d_0 widens the crossing region and increases $g_{\min}$. Increasing A_2 narrows the gap as $1/\sqrt{A_2}$. Increasing A_1 pushes s^* toward 1 and narrows δ_s through $(A_1+1)^{-2}$.

The runtime consequence is immediate. An optimal local schedule must target the crossing window, so s^* must be known to additive precision $O(\delta_s)$. For $d_0 = O(1)$ with polynomial spectral prefactors, this is roughly $2^{-n/2}$ precision up to polynomial factors [10]. The information demand is the bottleneck.

This is where Chapters 5–8 connect tightly. Chapter 5 builds the AQO problem formalism around this rank-one path. Chapter 6 derives global gap bounds outside and near the crossing window. Chapter 7 constructs

the optimal local schedule and runtime in this regime. Chapter 8 shows the computational price of the required spectral information: approximating A_1 to additive precision $\varepsilon < 1/(72(n-1))$ is NP-hard, while near-exact estimation at $\varepsilon = 2^{-\mathrm{poly}(n)}$ is #P-hard [10]. Combined with the unstructured adiabatic lower bound [39], this gives the central tension of the thesis. The Grover-like scaling is achievable, but the instance-specific information needed to realize it can itself be hard to compute.

That is the exact handoff to Chapter 5. In the circuit model, unstructured minimum finding is already characterized. In AQO, matching the same asymptotic law requires controlling crossing geometry and schedule design under nontrivial information constraints.

Chapter 5

Adiabatic Quantum Optimization

In the circuit model, unstructured optimization is already understood. Given a black-box cost function on $N = 2^n$ bit-strings, Grover's algorithm and its generalizations find a minimizer in $O(\sqrt{N/d_0})$ queries, where d_0 is the number of optima [1, 36]. The algorithm needs no prior knowledge of the cost function's structure. Amplitude amplification gathers what it needs adaptively, one oracle query at a time. No spectral parameter is computed in advance, no schedule is tuned to a gap profile, and no preprocessing competes with the search cost itself.

Adiabatic quantum computation is polynomially equivalent to the circuit model [47], so the same speedup exists in principle. The obstruction is different. The evolution Hamiltonian $H(s)$ interpolates continuously between an initial Hamiltonian H_0 and the problem Hamiltonian H_z, and the runtime is controlled by the spectral gap of $H(s)$ along the entire path. The location of the avoided crossing, the sharpness of the minimum gap, and the reopening rate all matter. Matching the Grover speedup now requires controlling spectral features that depend on the full degeneracy structure of H_z.

The adiabatic version of Grover's algorithm, due to Roland and Cerf [65], finds a single marked item among $N = 2^n$ by slowly interpolating between a uniform superposition and a problem Hamiltonian that penalizes all unmarked items. The crossing between the two lowest energy levels occurs at $s = 1/2$, its position independent of the Hamiltonian's spectrum. The minimum spectral gap scales as $1/\sqrt{N}$, and a schedule that slows near the crossing achieves the optimal $O(\sqrt{N})$ runtime.

Consider a cost function encoded in an n-qubit Hamiltonian diagonal in the computational basis, with M distinct energy levels, arbitrary degeneracies, and a spectral gap that may vary with the number of qubits. The ground states encode solutions to a combinatorial optimization problem. Can the adiabatic approach still match the $\Theta(\sqrt{N})$ lower bound for unstructured search [39]?

The bound applies directly to our setup. Farhi et al. proved that when H_0 is a rank-one projector onto the uniform superposition, no schedule can find the ground state in time $o(\sqrt{N/d_0})$, regardless of the cost function. Their proof constructs N equivalent Hamiltonians related by Fourier shifts and applies a continuous-time analogue of the BBBV argument [2]. Partial answers came first. Žnidarič and Horvat [66] showed via analytical and heuristic arguments that the minimum gap scales as $\sqrt{d_0/2^n}$ for 3-SAT instances and identified the crossing position, but did not rigorously bound the runtime. Hen [67] proved a quadratic speedup for a random Hamiltonian whose energy distribution makes the crossing position spectrum-independent, sidestepping the central difficulty.

The answer in full generality is yes, and in our view that is the surprising part. But it comes with a sharp caveat. The spectrum of the interpolated Hamiltonian is much richer than in the Grover case. Instead of a two-level system plus a degenerate bulk, one gets M interacting energy levels in a symmetric subspace, with higher-state avoided crossings that obscure the lowest gap. The ground-state crossing position depends nontrivially on the degeneracy structure of H_z. The minimum gap still scales as $\Theta(1/\sqrt{N})$ up to spectral factors, but it occurs at a position that must be known to exponential precision for the schedule to be correct.

For a general diagonal problem Hamiltonian, $H(s)$ has a single avoided crossing at position $s^* = A_1/(A_1+1)$, where A_1 is a spectral parameter determined by the degeneracy structure. The minimum spectral gap at the crossing scales as $\Theta(\sqrt{d_0/(NA_2)})$, and the gap grows linearly on both sides. Chapter 6 proves the gap bounds outside the crossing window, and Chapter 7 derives the optimal runtime. Chapter 8 then shows where the edge comes from. Computing s^* is NP-hard.

5.1 From Cost Function to Adiabatic Path

We now formalize the optimization setting and the interpolation path. Consider an n-qubit Hamiltonian H_z that is diagonal in the computational basis.

$$H_z = \sum_{z\in\{0,1\}^n} E_z \left|z\right\rangle \left\langle z\right|, \tag{5.1.1}$$

where E_z is the energy assigned to bit-string z. Since H_z acts diagonally, it encodes a classical cost function. The energy E_z is the cost of configuration z, and the ground states are the optimal solutions. Without loss of generality, we rescale and shift so that all eigenvalues lie in $[0, 1]$.

Suppose H_z has M distinct energy levels with eigenvalues

$$0 \le E_0 < E_1 < \cdots < E_{M-1} \le 1. \tag{5.1.2}$$

For each level k, the set of bit-strings at that energy is

$$\Omega_k = \{z \in \{0,1\}^n : H_z \left|z\right\rangle = E_k \left|z\right\rangle\}, \tag{5.1.3}$$

with degeneracy $d_k = |\Omega_k|$. The degeneracies partition the full Hilbert space, so $\sum_{k=0}^{M-1} d_k = 2^n = N$. The spectral gap of the problem Hamiltonian is $\Delta = E_1 - E_0$, the energy difference between the ground state and the first excited level.

NP-hard optimization problems such as MaxCut and QUBO encode directly as ground states of the 2-local Ising Hamiltonian [11, 12].

$$H_\sigma = \sum_{\langle i,j\rangle} J_{ij}\sigma_z^i\sigma_z^j + \sum_{j=1}^{n} h_j\sigma_z^j, \tag{5.1.4}$$

where $J_{ij}, h_j \in \{-m, -m+1, \ldots, m\}$ for some constant positive integer m. Since each eigenvalue is an integer linear combination of at most $\binom{n}{2} + n$ couplings bounded by m, the eigenvalues lie in $\{-L, -L+1, \ldots, L\}$ for $L = O(mn^2)$, giving at most $2L+1 \in \text{poly}(n)$ distinct energy levels. After normalization to unit operator norm, consecutive eigenvalues differ by at least $1/(2L) \ge 1/\text{poly}(n)$, so the spectral gap satisfies $\Delta \ge 1/\text{poly}(n)$.

Unstructured search also fits this framework. It has $M = 2$ energy levels, a single ground state ($d_0 = 1$) with energy $E_0 = 0$, and $N-1$ excited states ($d_1 = N-1$) at energy $E_1 = 1$. The ground state is the "marked item." Classical search requires $\Theta(N)$ queries, while Grover's circuit algorithm requires $\Theta(\sqrt{N})$ [1, 2].

The adiabatic Hamiltonian interpolates between a rank-one projector and H_z. The initial Hamiltonian is

$$H_0 = -\left|\psi_0\right\rangle \left\langle\psi_0\right|, \qquad \left|\psi_0\right\rangle = \left|+\right\rangle^{\otimes n} = \frac{1}{\sqrt{N}} \sum_{z\in\{0,1\}^n} \left|z\right\rangle. \tag{5.1.5}$$

Every computational basis state receives equal amplitude, so $\left|\psi_0\right\rangle$ introduces no bias toward any particular solution.

The adiabatic Hamiltonian is the linear interpolation

$$H(s) = -(1-s)\left|\psi_0\right\rangle \left\langle\psi_0\right| + sH_z, \qquad s \in [0,1]. \tag{5.1.6}$$

At $s = 0$, the ground state is $\left|\psi_0\right\rangle$ with energy -1, and all other states have energy 0. At $s = 1$, the Hamiltonian is H_z itself, and its ground states encode the solutions. The adiabatic theorem guarantees that if the schedule $s(t)$ traverses $[0, 1]$ slowly enough, the evolved state remains close to the instantaneous ground state throughout, arriving at the end in a state with high overlap with the ground space of H_z.

A rank-one H_0 produces exactly one avoided crossing between the two lowest energy levels. That single crossing is the structural reason the spectral analysis in Chapters 5–7 is possible at all. At $s = 0$, the spectrum has a non-degenerate ground state at -1 and an $(N-1)$-fold degenerate level at 0. As s increases, the degeneracy splits according to H_z. Because $H_0 = -\left|\psi_0\right\rangle \left\langle\psi_0\right|$ has rank one, all coupling between eigenstates of sH_z factors through $\left|\psi_0\right\rangle$. The matrix element $\left\langle k\right| H_0 \left|j\right\rangle = -\sqrt{d_k d_j}/N$ is nonzero for all pairs, yet the perturbation has only one degree of freedom, so eigenvalues repel through a single channel. Generic AQC Hamiltonians may exhibit multiple crossings requiring qualitatively different techniques [44, 68, 61]. Here, there is one.

The standard alternative to the rank-one projector is the transverse-field driver $H_0 = -\sum_{j=1}^{n} \sigma_x^j$, which is the default in quantum annealing hardware and in much of the AQC literature [44]. It couples every pair of computational basis states that differ in a single qubit, producing a dense web of avoided crossings throughout the interpolation. For random instances of NP-complete problems, Altshuler, Krovi, and Roland [43] showed

that the resulting spectrum exhibits Anderson localization. One then gets exponentially many avoided crossings with exponentially small gaps, and no known analytical technique yields tight gap bounds in that regime. The rank-one projector avoids this entirely. Because $|\psi_0\rangle\langle\psi_0|$ has a single non-zero eigenvalue, all coupling between eigenstates of sH_z flows through one channel, producing one crossing that can be analyzed exactly. The tractability of Chapters 5–7 is a direct consequence of this choice. Whether comparable results can be obtained for the transverse-field driver remains open. The Discussion of [10] identifies this as a central challenge.

In the unstructured case, $H(s) = -(1-s)|\psi_0\rangle\langle\psi_0| + s(I - |w\rangle\langle w|)$, where $|w\rangle$ is the marked item. Up to a global energy shift of s, this is the Roland-Cerf Hamiltonian [65]. The spectrum has $N-2$ states at energy s (degenerate, orthogonal to both $|\psi_0\rangle$ and $|w\rangle$) and two states whose energies depend on s and undergo an avoided crossing near $s = 1/2$.

5.2 Spectral Parameters

In the Roland-Cerf setting, the crossing position ($s^* = 1/2$), its width, and the minimum gap are all determined by a single quantity, N. For a general problem Hamiltonian H_z with M energy levels and arbitrary degeneracies, no single number suffices. The crossing position depends on the full eigenvalue structure of H_z, not only on E_0 and E_1. We therefore need quantities that compress this M-dimensional information into parameters that directly control the algorithm, namely the crossing location, the sharpness of the minimum gap, and the reopening rate.

Definition 5.2.1 (Spectral parameters)**.** *For the problem Hamiltonian H_z with eigenvalues $E_0 < E_1 < \cdots < E_{M-1}$ and degeneracies d_k, define*

$$A_p = \frac{1}{N}\sum_{k=1}^{M-1}\frac{d_k}{(E_k - E_0)^p}, \qquad p \in \mathbb{N}. \tag{5.2.1}$$

Each excited level contributes its degeneracy d_k weighted by the inverse p-th power of its distance to the ground energy. Larger p gives more weight to near-ground levels. Concretely, A_1 uses weight $1/(E_k - E_0)$, while A_2 uses $1/(E_k - E_0)^2$. A level at energy $E_0 + \varepsilon$ therefore contributes $O(1/\varepsilon)$ to A_1 but $O(1/\varepsilon^2)$ to A_2. The parameter A_1 determines the crossing position, and A_2 determines how sharp the crossing is. Normalization by $N = 2^n$ makes A_p an average over the full Hilbert space.

When $M = 2$, $d_0 = 1$, $d_1 = N - 1$, $E_0 = 0$, and $E_1 = 1$, we get

$$A_p = \frac{N-1}{N} \approx 1 \quad \text{for all } p, \tag{5.2.2}$$

since $E_1 - E_0 = 1$. The spectral parameters are trivial in this case, which is precisely why the Roland-Cerf analysis is simple.

For a general Ising Hamiltonian with $\Delta \geq 1/\text{poly}(n)$ and $M \in \text{poly}(n)$, the bound $A_1 \leq (1 - d_0/N)/\Delta$ gives $A_1 = O(\text{poly}(n))$. The bound $A_2 \geq 1 - d_0/N$ then guarantees A_2 stays constant-order whenever $d_0 \ll N$.

A_1 determines the crossing position, $s^* = A_1/(A_1+1)$. The parameter A_2 enters the minimum spectral gap, $g_{\min} = \Theta(\sqrt{d_0/(NA_2)})$. The gap scales as $\sqrt{d_0/N}$, so more ground states strengthen the coupling and widen the crossing. Both parameters appear in the runtime:

$$T = O\left(\frac{\sqrt{A_2}}{A_1(A_1+1)\Delta^2}\sqrt{\frac{N}{d_0}}\right).$$

Since every eigenvalue gap satisfies $E_k - E_0 \leq 1$ and the total excited degeneracy is $\sum_{k\geq 1} d_k = N - d_0$, we have

$$A_2 \geq \frac{1}{N}\sum_{k=1}^{M-1} d_k = 1 - \frac{d_0}{N}. \tag{5.2.3}$$

For $d_0 \ll N$ (few solutions), $A_2 \geq 1 - 1/N$ is close to 1. We also have $A_1 \leq (1 - d_0/N)/\Delta$, since $(E_k - E_0)^{-1} \leq \Delta^{-1}$ for all $k \geq 1$. A lower bound follows by the same comparison: because $E_k - E_0 \geq \Delta$, termwise comparison gives $A_1 \geq A_2\Delta$. Since $E_k - E_0 \leq 1$, we also have $A_1 \leq A_2$. Hence

$$A_2\Delta \leq A_1 \leq A_2.$$

The two-level approximation near the crossing is accurate only when the crossing window $\delta_s = O(\sqrt{d_0 A_2/N})$ is narrow compared to $[0, 1]$. Since $\delta_s/s^* = O((1/\Delta)\sqrt{d_0/(A_2 N)})$, this requires the spectral parameters to be polynomially bounded relative to N.

Definition 5.2.2 (Spectral condition)**.** *The problem Hamiltonian H_z satisfies the spectral condition if there exists a constant $c \ll 1$ such that*

$$\frac{1}{\Delta}\sqrt{\frac{d_0}{A_2 N}} < c. \tag{5.2.4}$$

The quantity on the left is, up to constants, the ratio between the crossing-window width and the problem-Hamiltonian spectral gap Δ. When this ratio is small, the two-level approximation near the crossing is accurate. Higher levels stay perturbative, and the window occupies only a small part of $[0, 1]$. The appendix of [10] shows that $c \approx 0.02$ is sufficient. When the condition fails, the argument breaks in a specific place. The eigenvalue equation is still valid, but the quadratic truncation in δ (Eq. (5.4.3)) requires $|\delta| \ll s\Delta$. That fails when many excited levels crowd near E_0. The result is a genuine multi-crossing regime, exemplified by transverse-field dynamics on random NP-complete instances [43]. The spectral condition therefore marks the boundary between the single-crossing regime of Chapters 5–7 and a regime that remains analytically intractable [68].

For any H_z with $\Delta > (1/c)\sqrt{d_0/N}$, the condition holds, using $A_2 \geq 1 - d_0/N$. For the Ising Hamiltonian with $\Delta \geq 1/\mathrm{poly}(n)$ and d_0 not scaling with N, the left side is exponentially small in n, so the condition is easily satisfied. With $\Delta = 1$ and $d_0 = 1$ (unstructured search), the left side is $1/\sqrt{N}$, well below any constant c for $N \geq 2$.

5.3 Symmetry Reduction

The Hilbert space of $H(s)$ has dimension $N = 2^n$, exponentially large in the number of qubits. Direct spectral analysis is intractable. But the problem Hamiltonian H_z has only M distinct energy levels, and the initial state $|\psi_0\rangle$ treats all bit-strings at the same energy identically. This permutation symmetry within each degenerate subspace reduces the eigenvalue problem from N dimensions to M.

For each energy level k, define the symmetric state

$$|k\rangle = \frac{1}{\sqrt{d_k}} \sum_{z \in \Omega_k} |z\rangle\,, \qquad 0 \leq k \leq M-1. \tag{5.3.1}$$

These M states are orthonormal: $\langle j\,|\,k\rangle = \delta_{jk}$. They span the M-dimensional symmetric subspace

$$\mathcal{H}_S = \mathrm{span}\,\{|k\rangle : 0 \leq k \leq M-1\}\,. \tag{5.3.2}$$

In this basis, the problem Hamiltonian has M non-degenerate eigenvalues.

$$H_z = \sum_{k=0}^{M-1} E_k\,|k\rangle\langle k| \quad \text{on } \mathcal{H}_S, \tag{5.3.3}$$

and the initial state decomposes as

$$|\psi_0\rangle = \sum_{k=0}^{M-1} \sqrt{\frac{d_k}{N}}\,|k\rangle\,. \tag{5.3.4}$$

Since $|\psi_0\rangle \in \mathcal{H}_S$ and both H_z and $|\psi_0\rangle\langle\psi_0|$ map $\mathcal{H}_S$ to itself, the adiabatic Hamiltonian $H(s)$ leaves $\mathcal{H}_S$ invariant. The time evolution starting from $|\psi_0\rangle$ remains in $\mathcal{H}_S$ for all s.

The complement $\mathcal{H}_S^\perp$ has dimension $N-M$ and is spanned by states orthogonal to $|\psi_0\rangle$ within each degenerate subspace. For each level k, order the bit-strings in Ω_k as $z_k^{(1)}, \ldots, z_k^{(d_k)}$ and define the Fourier basis

$$|k^{(\ell)}\rangle = \frac{1}{\sqrt{d_k}} \sum_{\ell'=1}^{d_k} \exp\left[\frac{i2\pi\ell\ell'}{d_k}\right] |z_k^{(\ell')}\rangle\,, \qquad 1 \leq \ell \leq d_k - 1. \tag{5.3.5}$$

Note that $|k^{(0)}\rangle = |k\rangle$ is the symmetric state already in $\mathcal{H}_S$. The remaining $d_k - 1$ states for each level k form a basis for $\mathcal{H}_S^\perp$.

$$\mathcal{H}_S^\perp = \mathrm{span}\left\{|k^{(\ell)}\rangle : 0 \leq k \leq M-1,\ 1 \leq \ell \leq d_k - 1\right\}. \tag{5.3.6}$$

Each $|k^{(\ell)}\rangle$ is an eigenstate of $H(s)$ with eigenvalue sE_k:

$$H(s)\,|k^{(\ell)}\rangle = -(1-s)\,|\psi_0\rangle \underbrace{\langle\psi_0\,|\,k^{(\ell)}\rangle}_{=0} + sE_k\,|k^{(\ell)}\rangle = sE_k\,|k^{(\ell)}\rangle\,. \tag{5.3.7}$$

The inner product vanishes because $|k^{(\ell)}\rangle$ is orthogonal to $|k\rangle = |k^{(0)}\rangle$ by construction, and $|\psi_0\rangle$ is a linear combination of the $|k\rangle$ states. Thus, out of the full 2^n-dimensional Hilbert space, only M dimensions participate in the adiabatic evolution. The remaining $N - M$ states are spectators. They are exact eigenstates with known eigenvalues sE_k and have zero overlap with the initial state. For Ising Hamiltonians, $M = O(\text{poly}(n))$, so the full dynamics lives in a polynomial-dimensional subspace.

Henceforth, $H(s)$ denotes its restriction to the symmetric subspace $\mathcal{H}_S$:

$$H(s) = -(1-s)\,|\psi_0\rangle\langle\psi_0| + s\sum_{k=0}^{M-1} E_k\,|k\rangle\langle k|\,. \tag{5.3.8}$$

This is a rank-one perturbation of the diagonal matrix sH_z, the setting of the Golub eigenvalue interlacing results [69].

Lemma 5.3.1 (Eigenvalue equation)**.** *Let $H(s)$ be the adiabatic Hamiltonian restricted to $\mathcal{H}_S$ as in Eq. (5.3.8). Then $\lambda(s)$ is an eigenvalue of $H(s)$ if and only if*

$$\frac{1}{1-s} = \frac{1}{N}\sum_{k=0}^{M-1}\frac{d_k}{sE_k - \lambda(s)}. \tag{5.3.9}$$

Proof. Let $|\psi\rangle = \sum_{k=0}^{M-1}\alpha_k\,|k\rangle$ be an eigenstate of $H(s)$ with eigenvalue λ, and set $\gamma = \langle\psi_0\rangle\,\psi$. Acting with $H(s)$ on $|\psi\rangle$ gives

$$H(s)\,|\psi\rangle = s\sum_{k=0}^{M-1} E_k\alpha_k\,|k\rangle - (1-s)\gamma\,|\psi_0\rangle = \lambda\sum_{k=0}^{M-1}\alpha_k\,|k\rangle\,. \tag{5.3.10}$$

Comparing coefficients of $|k\rangle$ and using $\langle\psi_0\rangle\,k = \sqrt{d_k/N}$ gives

$$\alpha_k = \frac{(1-s)\gamma\sqrt{d_k/N}}{sE_k - \lambda}. \tag{5.3.11}$$

Since $\gamma = \langle\psi_0\rangle\,\psi = (1/\sqrt{N})\sum_k \alpha_k\sqrt{d_k}$, substituting Eq. (5.3.11) yields

$$1 = \frac{1-s}{N}\sum_{k=0}^{M-1}\frac{d_k}{sE_k - \lambda}, \tag{5.3.12}$$

which is equivalent to Eq. (5.3.9). Each step is reversible: given a solution λ of Eq. (5.3.9), the coefficients in Eq. (5.3.11) define an eigenstate (after normalization), provided $\gamma \neq 0$. The case $\gamma = 0$ corresponds to $\lambda = sE_k$ for some k, which are the eigenvalues in $\mathcal{H}_S^{\perp}$ already accounted for. □

Viewed as a function of λ, the right-hand side of Eq. (5.3.9) is a sum of M terms, each decreasing with a vertical asymptote at $\lambda = sE_k$. Between consecutive poles sE_{k-1} and sE_k, the function decreases monotonically from $+\infty$ to $-\infty$, producing exactly one root per interval. Below the lowest pole sE_0, there is one additional root. The total count is M eigenvalues in $\mathcal{H}_S$, consistent with the dimension.

The two lowest eigenvalues are $\lambda_0(s) < sE_0$ (ground state) and $\lambda_1(s) \in (sE_0, sE_1)$ (first excited state). The spectral gap is $g(s) = \lambda_1(s) - \lambda_0(s) > 0$. However, this ordering information alone does not yield a useful quantitative upper bound on $g(s)$ uniformly over $s \in [0,1]$. Extracting tight bounds requires analyzing the eigenvalue equation in the vicinity of the crossing.

For $M = 2$, Eq. (5.3.9) becomes

$$\frac{1}{1-s} = \frac{1}{N}\cdot\frac{1}{-\lambda} + \frac{N-1}{N}\cdot\frac{1}{s-\lambda}, \tag{5.3.13}$$

where we set $E_0 = 0$ and $E_1 = 1$. Clearing denominators produces the quadratic $N\lambda^2 - N(2s-1)\lambda - s(1-s) = 0$, whose two roots give the ground and first excited energies:

$$\lambda_{\pm}(s) = \frac{2s-1}{2} \pm \frac{1}{2}\sqrt{(2s-1)^2 + \frac{4s(1-s)}{N}}. \tag{5.3.14}$$

At $s = 0$, the ground energy is $\lambda_- = -1$ and the first excited energy is $\lambda_+ = 0$, consistent with the spectrum of $H(0) = -\,|\psi_0\rangle\langle\psi_0|$. The gap $g(s) = \lambda_+(s) - \lambda_-(s)$ simplifies to

$$g(s) = \sqrt{(2s-1)^2 + \frac{4s(1-s)}{N}}, \tag{5.3.15}$$

which is minimized at $s = 1/2$ exactly, giving $g_{\min} = 1/\sqrt{N}$. This is the Roland-Cerf gap. The general theory of the next section reproduces this scaling as a special case.

5.4 The Avoided Crossing

The eigenvalue equation (Lemma 5.3.1) characterizes the spectrum of $H(s)$ implicitly. To extract explicit formulas for s^*, δ_s, and $g_{\min}$, we analyze it near the ground-state energy. Near the crossing, the ground and first excited states behave like a two-level system, while higher levels enter as a perturbation controlled by the spectral condition.

The two lowest eigenvalues have the form $\lambda(s) = sE_0 + \delta(s)$, where $\delta(s)$ is a correction to the trivial energy sE_0. Writing the eigenvalue as a perturbation of the nearest pole isolates the ground-state contribution and converts the implicit equation into an explicit power series. This is a standard technique for rank-one updates of diagonal eigenvalue problems [69]. Substituting into Eq. (5.3.9) gives

$$-\frac{d_0}{N\delta} + \frac{1}{N}\sum_{k=1}^{M-1} \frac{d_k}{s(E_k - E_0) - \delta} = \frac{1}{1-s}. \tag{5.4.1}$$

The first term has a pole at $\delta = 0$. The sum has poles at $\delta = s(E_k - E_0)$ for $k \geq 1$. When $|\delta| \ll s\Delta$ (guaranteed by the spectral condition), the sum can be expanded in powers of $\delta/(s(E_k - E_0))$:

$$\frac{1}{N}\sum_{k=1}^{M-1} \frac{d_k}{s(E_k - E_0) - \delta} = \frac{1}{s}\left(A_1 + \frac{\delta}{s}A_2 + \frac{\delta^2}{s^2}A_3 + \cdots\right). \tag{5.4.2}$$

Truncating at the A_2 term and rearranging Eq. (5.4.1) gives a quadratic in δ whose two roots are the corrections $\delta_0^+(s)$ and $\delta_0^-(s)$ for the first excited and ground states, respectively:

$$\delta_0^{\pm}(s) = \frac{s(A_1+1)}{2A_2(1-s)}\left[(s-s^*) \pm \sqrt{(s^*-s)^2 + \frac{4A_2 d_0}{N(A_1+1)^2}(1-s)^2}\right], \tag{5.4.3}$$

Here $\delta_0^+(s) > 0$ corresponds to the first excited state and $\delta_0^-(s) < 0$ to the ground state. The superscript indicates the sign of the correction relative to sE_0. The crossing position is

$$s^* = \frac{A_1}{A_1 + 1}. \tag{5.4.4}$$

The problem Hamiltonian has M eigenvalues and M degeneracies, so in principle there are $2M$ free spectral parameters. Yet the crossing location depends on one weighted average, A_1. This reduction is what makes a closed-form schedule possible despite rich spectral structure. For Ising Hamiltonians with $\Delta \geq 1/\text{poly}(n)$, A_1 is polynomially bounded above. In the hard-search regime $d_0 \ll N$, one also has $A_1 = \Omega(1)$, so s^* stays away from 0. As $A_1 \to \infty$ (many levels close to the ground state), $s^* \to 1$. For small A_1, s^* moves toward 0.

The crossing position is the balance point in the eigenvalue equation, $A_1/s^* = 1/(1-s^*)$. The left side is the aggregate pull of the excited spectrum toward sE_0, and the right side is the projector contribution. At $s = s^*$, the linear coefficient in the quadratic for δ (Eq. (5.4.3)) vanishes, so the roots $\delta_0^{\pm}$ are symmetric about zero. The minimum gap is then set by the constant term d_0/N, which is why ground-state degeneracy controls the opening size.

How good is the truncation? The actual roots $\delta_{\pm}(s)$ of the full equation differ from $\delta_0^{\pm}(s)$ by a relative error controlled by the spectral condition. The next result makes this precise. Its proof uses the intermediate value theorem on the full equation after bounding the remainder with A_3 and the spectral condition. The technique was developed for optimal spatial search via continuous-time quantum walks [70], where the same rank-one perturbation structure appears with a graph Laplacian replacing the diagonal Hamiltonian. The adaptation to the AQO setting appears in [10].

Lemma 5.4.1 (Validity of approximation)**.** *Let H_z satisfy the spectral condition (Definition 5.2.2) with constant $c \approx 0.02$, and define*

$$\delta_s = \frac{2}{(A_1+1)^2}\sqrt{\frac{d_0 A_2}{N}}. \tag{5.4.5}$$

Then for any $s \in \mathcal{I}_{s^*} = [s^* - \delta_s,\ s^* + \delta_s]$, there exists a constant $\eta \ll 1$ such that the two lowest eigenvalues of $H(s)$ satisfy

$$\delta_+(s) \in \left((1-\eta)\,\delta_0^+(s),\ (1+\eta)\,\delta_0^+(s)\right), \tag{5.4.6}$$

$$\delta_-(s) \in \left((1+\eta)\,\delta_0^-(s),\ (1-\eta)\,\delta_0^-(s)\right), \tag{5.4.7}$$

where $\delta_0^{\pm}(s)$ are given by Eq. (5.4.3).

The proof evaluates the full equation (5.4.1) at $\delta_0^{\pm}(1\pm\eta)$ and shows, using the spectral condition to bound the truncated Taylor remainder, that the full equation changes sign between these points. The intermediate value theorem then guarantees a root in the interval. The spectral condition enters through the bound $|\delta_0^{\pm}(s)|/(s\Delta) \leq \kappa c < 1$, where κ is a constant depending on c, ensuring the geometric series in the Taylor expansion converges. The constant $c \approx 0.02$ is sufficient for $\eta \leq 0.1$. The complete calculation appears in the appendix of [10].

Since both corrections are approximated to within $1 \pm \eta$, the spectral gap $g(s) = \delta_+(s) - \delta_-(s)$ is within a factor of $1 \pm 2\eta$ of $\delta_0^+(s) - \delta_0^-(s)$, which evaluates to

$$g(s) = (1 \pm 2\eta) \cdot \frac{s(A_1+1)}{A_2(1-s)} \sqrt{(s^*-s)^2 + \frac{4A_2 d_0}{N(A_1+1)^2}(1-s)^2}. \tag{5.4.8}$$

At $s = s^*$, the first term under the square root vanishes, leaving only the second:

$$g_{\min} = g(s^*) \geq (1-2\eta) \cdot \frac{2A_1}{A_1+1}\sqrt{\frac{d_0}{NA_2}}. \tag{5.4.9}$$

The gap scales as $\sqrt{d_0/N}$ with corrections from spectral structure. The factor $2A_1/(A_1+1)$ captures crossing position. A crossing near the boundary ($s^* \to 0$ or $s^* \to 1$) reduces the gap. The factor $\sqrt{d_0/N}$ is the Grover-like contribution. More solutions (larger d_0) increase the gap and reduce runtime. The factor $1/\sqrt{A_2}$ encodes spectral structure beyond the simplest two-level case.

An exact algebraic identity connects s^*, δ_s, and the leading-order minimum gap. Writing $\hat{g} = \frac{2A_1}{A_1+1}\sqrt{\frac{d_0}{NA_2}}$ for the leading-order expression, direct substitution gives

$$\frac{s^*(A_1+1)^2}{A_2} \cdot \delta_s = \hat{g}, \tag{5.4.10}$$

and by Eq. (5.4.9), $g_{\min} \geq (1-2\eta)\hat{g}$. This relation will be used in Chapter 7 to verify the runtime calculation.

Three regions partition $[0,1]$ based on the crossing.

$$\mathcal{I}_{s\leftarrow} = [0,\, s^*-\delta_s), \qquad \mathcal{I}_{s^*} = [s^*-\delta_s,\, s^*+\delta_s], \qquad \mathcal{I}_{s\rightarrow} = (s^*+\delta_s,\, 1]. \tag{5.4.11}$$

Lemma 5.4.2 (Gap within the crossing window)**.** *Let H_z satisfy the spectral condition with constant c, and define*

$$\kappa' = \frac{(1+2\eta)(1+2c)}{(1-2\eta)(1-2c)}\sqrt{1+(1-2c)^2}. \tag{5.4.12}$$

Then for any $s \in \mathcal{I}_{s^*}$,

$$g_{\min} \leq g(s) \leq \kappa' \cdot g_{\min}. \tag{5.4.13}$$

Proof. The lower bound is immediate from the definition of $g_{\min}$ as the minimum over $\mathcal{I}_{s^*}$. For the upper bound, start from Eq. (5.4.8) with $|s-s^*| \leq \delta_s$:

$$g(s) \leq \frac{s(A_1+1)}{A_2(1-s)}\sqrt{\delta_s^2 + \frac{4A_2 d_0}{N(A_1+1)^2}(1-s)^2}. \tag{5.4.14}$$

Factoring out $(A_1+1)\delta_s(1-s)$ under the square root and using $s/s^* \leq 1 + \delta_s/s^*$:

$$g(s) \leq \frac{s^*(A_1+1)^2}{A_2}\delta_s \cdot \frac{s}{s^*} \cdot \sqrt{\frac{1}{(1-s)^2(A_1+1)^2} + 1}. \tag{5.4.15}$$

The first factor equals $\hat{g}$ by Eq. (5.4.10). The spectral condition gives $\delta_s/(1-s^*) \leq 2c$ and $\delta_s/s^* \leq 2c$. To see the first, compute

$$\frac{\delta_s}{1-s^*} = \frac{2}{1+A_1}\sqrt{\frac{d_0 A_2}{N}} = \frac{2A_2\Delta}{1+A_1} \cdot \frac{1}{\Delta}\sqrt{\frac{d_0}{A_2 N}} \leq 2s^* c \leq 2c, \tag{5.4.16}$$

where we used $A_2\Delta/(1+A_1) \leq A_1/(1+A_1) = s^*$. The bound $\delta_s/s^* \leq 2c$ follows similarly. Substituting into the upper bound:

$$g(s) \leq (1+2\eta)\hat{g} \cdot (1+2c)\sqrt{1+(1-2c)^2} \leq \kappa' \cdot g_{\min}, \tag{5.4.17}$$

where the factor $(1+2\eta)$ comes from the upper approximation in Eq. (5.4.8), and the last step uses $\hat{g} \leq g_{\min}/(1-2\eta)$. □

Inside $\mathcal{I}_{s^*}$, the gap is $\Theta(g_{\min})$. Outside, it is strictly larger, as the next section establishes. The avoided crossing is localized.

Specializing to unstructured search, with $A_1 = A_2 = (N-1)/N$:

$$s^* = \frac{(N-1)/N}{(N-1)/N+1} = \frac{N-1}{2N-1} \approx \frac{1}{2}, \tag{5.4.18}$$

$$g_{\min} = \frac{2(N-1)/(2N-1)}{\sqrt{N\cdot(N-1)/N}} = \frac{2(N-1)}{(2N-1)\sqrt{N-1}} \approx \frac{1}{\sqrt{N}}, \tag{5.4.19}$$

$$\delta_s = \frac{2N^2}{(2N-1)^2}\sqrt{\frac{N-1}{N^2}} \approx \frac{1}{2\sqrt{N}}. \tag{5.4.20}$$

The crossing is at $s^* \approx 1/2$, the minimum gap scales as $1/\sqrt{N}$, and the window width scales as $1/\sqrt{N}$. These agree asymptotically with the exact quadratic solution in Eq. (5.3.15), confirming the general theory reproduces the known scaling. The small discrepancy between $s^* = (N-1)/(2N-1)$ and the exact minimum at $s = 1/2$ is a higher-order effect of the two-level truncation, vanishing as $O(1/N)$.

5.5 Gap Structure

The adiabatic schedule requires the gap everywhere, not just near the crossing. The local adaptive schedule speeds up where the gap is large and slows where it is small, so the runtime depends on the gap profile across the full interval $[0,1]$. Inside $\mathcal{I}_{s^*}$, the gap is $\Theta(g_{\min})$. Outside it, the gap grows linearly. Proving this split requires different techniques on the two sides, and that split drives the structure of Chapter 6.

Lemma 5.5.1 (Gap to the left of the crossing)**.** *For any $s \in \mathcal{I}_{s^*\leftarrow} = [0,\, s^* - \delta_s)$, the spectral gap of $H(s)$ satisfies*

$$g(s) \geq \frac{A_1(A_1+1)}{A_2}(s^* - s). \tag{5.5.1}$$

Why does this hold? One route uses the variational principle. An explicit ansatz $|\phi\rangle$ gives an upper bound $\lambda_0(s) \leq \langle\phi|\, H(s)\, |\phi\rangle$, while the eigenvalue equation gives the lower bound $\lambda_1(s) \geq sE_0$. The ansatz is

$$|\phi\rangle = \frac{1}{\sqrt{A_2 N}} \sum_{k=1}^{M-1} \frac{\sqrt{d_k}}{E_k - E_0} |k\rangle\,. \tag{5.5.2}$$

This ansatz concentrates amplitude near the ground energy and yields a tight upper bound on $\lambda_0(s)$. A second route uses concavity. Because $\lambda_0(s) = \min_{|\psi\rangle} \langle\psi|\, H(s)\, |\psi\rangle$ is the pointwise minimum of linear functions in s, it is concave. The tangent line at s^* therefore lies above $\lambda_0(s)$. Combining that tangent bound with $\lambda_1(s) \geq sE_0$ reproduces Eq. (5.5.1). Chapter 6 develops both arguments in detail.

Lemma 5.5.2 (Gap to the right of the crossing)**.** *Assume $A_1 \geq 1/2$ (equivalently $s^* \geq 1/3$). Let $k = 1/4$, $a = 4k^2\Delta/3$, and*

$$s_0 = s^* - \frac{k\, g_{\min}(1-s^*)}{a - k\, g_{\min}}. \tag{5.5.3}$$

Then for all $s \geq s^*$, the spectral gap of $H(s)$ satisfies

$$g(s) \geq \frac{\Delta}{30} \cdot \frac{s - s_0}{1 - s_0}. \tag{5.5.4}$$

This bound is linear in $s - s_0$, with slope proportional to Δ. The proof strategy differs from the left side. One places a line $\gamma(s) = sE_0 + \beta(s)$ between the two lowest eigenvalues and then uses Sherman-Morrison [71] to control the resolvent norm $\|R_{H(s)}(\gamma)\|$. This yields $g(s) \geq 2/\|R_{H(s)}(\gamma)\|$. The constants $k = 1/4$ and $a = 4k^2\Delta/3$ are chosen so that the auxiliary function $f(s)$ decreases monotonically on $[s^*, 1]$, producing the clean slope constant $\Delta/30$.

At the window boundary, both bounds match $g_{\min}$ in order. At $s = s^* - \delta_s$, the left bound gives

$$g(s^* - \delta_s) \geq \frac{A_1(A_1+1)}{A_2} \cdot \delta_s = \frac{2A_1}{A_1+1}\sqrt{\frac{d_0}{NA_2}} = \hat{g}, \tag{5.5.5}$$

which satisfies $\hat{g} = \Theta(g_{\min})$ by Eq. (5.4.9). At $s = s^*$ (right boundary start), $\beta(s^*) \geq k\, g_{\min}$, so $g(s^*) \geq 2k\, g_{\min}/(1 + f(s^*)) = O(g_{\min})$ since $f(s^*) = \Theta(1)$. The gap profile is therefore continuous across region boundaries. It dips to $g_{\min}$ at s^* and rises linearly on both sides.

With the gap profile in hand, runtime follows from the optimal local adaptive schedule [45, 65], where $ds/dt \propto g(s)^2$. Evolution therefore slows quadratically as the gap decreases. The total runtime is

$$T \propto \int_0^1 \frac{ds}{g(s)^2}, \tag{5.5.6}$$

split across the three regions. In the left and right regions, linear gap growth gives $1/g(s)^2 \propto 1/(s-s^*)^2$, so each outer contribution scales like $1/\delta_s$ at the window boundary. Inside the window, the gap is approximately constant at $g_{\min}$ and contributes $2\delta_s/g_{\min}^2$. This window term dominates. The bottleneck is therefore a $\Theta(1/\sqrt{N})$-wide interval around s^*.

$$\frac{\delta_s}{g_{\min}^2} \propto \frac{\sqrt{A_2}}{A_1(A_1+1)\Delta^2}\sqrt{\frac{N}{d_0}}, \tag{5.5.7}$$

yielding the optimal runtime [10]. For the Ising Hamiltonian with $A_1, A_2 = O(\text{poly}(n))$ and $\Delta \geq 1/\text{poly}(n)$, this gives $T = \widetilde{O}(\sqrt{N/d_0})$, matching the Grover lower bound up to polylogarithmic factors. Chapter 7 carries out this calculation rigorously.

5.6 What Remains

At this point, the structure is in place and the remaining steps are focused. Chapter 6 proves the outer-region gap bounds. Chapter 7 converts those bounds into the optimal runtime. Chapter 8 accounts for the pre-computation cost required to realize that schedule.

Given the complete gap profile, the optimal runtime is

$$T = O\left(\frac{1}{\varepsilon} \cdot \frac{\sqrt{A_2}}{A_1(A_1+1)\Delta^2} \cdot \sqrt{\frac{N}{d_0}}\right), \tag{5.6.1}$$

where ε is the target error. For Ising Hamiltonians, this is $\widetilde{O}(\sqrt{N/d_0})$, matching the lower bound of Farhi, Goldstone, and Gutmann [39]. Adiabatic quantum optimization achieves the Grover speedup. Chapter 7 derives this rigorously.

The local adaptive schedule requires s^* to precision $O(\delta_s) = O(2^{-n/2})$, so A_1 must be known at comparable precision. Approximating A_1 is already hard much earlier on this scale. At additive error $1/\text{poly}(n)$, two oracle queries suffice to solve 3-SAT, so the task is NP-hard. Exact computation of A_1, or approximation to $O(2^{-\text{poly}(n)})$, is #P-hard because polynomial interpolation recovers all degeneracies d_k from $O(\text{poly}(n))$ exact queries. Chapter 8 proves both statements and quantifies the resulting precision gap.

In the circuit model, Grover's algorithm reaches $\widetilde{O}(\sqrt{N/d_0})$ without pre-computing any spectral parameter. Oracle queries gather the needed information during execution. In the adiabatic framework, by contrast, the schedule is fixed before evolution starts, which forces NP-hard pre-computation. In our view, this asymmetry is not a proof artifact. It reflects a genuine model-level difference. The adiabatic speedup is real, but it is conditional on solving a hard preprocessing problem first [10]. Chapter 9 makes this tradeoff explicit through an uninformed-schedule separation, an interpolation theorem for partial information, and an adaptive measurement protocol that bypasses classical hardness.

In the unstructured case, the limitation vanishes: $A_1 = (N-1)/N \approx 1$ is trivially known, so $s^* \approx 1/2$ requires no hard computation. The complexity arises only for problem Hamiltonians with rich spectral structure, where the degeneracies d_k and energy gaps $E_k - E_0$ are not known in advance. The Ising Hamiltonian encoding an NP-hard problem is precisely such a case.

Chapter 6

Spectral Analysis

Chapter 5 established the crossing window $\mathcal{I}_{s^*}$ where the spectral gap satisfies $g(s) = \Theta(g_{\min})$, and it stated the outer-region bounds. The left side has a linear lower bound (Lemma 5.5.1), and so does the right side (Lemma 5.5.2). This chapter proves both lemmas.

The two proofs use different tools because the spectrum behaves differently on the two sides of the crossing. To the left of s^*, the ground energy $\lambda_0(s)$ sits below sE_0 while the first excited energy $\lambda_1(s)$ sits above it. A variational argument then gives a sharp linear gap bound. To the right of s^*, eigenvalues of sH_z crowd the interval $[sE_0, sE_1]$, and that variational strategy loses traction. There we switch to a resolvent argument plus Sherman-Morrison for rank-one perturbations. This split is the technical core of the chapter, and it yields the piecewise profile needed in Chapter 7. The profile is steep on the left, flatter on the right, and nearly flat inside the window.

6.1 Gap to the Left of the Crossing

The eigenvalue equation (Lemma 5.3.1) places the ground state energy at $\lambda_0(s) < sE_0$ and the first excited energy at $\lambda_1(s) \in (sE_0, sE_1)$. This already proves $g(s) > 0$. It does not yet give the quantitative lower bound needed for the runtime integral. What we need is a bound that makes the left-side linear reopening explicit.

The strategy is to tighten the upper bound on $\lambda_0(s)$. Two routes give the same linear form. The first uses the variational principle. For any normalized state $|\phi\rangle$, the ground energy satisfies $\lambda_0(s) \le \langle\phi| H(s) |\phi\rangle$, so a carefully chosen ansatz directly yields a bound. The second uses concavity. Because $\lambda_0(s) = \min_{|\psi\rangle} \langle\psi| H(s) |\psi\rangle$ is the pointwise minimum of affine functions in s, it is concave, and every tangent line lies above it. We start with the variational route because it keeps the constants explicit.

Lemma 6.1.1 (Gap to the left of the crossing)**.** *For any $s \in \mathcal{I}_{s\leftarrow} = [0,\, s^* - \delta_s)$, the spectral gap of $H(s)$ satisfies*

$$g(s) \ge \frac{A_1(A_1+1)}{A_2}\,(s^* - s)\,. \tag{6.1.1}$$

Proof. We upper-bound $\lambda_0(s)$ via the variational principle and lower-bound $\lambda_1(s)$ from the eigenvalue equation.

The ansatz must live in the span of $\{|k\rangle : k \ge 1\}$, orthogonal to the ground-state component $|0\rangle$, and should concentrate amplitude on levels close to E_0 where the energy expectation is lowest. The natural weighting is the inverse energy gap, because levels near E_0 should carry more amplitude. Unit normalization then fixes the scale, so we define

$$|\phi\rangle = \frac{1}{\sqrt{A_2 N}} \sum_{k=1}^{M-1} \frac{\sqrt{d_k}}{E_k - E_0}\,|k\rangle\,. \tag{6.1.2}$$

This weighting also arises in first-order perturbation theory. The correction to the ground state $|E_0\rangle$ of sH_z due to the perturbation $-(1-s)\,|\psi_0\rangle\langle\psi_0|$ has coefficients proportional to $\langle E_k\rangle\,\psi_0/(E_k - E_0) = \sqrt{d_k/N}/(E_k - E_0)$, which matches the form above up to normalization. Normalization is immediate.

$$\langle\phi\rangle\,\phi = \frac{1}{A_2 N} \sum_{k=1}^{M-1} \frac{d_k}{(E_k - E_0)^2} = \frac{A_2}{A_2} = 1. \tag{6.1.3}$$

To compute $\langle\phi| H(s) |\phi\rangle$, decompose $H(s) = -(1-s)\,|\psi_0\rangle\langle\psi_0| + s(H_z - E_0) + sE_0$. Each term contributes separately.

The projector term gives

$$-(1-s)\left|\langle\psi_0\rangle\,\phi\right|^2 = -(1-s)\left(\frac{1}{\sqrt{A_2 N}}\sum_{k=1}^{M-1}\frac{d_k}{(E_k-E_0)\sqrt{N}}\right)^2 = -(1-s)\frac{A_1^2}{A_2}, \tag{6.1.4}$$

where $\langle\psi_0\rangle\,\phi = A_1/\sqrt{A_2}$ follows from $\langle\psi_0\rangle\,k = \sqrt{d_k/N}$ and the definition of A_1.

The shifted diagonal term gives

$$s\,\langle\phi|\,(H_z - E_0)\,|\phi\rangle = \frac{s}{A_2 N}\sum_{k=1}^{M-1}\frac{d_k}{(E_k-E_0)^2}\cdot(E_k-E_0) = \frac{s}{A_2 N}\sum_{k=1}^{M-1}\frac{d_k}{E_k-E_0} = \frac{s\,A_1}{A_2}. \tag{6.1.5}$$

The constant term contributes $sE_0\,\langle\phi\rangle\,\phi = sE_0$. Combining the three terms gives

$$\lambda_0(s) \le \langle\phi|\,H(s)\,|\phi\rangle = sE_0 - (1-s)\frac{A_1^2}{A_2} + s\frac{A_1}{A_2} = sE_0 + \frac{A_1}{A_2}\left(s(1+A_1) - A_1\right). \tag{6.1.6}$$

Since $s^*(1+A_1) = A_1$, we have $s(1+A_1) - A_1 = (1+A_1)(s-s^*) = (s-s^*)/(1-s^*)$, so

$$\lambda_0(s) \le sE_0 + \frac{A_1}{A_2}\cdot\frac{s-s^*}{1-s^*}. \tag{6.1.7}$$

For $s < s^*$, the second term is negative, confirming $\lambda_0(s) < sE_0$.

For the first excited state, the eigenvalue equation (Lemma 5.3.1) confines $\lambda_1(s)$ to the interval (sE_0, sE_1), so

$$\lambda_1(s) \ge sE_0. \tag{6.1.8}$$

The gap is therefore

$$g(s) = \lambda_1(s) - \lambda_0(s) \ge sE_0 - sE_0 - \frac{A_1}{A_2}\cdot\frac{s-s^*}{1-s^*} = \frac{A_1}{A_2}\cdot\frac{s^*-s}{1-s^*}. \tag{6.1.9}$$

Since $1/(1-s^*) = A_1 + 1$, we obtain $g(s) \ge A_1(A_1+1)(s^*-s)/A_2$. □

At the left boundary of the crossing window, $s = s^* - \delta_s$, the bound gives

$$g(s^* - \delta_s) \ge \frac{A_1(A_1+1)}{A_2}\cdot\delta_s = \hat{g}, \tag{6.1.10}$$

using $A_1(A_1+1)\delta_s/A_2 = \hat{g}$ from Eq. (5.4.10). Since $g_{\min} = (1 \pm O(\eta))\hat{g}$ from Eq. (5.4.9), the gap at the window boundary is $\Theta(g_{\min})$. The three-region decomposition is therefore tight because the left bound meets the window bound at the boundary rather than leaving a gap between them.

An alternative derivation uses concavity. Since $\lambda_0(s) = \min_{|\psi\rangle}\langle\psi|\,H(s)\,|\psi\rangle$ is the pointwise minimum of affine functions in s, it is concave. The Hellmann-Feynman theorem [16] gives the second derivative explicitly.

$$\ddot{\lambda}_0(s) = -2\sum_{j\ge 1}\frac{|\,\langle\phi_j(s)|\,\dot{H}\,|\phi_0(s)\rangle\,|^2}{\lambda_j(s)-\lambda_0(s)} \le 0,$$

where $\dot{H} = H_z + |\psi_0\rangle\langle\psi_0|$ and $|\phi_j(s)\rangle$ are the instantaneous eigenstates. Concavity implies that every tangent line lies above the function. In particular, the tangent at s^* gives $\lambda_0(s) \le \lambda_0(s^*) + \lambda_0'(s^*)(s-s^*)$, an upper bound of the same form as (6.1.7), though the variational approach gives slightly sharper constants.

When $M = 2$ ($d_0 = 1$, $d_1 = N-1$, $E_0 = 0$, $E_1 = 1$), the ansatz reduces to $|\phi\rangle = |1\rangle$, and the bound becomes

$$g(s) \ge \frac{(N-1)/N\cdot(2N-1)/N}{(N-1)/N}\left(\frac{1}{2}-s\right) = \frac{2N-1}{N}\left(\frac{1}{2}-s\right) \approx 2\left(\frac{1}{2}-s\right). \tag{6.1.11}$$

The exact gap $g(s) = \sqrt{(2s-1)^2 + 4s(1-s)/N}$ at $s = 1/4$ equals $\sqrt{1/4 + 3/(4N)} \approx 1/2$, while the bound gives $(2N-1)/(4N) \approx 1/2$. The bound is tight near s^* and only becomes loose as s approaches 0, where the true gap approaches 1 while the bound continues growing.

6.2 Gap to the Right of the Crossing

The variational principle cannot bound the gap to the right of s^*. It bounds ground energies from above, not excited energies from below, and what we need on the right is a lower bound on $\lambda_1(s) - \lambda_0(s)$ that captures the linear reopening of the gap.

The obstacle is structural. On the left, $\lambda_1(s)$ is bounded below by sE_0 from the eigenvalue equation, which gives a clean anchor point. On the right, $\lambda_1(s)$ still lies between sE_0 and sE_1, but now many higher branches pass through the same interval and generate their own avoided crossings. We need a method that controls spectral distance without tracking individual branches one by one. The eigenvalue equation (Lemma 5.3.1) characterizes the full spectrum implicitly, but it does not directly give the linear-in-$(s - s^*)$ lower bound we need.

The resolvent provides exactly this. For a self-adjoint operator A with spectrum $\sigma(A)$ and any $\lambda \notin \sigma(A)$, the resolvent

$$R_A(\lambda) = (\lambda I - A)^{-1} \tag{6.2.1}$$

is a bounded operator whose norm equals the inverse distance from λ to the spectrum:

$$\|R_A(\lambda)\| = \frac{1}{\operatorname{dist}(\lambda,\, \sigma(A))}. \tag{6.2.2}$$

This follows from the spectral theorem. In the eigenbasis of A with eigenvalues $\{\lambda_j\}$, the resolvent is diagonal with entries $1/(\lambda - \lambda_j)$, so its operator norm is $\max_j |1/(\lambda - \lambda_j)| = 1/\min_j |\lambda - \lambda_j|$. If a point γ lies between two consecutive eigenvalues λ_0 and λ_1, then $\operatorname{dist}(\gamma, \sigma(A)) = \min(\gamma - \lambda_0, \lambda_1 - \gamma) \leq g/2$, since the minimum of two non-negative numbers summing to g is at most $g/2$. Therefore $\|R_A(\gamma)\| = 1/\operatorname{dist}(\gamma, \sigma(A)) \geq 2/g$, and the useful contrapositive is

$$g(s) \geq \frac{2}{\|R_{H(s)}(\gamma)\|}. \tag{6.2.3}$$

The spectral-gap problem has become a norm problem. A lower bound on the gap is now an upper bound on a resolvent norm.

This resolvent approach to rank-one perturbations has precedent in spatial search. Childs and Goldstone [72] used it to prove $O(\sqrt{N})$ search time on the complete graph. Chakraborty, Novo, and Roland [73, 70] then extended the method to broad graph families via Sherman-Morrison.

The algebraic structure is the same as in our Hamiltonian $H(s) = sH_z - (1-s)\,|\psi_0\rangle\langle\psi_0|$, with a graph Laplacian replaced by a diagonal cost Hamiltonian. We therefore import the same mechanism, with graph parameters replaced by A_1 and A_2.

Spatial search via continuous-time quantum walks asks for a marked vertex in a graph G on N vertices by evolving $|s\rangle = (1/\sqrt{N})\sum_v |v\rangle$ under $H_{\text{search}} = -\gamma L - \sum_{v\in S} |v\rangle\langle v|$, where L is the graph Laplacian and $\gamma > 0$ is tunable [72]. When $|S| = 1$, the oracle term is rank one (and low rank more generally). The dictionary to our setting is direct. L plays the role of sH_z, the oracle projector plays the role of $(1-s)\,|\psi_0\rangle\langle\psi_0|$, the graph spectral gap corresponds to Δ, and effective resistance plays the role of A_2.

In both settings, one places a line $\gamma(s)$ between the two lowest eigenvalues, applies Sherman-Morrison to split the resolvent into a known diagonal part plus a correction term, and then bounds that correction. The method works because rank-one perturbations of diagonal operators always admit this inversion step, reducing the gap problem to one rational bound.

The constants $k = 1/4$ and $f(s^*) = 4$ are not accidents of this specific Hamiltonian. They come from the same line-placement optimization that appears whenever a rank-one perturbation is handled this way. The optimization balances denominator positivity against numerator growth in $f(s)$. In that sense the constants are structural. They do not depend on whether the unperturbed part is a graph Laplacian or a diagonal cost Hamiltonian.

Since $H(s) = sH_z - (1-s)\,|\psi_0\rangle\langle\psi_0|$ is a rank-one perturbation of sH_z, we can invert its resolvent explicitly. The Sherman-Morrison identity [71] states that for an invertible operator A and vectors $|u\rangle, \langle v|$,

$$(A + |u\rangle\langle v|)^{-1} = A^{-1} - \frac{A^{-1}\,|u\rangle\langle v|\,A^{-1}}{1 + \langle v|\,A^{-1}\,|u\rangle}, \tag{6.2.4}$$

provided $1 + \langle v|\,A^{-1}\,|u\rangle \neq 0$. Applying this to the resolvent of $H(s)$ decomposes it into the resolvent of sH_z (whose spectrum is known explicitly) and a correction from the rank-one term $-(1-s)\,|\psi_0\rangle\langle\psi_0|$. The triangle inequality then yields an upper bound on $\|R_{H(s)}(\gamma)\|$.

We choose a line $\gamma(s)$ between $\lambda_0(s)$ and $\lambda_1(s)$ for all $s \geq s^*$. Then we apply Sherman-Morrison, bound each contribution in terms of A_1 and A_2, and convert the resulting resolvent estimate into a linear lower bound on $g(s)$.

The simplest line starts at sE_0 when $s = s^*$ and ends between E_0 and E_1 at $s = 1$. Take $\beta(s) = a(s - s^*)/(1 - s^*)$ with $a < \Delta$, and set $\gamma(s) = sE_0 + \beta(s)$. For $a = \Delta/6$, one can show $f(s) \leq 1$ for all $s \geq s^*$. This yields $g(s) \geq \beta(s) = (\Delta/6)(s - s^*)/(1 - s^*)$. The bound is valid but too weak where the runtime is decided. At the window boundary $s = s^* + \delta_s$, it gives $g(s^* + \delta_s) \geq (\Delta/6) \cdot \delta_s/(1 - s^*) = (\Delta A_2)/(6A_1) \cdot g_{\min}$. Since $\Delta A_2 \leq A_1$, this is at most $g_{\min}/6$, and it can be polynomially smaller when $\Delta A_2 \ll A_1$. At $s = s^*$, the same estimate collapses to $g(s^*) \geq 0$, which misses the true minimum gap entirely.

The failure has a geometric explanation. At s^*, the ground energy $\lambda_0(s^*)$ sits $g_{\min}/2$ below s^*E_0. The line $\gamma(s)$ passes through s^*E_0 at $s = s^*$, so it has no safety margin from the lower branch. At a midpoint between two eigenvalues, the resolvent norm is $2/g$. At a point that touches one eigenvalue, it diverges. So the line must start at $O(g_{\min})$ distance from both branches.

The fix is to shift the line origin from s^* to a point $s_0 < s^*$ so that $\beta(s^*) = k\, g_{\min}$ for a constant $k < 1$. With $\beta(s) = a(s - s_0)/(1 - s_0)$, the constraint $\beta(s^*) = k\, g_{\min}$ determines

$$s_0 = s^* - \frac{k\, g_{\min}(1 - s^*)}{a - k\, g_{\min}}. \tag{6.2.5}$$

The line now passes through $\gamma(s^*) = s^*E_0 + k\, g_{\min}$, which lies between $\lambda_0(s^*)$ and $\lambda_1(s^*)$ when k is chosen appropriately. The price is that $s_0 < s^*$ introduces extra terms in the monotonicity analysis for $f(s)$. We therefore need a careful choice of a.

Lemma 6.2.1 (Gap to the right of the crossing)**.** *Assume $A_1 \geq 1/2$. Let $k = 1/4$, $a = 4k^2\Delta/3 = \Delta/12$, and s_0 as in Eq. (6.2.5). Then for all $s \geq s^*$, the spectral gap of $H(s)$ satisfies*

$$g(s) \geq \frac{\Delta}{30} \cdot \frac{s - s_0}{1 - s_0}. \tag{6.2.6}$$

Proof. Set $\gamma(s) = sE_0 + \beta(s)$ with $\beta(s) = a(s - s_0)/(1 - s_0)$. We bound $\|R_{H(s)}(\gamma)\|$ from above using the Sherman-Morrison formula.

Since $H(s) = sH_z - (1 - s)\,|\psi_0\rangle\langle\psi_0|$, the resolvent of $H(s)$ at γ satisfies, via Eq. (6.2.4) and the triangle inequality,

$$\|R_{H(s)}(\gamma)\| \leq \|R_{sH_z}(\gamma)\| + (1 - s)\frac{\|R_{sH_z}(\gamma)\,|\psi_0\rangle\langle\psi_0|\,R_{sH_z}(\gamma)\|}{1 + (1 - s)\,\langle\psi_0|\,R_{sH_z}(\gamma)\,|\psi_0\rangle}. \tag{6.2.7}$$

The unperturbed resolvent $R_{sH_z}(\gamma)$ is diagonal in the $|k\rangle$ basis with entries $1/(\gamma - sE_k) = 1/(\beta - s(E_k - E_0))$ for $k \geq 1$ and $1/\beta$ for $k = 0$. The nearest eigenvalue of sH_z to γ is sE_0, at distance β, so $\|R_{sH_z}(\gamma)\| = 1/\beta$.

We now bound the numerator and denominator of the second term separately. Both bounds use $\beta(s) \leq s(E_k - E_0)/2$ for all $k \geq 1$, so the Taylor series in $\beta/(s(E_k - E_0))$ converges quickly. Here $\beta(s) \leq a = \Delta/12$, while $s(E_k - E_0) \geq s^*\Delta \geq \Delta/3$ because $s^* = A_1/(A_1 + 1) \geq 1/3$ when $A_1 \geq 1/2$. Therefore $\beta \leq \Delta/12 < \Delta/6 \leq s(E_k - E_0)/2$, as required. The condition $A_1 \geq 1/2$ also marks the nontrivial search regime. Since $A_1 \geq 1 - d_0/N$, the complementary case $A_1 < 1/2$ implies $d_0 > N/2$, where random sampling already succeeds with constant probability.

Numerator bound. The squared norm of $R_{sH_z}(\gamma)\,|\psi_0\rangle$ expands as

$$\|R_{sH_z}(\gamma)\,|\psi_0\rangle\|^2 = \frac{d_0}{N\beta^2} + \frac{1}{N}\sum_{k=1}^{M-1}\frac{d_k}{\big(s(E_k - E_0) - \beta\big)^2}. \tag{6.2.8}$$

Using $s(E_k - E_0) - \beta \geq s(E_k - E_0)/2$, each term in the sum is at most $4d_k/(Ns^2(E_k - E_0)^2)$, giving

$$\|R_{sH_z}(\gamma)\,|\psi_0\rangle\langle\psi_0|\,R_{sH_z}(\gamma)\| \leq \|R_{sH_z}(\gamma)\,|\psi_0\rangle\|^2 \leq \frac{d_0}{N\beta^2} + \frac{4A_2}{s^2}. \tag{6.2.9}$$

Denominator bound. Expanding the expectation value gives

$$\begin{aligned} 1 + (1 - s)\,\langle\psi_0|\,R_{sH_z}(\gamma)\,|\psi_0\rangle &= 1 + \frac{(1 - s)d_0}{N\beta} - \frac{1 - s}{N}\sum_{k=1}^{M-1}\frac{d_k}{s(E_k - E_0) - \beta} \\ &= 1 + \frac{(1 - s)d_0}{N\beta} - \frac{1 - s}{s}\sum_{k=1}^{M-1}\frac{d_k}{N(E_k - E_0)}\sum_{\ell=0}^{\infty}\left(\frac{\beta}{s(E_k - E_0)}\right)^{\ell}. \end{aligned} \tag{6.2.10}$$

Using $\beta/(s(E_k - E_0)) \leq 1/2$ to bound the geometric series by $1 + 2\beta/(s(E_k - E_0))$ gives

$$1 + (1 - s)\,\langle\psi_0|\,R_{sH_z}(\gamma)\,|\psi_0\rangle \geq 1 + \frac{(1 - s)d_0}{N\beta} - (1 - s)\left(\frac{A_1}{s} + \frac{2A_2\beta}{s^2}\right). \tag{6.2.11}$$

Collecting terms. Substituting the bounds (6.2.9) and (6.2.11) into (6.2.7) and factoring gives

$$\|R_{H(s)}(\gamma)\| \le \frac{1}{\beta}\,(1+f(s))\,, \tag{6.2.12}$$

and

$$f(s) = \frac{\frac{d_0}{N}\,s^2(1-s) + 4A_2\beta^2(1-s)}{\frac{d_0}{N}\,s^2(1-s) + \beta\,s\,\dfrac{s-s^*}{1-s^*} - 2A_2\beta^2(1-s)}. \tag{6.2.13}$$

To obtain this form, multiply numerator and denominator of the second term in (6.2.7) by β, then multiply by $s^2(1-s)$ to clear fractions. The key step is rewriting the denominator's constant-plus-linear terms using $A_1 = s^*/(1-s^*)$:

$$1 - \frac{(1-s)A_1}{s} + \frac{(1-s)d_0}{N\beta} = \frac{s-s^*}{s(1-s^*)} + \frac{(1-s)d_0}{N\beta}, \tag{6.2.14}$$

since $1 - A_1(1-s)/s = (s - A_1(1-s))/s = (s - s^*(1-s)/(1-s^*))/s = (s(1-s^*) - s^*(1-s))/(s(1-s^*)) = (s-s^*)/(s(1-s^*))$. Multiplying through by $\beta s^2(1-s)$ and collecting the Taylor-bounded terms into the $A_2\beta^2$ contributions gives Eq. (6.2.13). The fraction d_0/N measures the density of ground states in the computational basis.

The numerator of $f(s)$ measures how strongly the rank-one perturbation can amplify the resolvent norm. The d_0/N term comes from the $|0\rangle$ component of $|\psi_0\rangle$, and the A_2 term comes from the excited components. The denominator records the opposing effect. As γ moves away from the crossing, the factor $\beta\,s(s-s^*)/(1-s^*)$ increases and pushes the resolvent back down. This is why $f(s^*)$ is only $O(1)$ near the crossing and why $f(s) \to 0$ as s approaches 1.

From (6.2.12) and (6.2.3), the spectral gap satisfies

$$g(s) \ge \frac{2\beta(s)}{1+f(s)} \ge \frac{2\beta(s)}{1+\max_{s\ge s^*} f(s)}. \tag{6.2.15}$$

If f is monotonically decreasing on $[s^*, 1]$, then $\max_{s\ge s^*} f(s) = f(s^*)$, and the bound becomes $g(s) \ge 2\beta(s)/(1+f(s^*))$, which is linear in $s - s_0$.

Monotonicity of f. We show $f'(s) < 0$ for $s \in [s^*, 1]$. Write $f = u/v$, so the sign of f' is the sign of $u'v - uv'$. The derivative algebra is long, so it helps to name the structure before expanding. After cancellation, three terms remain. Two are negative. One is positive and proportional to $(d_0/N)\,s_0$, which appears because the line origin is shifted below s^*. The real work is to show that the negative terms dominate this positive contribution on all of $[s^*, 1]$. Write $f = u/v$ with

$$\begin{aligned} u &= \frac{d_0}{N}\,s^2(1-s) + 4A_2\beta^2(1-s), \\ v &= \frac{d_0}{N}\,s^2(1-s) + \beta\,s\,\frac{s-s^*}{1-s^*} - 2A_2\beta^2(1-s). \end{aligned} \tag{6.2.16}$$

Then $f' = (u'v - uv')/v^2$, so the sign of f' is determined by $u'v - uv'$.

Computing u' and v' using $\beta' = a/(1-s_0)$:

$$\begin{aligned} u' &= \frac{4aA_2\beta}{1-s_0}(2+s_0-3s) + \frac{d_0}{N}\,s(2-3s), \\ v' &= \frac{a(3s^2 - 2s(s^*+s_0) + s^*s_0)}{(1-s_0)(1-s^*)} - \frac{2aA_2\beta}{1-s_0}(2+s_0-3s) + \frac{d_0}{N}\,s(2-3s). \end{aligned} \tag{6.2.17}$$

Expanding $u'v$ and uv' and taking the difference produces exact cancellation of two terms. The canceled terms are $(d_0/N)^2 s^3(2-3s)(1-s)$ and $8aA_2^2\beta^3(1-s)(2+s_0-3s)/(1-s_0)$. The remainder has three terms [10]:

$$\begin{aligned} u'v - uv' = &-\frac{4aA_2\beta^2}{(1-s_0)(1-s^*)}\Big(s^2(1+s_0-s^*) - 2s\,s_0 + s^*s_0\Big) \\ &+ \frac{12aA_2\frac{d_0}{N}\beta}{1-s_0}\,s(1-s)^2\,s_0 \\ &- \frac{\frac{d_0}{N}\,s^2 a}{(1-s_0)(1-s^*)}\Big(-s^2(s^*+s_0-1) + 2s\,s_0s^* - s^*s_0\Big). \end{aligned} \tag{6.2.18}$$

The first and third terms are negative, while the middle term is positive. That middle term is the only one that contains $(d_0/N)\,s_0$, so it is exactly the cost of shifting the line origin below s^*. We now show that the first negative term controls it.

Factor out $-4aA_2\beta/(1-s_0)$ from the sum of the first two terms:

$$-\frac{4aA_2\beta}{1-s_0}\left(\frac{\beta}{1-s^*}\Big(s^2(1+s_0-s^*)-2s\,s_0+s^*s_0\Big)-\frac{3d_0}{N}\,s_0\,s(1-s)^2\right). \tag{6.2.19}$$

The quadratic $s^2(1+s_0-s^*)-2s\,s_0+s^*s_0$ is convex in s because $1+s_0-s^*>0$, and here $s_0<s^*$. Its minimizer lies at $s_m<s^*$, so throughout $[s^*,1]$ it stays above its value at s^*. At $s=s^*$ that value is $s^*(1-s^*)(s^*-s_0)>0$. The cubic $s(1-s)^2$ reaches its maximum at $s=1/3\le s^*$, so on $[s^*,1]$ it also stays below its value at s^*. Therefore the bracket in (6.2.19) is bounded below by its value at $s=s^*$:

$$\frac{a(s^*-s_0)^2}{1-s_0}-\frac{3d_0}{N}\,s_0(1-s^*)^2. \tag{6.2.20}$$

Using $s_0\le s^*$ and $s^*-s_0=k\,g_{\min}(1-s^*)/(a-k\,g_{\min})$, this is positive whenever

$$a<\frac{4}{3}k^2\frac{A_1}{A_2}. \tag{6.2.21}$$

Since $\Delta A_2\le A_1$ and $A_2\le\sum_{k\ge1}d_k/(N(E_k-E_0)^2)\le A_1/\Delta$, the choice $a=(4/3)k^2\Delta$ satisfies (6.2.21). With this choice, $u'v-uv'<0$ on $[s^*,1]$, so f is monotonically decreasing.

Evaluating $f(s^*)$. At $s=s^*$, $\beta(s^*)=k\,g_{\min}$. The term $\beta\,s(s-s^*)/(1-s^*)$ vanishes, so

$$f(s^*)=\frac{\frac{d_0}{N}\,s^{*2}(1-s^*)+4A_2k^2g_{\min}^2(1-s^*)}{\frac{d_0}{N}\,s^{*2}(1-s^*)-2A_2k^2g_{\min}^2(1-s^*)}. \tag{6.2.22}$$

Replacing $g_{\min}$ by its leading-order expression $\hat g=2s^*\sqrt{d_0/(NA_2)}$ from Eq. (5.4.9) (valid up to a $(1\pm O(\eta))$ factor that does not affect the final constant), we have $A_2k^2\hat g^2=4k^2s^{*2}d_0/N$. Substituting gives

$$f(s^*)=\frac{1+16k^2}{1-8k^2}. \tag{6.2.23}$$

For $k=1/4$, $f(s^*)=(1+1)/(1-1/2)=4$, so $1+f(s^*)=5$.

Final bound. From (6.2.15),

$$g(s)\ge\frac{2\beta(s)}{1+f(s^*)}=\frac{2a}{1+f(s^*)}\cdot\frac{s-s_0}{1-s_0}. \tag{6.2.24}$$

The prefactor evaluates to

$$\frac{2a}{1+f(s^*)}=\frac{2\cdot(4/3)k^2\Delta}{1+(1+16k^2)/(1-8k^2)}=\frac{4}{3}k^2\cdot\frac{1-8k^2}{1+4k^2}\cdot\Delta. \tag{6.2.25}$$

The function $P(k)=(4/3)k^2(1-8k^2)/(1+4k^2)$ is maximized at $k_{\rm opt}=\frac12\sqrt{\sqrt{3/2}-1}\approx0.237$, where $P(k_{\rm opt})=\frac13(5-2\sqrt6)\approx0.034$. For $k=1/4$:

$$P(1/4)=\frac{4}{3}\cdot\frac{1}{16}\cdot\frac{1/2}{5/4}=\frac{1}{30}. \tag{6.2.26}$$

Therefore $g(s)\ge(\Delta/30)(s-s_0)/(1-s_0)$. □

Specializing to $M=2$ and $\Delta=1$, the bound gives $g(s)\ge(1/30)(s-s_0)/(1-s_0)$, where $s_0=1/2-O(1/\sqrt N)$ is close to $s^*\approx1/2$ for large N. Near $s=3/4$, the exact gap from Eq. (5.3.15) is $g(3/4)=\sqrt{1/4+3/(4N)}\approx1/2$, while the bound gives approximately $(1/30)(1/4)/(1/2)=1/60$. The bound is conservative by a factor of approximately 30 but correctly captures the linear growth. This constant is the price of a clean, uniform bound valid for all problem Hamiltonians satisfying the spectral condition.

6.3 The Complete Gap Profile

Combining the results of this chapter with those of Chapter 5, the spectral gap $g(s)$ is bounded below across all of $[0, 1]$.

Theorem 6.3.1 (Complete gap profile)**.** *Let H_z satisfy the spectral condition (Definition 5.2.2) and assume $A_1 \geq 1/2$ (equivalently $s^* \geq 1/3$). The spectral gap of $H(s) = -(1-s)\,|\psi_0\rangle\langle\psi_0| + sH_z$ satisfies, for all $s \in [0, 1]$:*

$$g(s) \geq \begin{cases} \dfrac{A_1(A_1+1)}{A_2}\,(s^* - s)\,, & s \in \mathcal{I}_{s\leftarrow} = [0,\, s^* - \delta_s)\,, \\ g_{\min}, & s \in \mathcal{I}_{s^*} = [s^* - \delta_s,\, s^* + \delta_s]\,, \\ \dfrac{\Delta}{30} \cdot \dfrac{s - s_0}{1 - s_0}, & s \in \mathcal{I}_{s\rightarrow} = (s^* + \delta_s,\, 1]\,, \end{cases} \tag{6.3.1}$$

where $s_0 = s^* - k\,g_{\min}(1 - s^*)/(a - k\,g_{\min})$ with $k = 1/4$ and $a = \Delta/12$.

Proof. The three cases follow from Lemma 5.4.2 (window, proved in Chapter 5), Lemma 6.1.1 (left), and Lemma 6.2.1 (right). The right bound holds for all $s \geq s^*$ and therefore covers $\mathcal{I}_{s\rightarrow}$. The window bound $g(s) \geq g_{\min}$ is tighter than the right bound at s^* but weaker far from the crossing. □

The bounds match across region boundaries. At the left boundary $s = s^* - \delta_s$,

$$\frac{A_1(A_1+1)}{A_2} \cdot \delta_s = \hat{g} = \Theta(g_{\min}), \tag{6.3.2}$$

so the left bound at the window boundary is $\Theta(g_{\min})$, consistent with the window bound. At $s = s^*$, the right bound gives $g(s^*) \geq 2\beta(s^*)/(1 + f(s^*)) = 2k\,g_{\min}/5 = g_{\min}/10$, which is below $g_{\min}$ by a constant factor but still $O(g_{\min})$. The window bound provides the tighter estimate $g(s^*) = g_{\min}$.

The piecewise bounds are intentionally asymmetric. The left arm is steep, and the right arm is shallower. The variational method tracks the left slope closely. The resolvent method gives a weaker slope but remains valid through the spectral congestion on the right. Geometrically, the profile is a broad V centered at s^* with a narrow rounded minimum of width about $2\delta_s$. The left slope is $A_1(A_1+1)/A_2$, which is $O(\mathrm{poly}(n))$ for Ising instances. The right slope is $\Delta/(30(1 - s_0))$, set by the problem gap Δ. At the endpoints, $g(0) = 1$ for H_0 and $g(1) = \Delta$ for H_z.

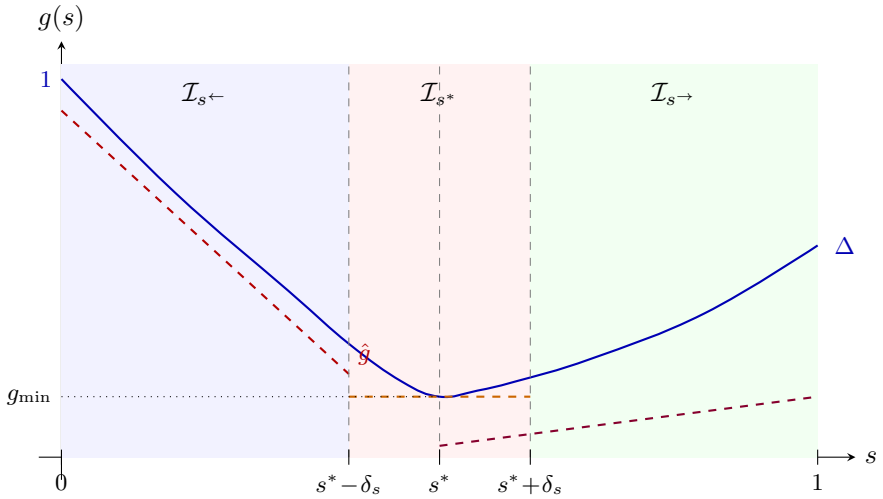

Figure 6.1: Schematic gap profile for $H(s)$. The solid curve shows the true spectral gap $g(s)$, which equals 1 at $s = 0$, dips to $g_{\min}$ at $s = s^*$, and recovers to Δ at $s = 1$. The left arm is steep (slope $A_1(A_1+1)/A_2$); the right arm is shallower (slope controlled by Δ). Dashed lines show the piecewise lower bounds from Theorem 6.3.1: linear on the left, constant $g_{\min}$ in the window, and linear on the right (reaching $\Delta/30$ at $s = 1$). The right bound is below $g_{\min}$ at s^* but remains $O(g_{\min})$.

Four parameters control the gap: A_1, A_2, d_0, and Δ. For any problem Hamiltonian H_z satisfying the spectral condition, Theorem 6.3.1 bounds $g(s)$ over all of $[0, 1]$ up to constants. The minimum is $g_{\min} = \Theta(\sqrt{d_0/(NA_2)})$

at $s^* = A_1/(A_1+1)$, and it is exponentially small in n when $d_0 = O(1)$. The crossing location depends only on A_1. More solutions (larger d_0) widen the gap, while richer near-ground spectral structure (larger A_2) narrows it. At $s = 1$, the gap returns to Δ, the spectral gap of H_z itself.

For unstructured search, the exact gap $g(s) = \sqrt{(2s-1)^2 + 4s(1-s)/N}$ and the piecewise bound from Theorem 6.3.1 can be compared directly. The left bound has slope $(2N-1)/N \approx 2$, matching the asymptotic slope of the exact gap, which approaches $2(1-1/N) \approx 2$ away from s^*. The window bound $g_{\min} = 1/\sqrt{N}$ is exact. The right bound has slope approximately $1/15$ near s^*, weaker than the true slope by a factor of 30, but sufficient for the runtime integral since the window dominates.

The window dominates the runtime integral. $\int_0^1 g(s)^{-2}\,ds$ splits across the three regions. In the left and right regions, $g(s) \sim C|s - s^*|$ for constants C, and

$$\int_{\delta_s}^{s^*} \frac{du}{(Cu)^2} = \frac{1}{C^2}\left(\frac{1}{\delta_s} - \frac{1}{s^*}\right) \leq \frac{1}{C^2\delta_s}, \tag{6.3.3}$$

which is $O(1/(C^2\delta_s))$. In the window, $g(s) \geq g_{\min}$ gives $\int_{s^*-\delta_s}^{s^*+\delta_s} g(s)^{-2}\,ds \leq 2\delta_s/g_{\min}^2$. The window contribution $\delta_s/g_{\min}^2 = \Theta(A_2^{3/2}/(A_1(A_1+1)) \cdot \sqrt{N/d_0})$ dominates the outer regions. Once the Δ-dependent right-arm term is included, the full integral yields the runtime

$$T = O\left(\frac{\sqrt{A_2}}{A_1(A_1+1)\Delta^2}\sqrt{\frac{N}{d_0}}\right),$$

which Chapter 7 derives rigorously.

Chapter 7

Optimal Schedule

The spectral gap of $H(s)$ is now bounded from below on all of $[0,1]$. Theorem 6.3.1 shows a piecewise form. The gap reaches $g_{\min}$ at s^*, then reopens with slope $A_1(A_1+1)/A_2$ on the left and $\Delta/30$ on the right. Chapter 5 already identified the key runtime integral, $\int_0^1 g(s)^{-2}\,ds$ (Eq. (5.5.6)), and showed that the crossing window dominates. The remaining issue is the adiabatic theorem itself. Its error bound determines which power of g controls runtime.

With a constant-rate theorem, runtime is controlled by $\int_0^1 g(s)^{-3}\,ds$. For the profile of Theorem 6.3.1, the crossing window contributes $\delta_s/g_{\min}^3$. In the two-level case $M=2$ with $g_{\min}=1/\sqrt{N}$, this gives $T=O(N)$ and no speedup over classical search. An adaptive schedule with $K'(s)$ scaled to the gap replaces $\int g^{-3}\,ds$ with $\int g^{-p}\,ds$ for $p\in(1,2)$. The resulting runtime

$$T = O\left(\frac{\sqrt{A_2}}{A_1(A_1+1)\Delta^2}\sqrt{\frac{N}{d_0}}\frac{1}{\varepsilon}\right)$$

matches Grover scaling up to explicit spectral prefactors.

7.1 How Theorem Choice Sets Runtime

The gap profile alone does not determine runtime. Translating spectral data into evolution time requires an adiabatic theorem, and different theorems permit different schedules. That choice changes the gap dependence and, in the running example, is exactly the difference between $O(N)$ and $O(\sqrt{N})$.

The earliest rigorous bounds, due to Jansen, Ruskai, and Seiler [17], apply to a constant schedule $K'(s)=T$ and give a transition probability of order $O(1/T^2)$. Their Theorem 3 states that for a state $\psi\in P(0)$, the probability of leaving the ground space satisfies

$$(\psi,[1-P(s)]U_\tau(s)\psi)\le A(s)^2, \tag{7.1.1}$$

where $A(s)\le (1/T)(\|H'\|/g^2)|_{\text{bdry}}+(1/T)\int_0^s(7\sqrt{m}\,\|H'\|^2/g^3+\|H'\|/g^2)\,ds'$, with m the multiplicity of the ground eigenvalue and the boundary term evaluated at $s=0$ and s. Setting $A(s)=\varepsilon$ and solving for T gives

$$T = O\left(\frac{1}{\varepsilon}\int_0^1 \frac{\|H'\|^2}{g(s)^3}\,ds\right). \tag{7.1.2}$$

With $M=2$ and $\|H'\|=O(1)$, the integral $\int_0^1 g^{-3}\,ds$ is dominated by the $O(1/\sqrt{N})$-wide window where $g\approx 1/\sqrt{N}$. Its contribution is $(1/\sqrt{N})\cdot N^{3/2}=N$. Therefore the JRS bound gives $T=O(N/\varepsilon)$, which matches classical search. A constant schedule allocates the same physical time per unit of s whether the gap is $O(1)$ or $O(1/\sqrt{N})$. That uniform allocation forces the g^{-3} dependence, so the narrow crossing window dominates and the quantum speedup disappears.

The resolution is to let the schedule depend on the gap. Roland and Cerf [65] introduced a *local* adiabatic condition. Instead of enforcing adiabaticity with one global timescale T, they enforce it infinitesimally on each segment $[s,s+ds]$. The standard criterion gives

$$\left|\frac{ds}{dt}\right| \le \frac{\varepsilon\, g(s)^2}{|\langle e_1(s)|H'(s)|e_0(s)\rangle|},$$

where e_0, e_1 are the ground and first excited states. Inverting this inequality yields

$$K'(s) = \frac{dt}{ds} \geq \frac{|\langle e_1|H'|e_0\rangle|}{\varepsilon\, g(s)^2}.$$

For the running example, $|\langle e_1|H'|e_0\rangle| = O(1)$ because $H'(s) = |\psi_0\rangle\langle\psi_0| + H_z$ is constant. Thus $K'(s) \propto 1/g(s)^2$, and the runtime becomes

$$T = \frac{C}{\varepsilon}\int_0^1 g(s)^{-2}\, ds. \tag{7.1.3}$$

The integral can be evaluated explicitly. Writing $g(s)^2 = (2s-1)^2 + 4s(1-s)/N$ and substituting $u = 2s-1$:

$$\int_0^1 g(s)^{-2}\, ds = \frac{1}{2}\int_{-1}^1 \frac{du}{u^2 + (1-u^2)/N} = \frac{1}{2}\int_{-1}^1 \frac{N\, du}{1 + (N-1)u^2}. \tag{7.1.4}$$

For large N, the substitution $v = \sqrt{N-1}\, u$ gives $\frac{N}{2\sqrt{N-1}}\int_{-\sqrt{N-1}}^{\sqrt{N-1}} \frac{dv}{1+v^2} = \frac{N}{2\sqrt{N-1}} \cdot 2\arctan\big(\sqrt{N-1}\big) = O(\sqrt{N})$, since $\arctan\big(\sqrt{N-1}\big) \to \pi/2$. Therefore $T = O(\sqrt{N}/\varepsilon)$, recovering the Grover speedup from a smooth, continuous-time evolution.

The Roland-Cerf construction requires exact knowledge of $g(s)$ at every point. For the running example with $M = 2$, this is feasible because the gap has the closed form in Eq. (5.3.15). For a general M-level problem Hamiltonian, the exact gap is unknown and only the piecewise bounds of Theorem 6.3.1 are available. If one substitutes a lower bound $g_0(s) \leq g(s)$, the schedule slows down conservatively because $1/g_0^2 \geq 1/g^2$, so the runtime increases only by constants. The difficulty shifts to error control: derivative terms in the adiabatic bound become sensitive to corners in g_0. The adaptive schedule of section 7.3 addresses this through the exponent $p \in (1, 2)$.

Several later results sharpened this picture. Boixo, Knill, and Somma [74] introduced eigenpath traversal, which replaces continuous evolution with projections onto ground states of intermediate Hamiltonians $H(s_0), H(s_1), \ldots, H(s_L)$. Their key ingredient is phase randomization between steps. It suppresses coherent accumulation of diabatic error, which otherwise recreates the usual $O(1/g_{\min}^2)$ behavior. Under that phase randomization, coherent errors from successive transitions no longer add constructively. Under the condition $\int g^{-p}\, ds = O(g_{\min}^{1-p})$, this gives $O(1/g_{\min})$ scaling. Cunningham and Roland [75] tightened constants and gave a continuous-time version that underlies section 7.2. Elgart and Hagedorn [18] followed a different route using Gevrey-smooth switching, obtaining superpolynomial suppression with runtime $T \geq K\, g^{-2}|\ln g|^{6\alpha}$. The schedule used here has a different practical advantage: it only needs a certified lower bound $g_0(s) \leq g(s)$, not the exact gap.

7.2 The Adiabatic Error Bound

The Schrödinger equation $i\, d|\psi\rangle/dt = H(s(t))|\psi\rangle$ governs the evolution under the time-dependent Hamiltonian $H(s)$, with $s : [0, T] \to [0, 1]$ parameterizing the interpolation. The density-matrix form $d\rho/dt = -i[H, \rho]$ is more convenient for the error analysis and also covers mixed states. We reparameterize time by $t = K(s)$, where $K : [0, 1] \to \mathbb{R}^+$ is differentiable and monotone increasing. The chain rule then gives

$$\frac{d\rho}{ds} = -iK'(s)[H(s), \rho(s)], \tag{7.2.1}$$

where $K'(s) = dK/ds > 0$ controls the instantaneous evolution rate. The total runtime is $T = K(1) = \int_0^1 K'(s)\, ds$. A large $K'(s)$ means slow evolution (long physical time per unit of s), allowing the state to track the ground state through a small-gap region. A small $K'(s)$ means fast evolution, appropriate where the gap is large and diabatic transitions are suppressed.

The error of the adiabatic evolution is the probability that the final state does not lie in the ground space of $H(1)$:

$$\varepsilon = 1 - \mathrm{Tr}[P(1)\rho(1)], \tag{7.2.2}$$

where $P(s)$ denotes the projector onto the ground eigenspace of $H(s)$ and $\rho(0) = P(0)$ (the system starts in the ground state of $H(0)$). The projector $P(s)$ and the ground energy $\lambda_0(s)$ are both functions of s, varying as the Hamiltonian interpolates from H_0 to H_z. The operator

$$(H(s) - \lambda_0(s))^+ = \sum_{j\geq 1} \frac{1}{\lambda_j(s) - \lambda_0(s)}\, |\phi_j(s)\rangle\langle\phi_j(s)| \tag{7.2.3}$$

is the pseudoinverse of $H(s) - \lambda_0(s)$: it acts as zero on the ground space and as $(\lambda_j - \lambda_0)^{-1}$ on the j-th excited eigenspace. Its operator norm is $1/g(s)$, so a small spectral gap amplifies the pseudoinverse.

Lemma 7.2.1 (Adiabatic error bound [10, 75])**.** *Let $H(s)$ be a twice-differentiable path of Hamiltonians with a continuous ground energy $\lambda_0(s)$ and a spectral gap $g(s) > 0$ for all $s \in [0,1]$. Let $K : [0,1] \to \mathbb{R}^+$ be a schedule with absolutely continuous derivative K'. Then the evolution (7.2.1) starting from $\rho(0) = P(0)$ satisfies*

$$\varepsilon \le \frac{1}{K'(1)} \left\| \left[P'(1),\, (H(1) - \lambda_0(1))^+\right] \right\| + \int_0^1 \frac{1}{K'} \left\| \left[P',\, (H - \lambda_0)^+\right]' \right\| ds + \int_0^1 \left| \left(\frac{1}{K'}\right)' \right| \left\| \left[P',\, (H - \lambda_0)^+\right] \right\| ds. \tag{7.2.4}$$

Proof. Since $\rho(0) = P(0)$, the error is $\varepsilon = \operatorname{Tr}[P(0)\rho(0)] - \operatorname{Tr}[P(1)\rho(1)] = |\operatorname{Tr}[P\rho]|_0^1$, so it suffices to track $\operatorname{Tr}[P(s)\rho(s)]$. Differentiating:

$$\frac{d}{ds}\operatorname{Tr}[P\rho] = \operatorname{Tr}[P'\rho] + \operatorname{Tr}[P\rho']. \tag{7.2.5}$$

The second term vanishes. Substituting the evolution equation (7.2.1): $\operatorname{Tr}[P\rho'] = -iK' \operatorname{Tr}[P[H,\rho]]$. Since $HP = \lambda_0 P$, the cyclic property gives $\operatorname{Tr}[P[H,\rho]] = \operatorname{Tr}[PH\rho - P\rho H] = \lambda_0 \operatorname{Tr}[P\rho] - \operatorname{Tr}[HP\rho] = 0$.

For $\operatorname{Tr}[P'\rho]$, write $Q = I - P$ and use the decomposition $P' = PP'Q + QP'P$, which holds because $PP'P = 0$ and $QP'Q = 0$.[i] Inserting $Q = (H - \lambda_0)^+(H - \lambda_0)$ and using the identities $(H - \lambda_0)\rho P = [H,\rho]P$ and $P\rho(H - \lambda_0) = -P[H,\rho]$ (both consequences of $HP = \lambda_0 P$), a cyclic rearrangement under the trace gives

$$\operatorname{Tr}[P'\rho] = \operatorname{Tr}\left[PP'(H - \lambda_0)^+[H,\rho]\right] - \operatorname{Tr}\left[(H - \lambda_0)^+ P'P[H,\rho]\right]. \tag{7.2.6}$$

Since $(H - \lambda_0)^+ P = P(H - \lambda_0)^+ = 0$ (the pseudoinverse annihilates the ground space), $PP'(H - \lambda_0)^+$ reduces to $P'(H - \lambda_0)^+$ and $(H - \lambda_0)^+ P'P$ reduces to $(H - \lambda_0)^+ P'$, so the two terms combine into a commutator:

$$\operatorname{Tr}[P'\rho] = \operatorname{Tr}\left[\left[P',\, (H - \lambda_0)^+\right][H,\rho]\right] = i(K')^{-1} \operatorname{Tr}\left[\left[P',\, (H - \lambda_0)^+\right]\rho'\right], \tag{7.2.7}$$

where the last equality substitutes $[H,\rho] = i(K')^{-1}\rho'$ from (7.2.1).

Integrating from 0 to 1 gives $\operatorname{Tr}[P\rho]\big|_0^1 = i\int_0^1 (K')^{-1} \operatorname{Tr}[[P',\, (H - \lambda_0)^+]\,\rho']\, ds$. Integration by parts, with $u = (K')^{-1}[P',\, (H - \lambda_0)^+]$ and $dv = \rho'\, ds$, transfers the derivative from ρ onto u:

$$\begin{aligned} \operatorname{Tr}[P\rho]\big|_0^1 = i(K'(1))^{-1} \operatorname{Tr}\left[\left[P'(1),\, (H(1) - \lambda_0(1))^+\right]\rho(1)\right] \\ - i\int_0^1 \operatorname{Tr}\left[\left((K')^{-1}\left[P',\, (H - \lambda_0)^+\right]' + \left((K')^{-1}\right)'\left[P',\, (H - \lambda_0)^+\right]\right)\rho\right] ds. \end{aligned} \tag{7.2.8}$$

The boundary term at $s = 0$ vanishes. Since $\rho(0) = P(0)$, the commutator trace expands as

$$\operatorname{Tr}\left[\left[P',\, (H - \lambda_0)^+\right] P\right] = \operatorname{Tr}[P'(H - \lambda_0)^+ P] - \operatorname{Tr}[(H - \lambda_0)^+ P'P].$$

For the first summand, $(H - \lambda_0)^+ P = 0$ (the pseudoinverse annihilates the ground-space projector), so $\operatorname{Tr}[P'(H - \lambda_0)^+ P] = 0$. For the second, cyclicity of the trace gives $\operatorname{Tr}[(H - \lambda_0)^+ P'P] = \operatorname{Tr}[P(H - \lambda_0)^+ P'] = 0$ by the same identity. Taking absolute values and bounding $|\operatorname{Tr}[A\rho]| \le \|A\|$ for any density matrix ρ yields (7.2.4). □

The error bound depends on $H(s)$ only through the commutator $[P', (H - \lambda_0)^+]$ and its derivative. The following bounds express these in terms of the Hamiltonian derivatives H', H'' and the spectral gap g, using the Riesz integral representation of the spectral projector introduced by Kato [16].

Lemma 7.2.2 (Projector derivative bounds [10])**.** *Under the conditions of Lemma 7.2.1:*

$$\|P'(s)\| \le \frac{2\|H'(s)\|}{g(s)}, \tag{7.2.9}$$

$$\left\| \left[P'(s),\, (H(s) - \lambda_0(s))^+\right] \right\| \le \frac{4\|H'(s)\|}{g(s)^2}, \tag{7.2.10}$$

$$\left\| \left[P'(s),\, (H(s) - \lambda_0(s))^+\right]' \right\| \le \frac{40\|H'(s)\|^2}{g(s)^3} + \frac{4\|H''(s)\|}{g(s)^2}. \tag{7.2.11}$$

[i] Differentiating $P^2 = P$ gives $P'P + PP' = P'$. Left-multiplying by P: $PP'P + PP' = PP'$, so $PP'P = 0$. Then $QP'Q = P' - PP' - P'P + PP'P = P' - P' = 0$.

Proof of (7.2.9). Let Γ be a circle in the complex plane centered at $\lambda_0(s)$ with radius $g(s)/2$. The Riesz integral representation gives

$$P(s) = \frac{1}{2\pi i} \oint_\Gamma R_{H(s)}(z)\, dz, \tag{7.2.12}$$

where $R_{H(s)}(z) = (zI - H(s))^{-1}$ is the resolvent. Differentiating with respect to s:

$$P'(s) = \frac{1}{2\pi i} \oint_\Gamma R_{H(s)}(z)\, H'(s)\, R_{H(s)}(z)\, dz, \tag{7.2.13}$$

using the resolvent identity $R'_H = R_H H' R_H$. On the contour Γ, every point z lies at distance exactly $g(s)/2$ from $\lambda_0(s)$ and at distance at least $g(s)/2$ from every other eigenvalue (since the nearest eigenvalue is $\lambda_1(s)$ at distance $g(s)$ from $\lambda_0(s)$). Therefore $\|R_{H(s)}(z)\| = 1/\mathrm{dist}(z, \sigma(H(s))) \le 2/g(s)$ on Γ. Bounding the integral:

$$\|P'(s)\| \le \frac{1}{2\pi} \oint_\Gamma \|R_H(z)\| \cdot \|H'(s)\| \cdot \|R_H(z)\|\, |dz| \le \frac{1}{2\pi} \left(\frac{2}{g}\right)^2 \|H'\| \cdot \pi g = \frac{2\|H'\|}{g}. \tag{7.2.14}$$

□

Bound (7.2.10) follows from (7.2.9): $\|[A, B]\| \le 2\|A\| \cdot \|B\|$ gives $\|[P', (H - \lambda_0)^+]\| \le 2 \cdot 2\|H'\|/g \cdot 1/g = 4\|H'\|/g^2$.

Bound (7.2.11) requires two intermediate results. Write $\widetilde{H} = H - \lambda_0$ for the shifted Hamiltonian. Its pseudoinverse satisfies

$$(\widetilde{H}^+)' = -\widetilde{H}^+ \widetilde{H}' \widetilde{H}^+ + P' \widetilde{H}^+ + \widetilde{H}^+ P', \tag{7.2.15}$$

where $\widetilde{H}' = H' - \lambda_0'$. To see this, split the difference quotient $(\widetilde{H}^+(s+h) - \widetilde{H}^+(s))/h$ using $Q = \widetilde{H}^+ \widetilde{H}$ and $P = I - Q$. The Q-part gives $\lim_{h\to 0} \widetilde{H}^+(s)(\widetilde{H}(s) - \widetilde{H}(s+h))\widetilde{H}^+(s+h)/h = -\widetilde{H}^+ \widetilde{H}' \widetilde{H}^+$, while the P-part, after adding and subtracting $P(s+h)\widetilde{H}^+(s+h)$ and $\widetilde{H}^+(s)P(s)$, yields $P'\widetilde{H}^+ + \widetilde{H}^+ P'$. Bounding the norm and using $|\lambda_0'| = |\langle \phi_0 | H' | \phi_0 \rangle| \le \|H'\|$ (Hellmann-Feynman):

$$\|(\widetilde{H}^+)'\| \le \frac{\|H'\| + |\lambda_0'|}{g^2} + \frac{4\|H'\|}{g^2} \le \frac{6\|H'\|}{g^2}. \tag{7.2.16}$$

The second intermediate result bounds P''. Differentiating $P' = (2\pi i)^{-1} \oint_\Gamma R_H H' R_H\, dz$ gives

$$P'' = \frac{1}{2\pi i} \oint_\Gamma (2R_H H' R_H H' R_H + R_H H'' R_H)\, dz, \tag{7.2.17}$$

where the two $R_H H' R_H H' R_H$ terms arise from differentiating each resolvent factor. Bounding by $\|R_H(z)\| \le 2/g$ on Γ and integrating over the contour of length πg:

$$\|P''\| \le \frac{1}{2\pi} \left(\frac{2}{g}\right)^3 2\|H'\|^2 \cdot \pi g + \frac{1}{2\pi} \left(\frac{2}{g}\right)^2 \|H''\| \cdot \pi g = \frac{8\|H'\|^2}{g^2} + \frac{2\|H''\|}{g}. \tag{7.2.18}$$

Now expand $[P', (H - \lambda_0)^+]' = [P'', (H - \lambda_0)^+] + [P', ((H - \lambda_0)^+)']$ and bound each commutator:

$$\|[P'', (H - \lambda_0)^+]\| \le \frac{2\|P''\|}{g} \le \frac{16\|H'\|^2}{g^3} + \frac{4\|H''\|}{g^2}, \tag{7.2.19}$$

and, using (7.2.9) and (7.2.16):

$$\|[P', ((H - \lambda_0)^+)']\| \le 2\|P'\| \cdot \|(\widetilde{H}^+)'\| \le 2 \cdot \frac{2\|H'\|}{g} \cdot \frac{6\|H'\|}{g^2} = \frac{24\|H'\|^2}{g^3}. \tag{7.2.20}$$

Summing gives $40\|H'\|^2/g^3 + 4\|H''\|/g^2$. A block-matrix decomposition of the commutator with respect to P and $Q = I - P$, tracking cross terms exactly rather than using submultiplicativity, replaces the coefficient 40 by ≈ 4.77 [10]; the asymptotic scaling is unchanged.

The simplest schedule is constant. It sets $K'(s) = T$, so evolution proceeds at a uniform rate regardless of the gap. Substituting the derivative bounds into the error bound (7.2.4) with $(1/K')' = 0$ gives the constant-rate result.

Theorem 7.2.3 (Constant-rate runtime)**.** *Under the conditions of Lemma 7.2.1, a constant schedule $K'(s) = T$ achieves error at most ε provided*

$$T \geq \frac{1}{\varepsilon}\left(\frac{4\|H'(1)\|}{g(1)^2} + \int_0^1 \frac{40\|H'(s)\|^2}{g(s)^3}\,ds + \int_0^1 \frac{4\|H''(s)\|}{g(s)^2}\,ds\right). \tag{7.2.21}$$

Proof. With constant K', the third term in (7.2.4) vanishes. Substituting bounds (7.2.10) and (7.2.11) into the remaining two terms:

$$\varepsilon \leq \frac{1}{T}\left(\frac{4\|H'(1)\|}{g(1)^2} + \int_0^1 \frac{40\|H'(s)\|^2}{g(s)^3}\,ds + \int_0^1 \frac{4\|H''(s)\|}{g(s)^2}\,ds\right). \tag{7.2.22}$$

Setting the right side equal to ε and solving for T gives (7.2.21). □

Since $H'' = 0$ for the linear interpolation $H(s) = -(1-s)\,|\psi_0\rangle\langle\psi_0| + sH_z$, and $H'(s) = |\psi_0\rangle\langle\psi_0| + H_z$ is constant with $\|H'\| = O(1)$, the dominant term in (7.2.21) is $\int_0^1 g(s)^{-3}\,ds$. From the gap profile of Theorem 6.3.1, the crossing window contributes

$$\int_{s^*-\delta_s}^{s^*} g(s)^{-3}\,ds \leq \frac{\delta_s}{g_{\min}^3} = \frac{A_2}{A_1(A_1+1)} \cdot g_{\min}^{-2}, \tag{7.2.23}$$

using $\delta_s = A_2 g_{\min}/(A_1(A_1+1))$ from Eq. (5.4.10). This gives $T_{\text{constant}} = O(\delta_s/(\varepsilon\, g_{\min}^3))$.

Specializing to $M = 2$ with $g_{\min} = 1/\sqrt{N}$, the exact gap $g(s) = \sqrt{(2s-1)^2 + 4s(1-s)/N}$ from Eq. (5.3.15) gives $\int_0^1 g(s)^{-3}\,ds = O(N)$. The dominant contribution comes from the $O(1/\sqrt{N})$ window where $g \approx 1/\sqrt{N}$. Hence $T_{\text{constant}} = O(N/\varepsilon)$, matching classical search. A constant-rate schedule therefore gives no quantum speedup. It wastes time where the gap is large and still moves too quickly near s^*.

7.3 The Adaptive Schedule

The constant schedule fails because it treats every value of s the same. The error bound (7.2.4) suggests the opposite strategy. Choose large $K'(s)$ where the gap is small and small $K'(s)$ where the gap is large. Since $K'(s) = dt/ds$, this means spending physical time where diabatic transitions are dangerous. The natural ansatz is $K'(s) \propto 1/g(s)^p$ for some $p \geq 1$. Then runtime scales as $T \propto \int_0^1 g(s)^{-p}\,ds$, while the error terms involve integrals of the form $\int g^{q-3}\,ds$.

The exponent p controls the runtime-error tradeoff. The family $K'(s) \propto 1/g_0(s)^p$ extends Roland-Cerf ($p = 2$) to a continuum of schedules. At $p = 1$, $\int g_0^{-1}\,ds$ is mild but the companion error integral $\int g_0^{-2}\,ds$ diverges for piecewise linear profiles. At $p = 2$, the scaling is favorable, but the schedule-variation term requires exact gap information. The useful regime is therefore $p \in (1, 2)$. There, $\int g_0^{-p}\,ds = O(g_{\min}^{1-p})$ and $\int g_0^{p-3}\,ds = O(g_{\min}^{p-2})$, whose product is always $O(g_{\min}^{-1})$. This is exactly the range where a certified lower bound $g_0 \leq g$ suffices.

The adaptive rate theorem, extending the eigenpath traversal framework of [75] to the continuous-time setting, formalizes this trade-off.

Theorem 7.3.1 (Adaptive rate [10])**.** *Let $H(s)$ satisfy the conditions of Lemma 7.2.1, and let $g_0 : [0,1] \to \mathbb{R}^+$ be an absolutely continuous function satisfying $g_0(s) \leq g(s)$ for all s. Suppose there exist $1 < p < 2$ (the endpoints are excluded: at $p = 1$ the B_1 integral diverges logarithmically, and at $p = 2$ the schedule variation term requires the exact gap) and constants $B_1, B_2 \geq 1$ such that*

$$\int_0^1 \frac{ds}{g_0(s)^p} \leq B_1\, g_{\min}^{1-p} \qquad \text{and} \qquad \int_0^1 \frac{ds}{g_0(s)^{3-p}} \leq B_2\, g_{\min}^{p-2}. \tag{7.3.1}$$

Assume additionally that $g_0(1) \geq g_{\min}$, that there exists $b \in (0,1]$ with $g_0(s) \geq b\, g_{\min}$ for all $s \in [0,1]$, and that $\sup_{s\in[0,1]} |g_0'(s)| < \infty$. Define

$$c = \sup_{s\in[0,1]} \left(4\|H'(s)\| + 40\|H'(s)\|^2 B_2 + 4\|H''(s)\| + 6p\,|g_0'(s)|\,\|H'(s)\|\,B_2\right). \tag{7.3.2}$$

The last term uses $|g_0'(s)|$ rather than $|g'(s)|$: since the schedule is defined in terms of g_0, the derivative $(K'^{-1})' \propto (g_0^p)'$ involves g_0'. Then the schedule

$$K'(s) = \frac{1}{\varepsilon} \cdot \frac{c}{g_0(s)^p \cdot g_{\min}^{2-p}} \tag{7.3.3}$$

achieves error at most ε, with total runtime

$$T = \int_0^1 K'(s)\,ds \le \frac{c\,B_1}{\varepsilon\,g_{\min}}. \tag{7.3.4}$$

Proof. Let ε_0 denote the actual error. Substituting (7.3.3) into the error bound (7.2.4): $(K')^{-1} = \varepsilon\,g_0^p\,g_{\min}^{2-p}/c$, and $|((K')^{-1})'| = (\varepsilon\,g_{\min}^{2-p}/c)\cdot p\,g_0^{p-1}\,|g_0'|$. The three terms become

$$\varepsilon_0 \le \frac{\varepsilon}{c}\,g_{\min}^{2-p}\Bigg(g_0(1)^p\,\big\|\big[P'(1),(H(1)-\lambda_0(1))^+\big]\big\| + \int_0^1 g_0^p\,\Big\|\big[P',(H-\lambda_0)^+\big]'\Big\|\,ds + \int_0^1 p\,g_0^{p-1}|g_0'|\,\big\|\big[P',(H-\lambda_0)^+\big]\big\|\,ds\Bigg). \tag{7.3.5}$$

Boundary term. Using bound (7.2.10) with $g_0 \le g$:

$$g_{\min}^{2-p}\,g_0(1)^p\cdot\frac{4\|H'(1)\|}{g(1)^2} \le 4\|H'(1)\|\,g_{\min}^{2-p}\,g_0(1)^{p-2} \le 4\|H'\|, \tag{7.3.6}$$

since $g_0(1) \ge g_{\min}$ and $p-2<0$ imply $g_0(1)^{p-2} \le g_{\min}^{p-2}$.

Commutator derivative integral. Using bound (7.2.11) and splitting:

$$g_{\min}^{2-p}\int_0^1 g_0^p\cdot\frac{40\|H'\|^2}{g^3}\,ds \le 40\|H'\|^2\,g_{\min}^{2-p}\int_0^1\frac{ds}{g_0^{3-p}} \le 40\|H'\|^2 B_2, \tag{7.3.7}$$

where $g_0^p/g^3 \le g_0^p/g_0^3 = 1/g_0^{3-p}$ since $g_0 \le g$, and the B_2 condition (7.3.1) absorbs $g_{\min}^{2-p}\cdot g_{\min}^{p-2} = 1$. Similarly, the H'' sub-term contributes

$$g_{\min}^{2-p}\int_0^1 g_0^p\cdot\frac{4\|H''\|}{g^2}\,ds \le 4\|H''\|\,g_{\min}^{2-p}\int_0^1\frac{ds}{g_0^{2-p}} \le 4\|H''\|, \tag{7.3.8}$$

since $g_0 \ge b\,g_{\min}$ and $p-2<0$ imply $g_0^{p-2} \le b^{p-2}g_{\min}^{p-2}$, giving $\int g_0^{p-2}\,ds = O(g_{\min}^{p-2})$ with the constant b^{p-2} absorbed into the O-notation.

Schedule variation integral. Using bound (7.2.10):

$$\begin{aligned} g_{\min}^{2-p}\int_0^1 p\,g_0^{p-1}|g_0'|\cdot\frac{4\|H'\|}{g^2}\,ds &\le 4p\,\|H'\|\,g_{\min}^{2-p}\int_0^1\frac{g_0^{p-1}\,|g_0'|}{g_0^2}\,ds \\ &= 4p\,\|H'\|\,g_{\min}^{2-p}\int_0^1 g_0^{p-3}\,|g_0'|\,ds. \end{aligned} \tag{7.3.9}$$

Using $\sup|g_0'| < \infty$, we have $\int g_0^{p-3}|g_0'|\,ds \le \sup|g_0'|\cdot\int g_0^{p-3}\,ds \le \sup|g_0'|\cdot B_2\,g_{\min}^{p-2}$. The resulting bound is $4p\sup|g_0'|\,\|H'\|\,B_2$. The constant c in (7.3.2) uses the factor $6p$ rather than $4p$; this is a valid overestimate that simplifies the expression without affecting the asymptotic result.

Collecting. Summing all contributions:

$$\varepsilon_0 \le \frac{\varepsilon}{c}\left(4\|H'\| + 40\|H'\|^2 B_2 + 4\|H''\| + 6p\sup|g_0'|\,\|H'\|\,B_2\right) \le \frac{\varepsilon}{c}\cdot c = \varepsilon. \tag{7.3.10}$$

Runtime. The total evolution time is

$$T = \int_0^1 K'\,ds = \frac{c}{\varepsilon}\,g_{\min}^{p-2}\int_0^1\frac{ds}{g_0^p} \le \frac{c}{\varepsilon}\,g_{\min}^{p-2}\cdot B_1\,g_{\min}^{1-p} = \frac{c\,B_1}{\varepsilon\,g_{\min}}. \tag{7.3.11}$$

□

Three terms compose the error. The first is a boundary term that depends on $g_0(1)$ and is $O(1)$. The second is an integral that pairs g_0^p from the schedule with g^{-3} from the derivative bounds, producing $\int g_0^{p-3}\,ds$. The third is a schedule-variation term from the non-constant K'. The parameter p balances the two integrals. B_1 bounds $\int g_0^{-p}\,ds$ (the runtime cost), while B_2 bounds $\int g_0^{p-3}\,ds$ (the error cost). Their product with $g_{\min}^{-1}$ gives the final runtime.

Corollary 7.3.2. *If $\int_0^1 g(s)^{-p}\,ds = O(g_{\min}^{1-p})$ for all $p>1$, and $\|H'\|$, $\|H''\|$, $|\lambda_0'|$, $|g'|$ are all $O(1)$, then $T = O(1/(\varepsilon\,g_{\min}))$.*

The runtime scales inversely with the minimum gap, which is optimal for quantum search [39]. The running example satisfies these conditions.

The integral $\int_0^1 g(s)^{-p}\,ds$ is dominated by the $O(1/\sqrt{N})$-wide window where $g \approx 1/\sqrt{N}$: the window's contribution is $(1/\sqrt{N}) \cdot N^{p/2} = N^{(p-1)/2}$, while outside the window $g = \Omega(|s-1/2|)$ and the integral converges. For any $p > 1$, this gives $O(g_{\min}^{1-p})$.

Lemma 7.3.3 (Grover gap integral)**.** *For the exact gap $g(s) = \sqrt{(2s-1)^2 + 4s(1-s)/N}$ of the running example ($M = 2$, $d_0 = 1$, $d_1 = N-1$),*

$$\int_0^1 g(s)^{-p}\,ds = O\left(N^{(p-1)/2}\right) = O\left(g_{\min}^{1-p}\right) \qquad \text{for all } p > 1. \tag{7.3.12}$$

Proof. The gap is symmetric about $s = 1/2$ and achieves its minimum $g_{\min} = 1/\sqrt{N}$ there. Split the integral at $1/2 - 1/\sqrt{N}$. In the window $[1/2 - 1/\sqrt{N},\, 1/2]$, bound $g \geq g_{\min}$:

$$\int_{1/2-1/\sqrt{N}}^{1/2} g^{-p}\,ds \leq \frac{1}{\sqrt{N}} \cdot N^{p/2} = N^{(p-1)/2}. \tag{7.3.13}$$

Outside the window, $g(s) \geq c|s - 1/2|$ for a constant $c > 0$ (the gap grows linearly away from the minimum). The change of variable $u = g(s)$, with $|ds/du| = O(1)$ since $|g'(s)| \leq 2$, gives

$$\int_0^{1/2-1/\sqrt{N}} g^{-p}\,ds \leq C \int_{1/\sqrt{N}}^{O(1)} u^{-p}\,du = O\left(N^{(p-1)/2}\right). \tag{7.3.14}$$

Combining and using the symmetry about $1/2$ gives the result. □

The other conditions of Corollary 7.3.2 are immediate: $\|H'\| = \||\psi_0\rangle\langle\psi_0| + H_z\| \leq 2$, $H'' = 0$, $|\lambda_0'| \leq \|H'\| \leq 2$ by the Hellmann-Feynman theorem, and $|g'(s)| \leq 2$ (from $|g'| = |4(1 - 1/N)(1/2 - s)/g| \leq 2$, since the numerator is at most $2g$). Therefore $T = O(\sqrt{N}/\varepsilon)$ for the running example with an adaptive schedule, compared to $T = O(N/\varepsilon)$ with a constant schedule. The adaptive schedule recovers the full Grover speedup.

The schedule $K'(s) \propto 1/g(s)^p$ concentrates the evolution time near the crossing: at $s = 1/2$, where $g \approx 1/\sqrt{N}$, the schedule rate is $K' \propto N^{p/2}$, while far from $1/2$, where $g = O(1)$, it is $K' = O(1)$. The algorithm spends $O(\sqrt{N})$ physical time traversing the window and $O(1)$ time traversing the rest of $[0, 1]$.

7.4 Runtime of Adiabatic Quantum Optimization

Applying Theorem 7.3.1 to $H(s) = -(1-s)\,|\psi_0\rangle\langle\psi_0| + sH_z$ with the gap profile of Theorem 6.3.1 requires three concrete steps. We construct a continuous lower bound $g_0(s)$ from the piecewise bounds, compute B_1 and B_2, and then evaluate the constant c.

The bounds from Theorem 6.3.1 are valid on their regions but do not meet continuously at $s^* - \delta_s$ and s^*. The left bound is too high at $s^* - \delta_s$, and the right bound is too low at s^*. Since Theorem 7.3.1 requires g_0 to be absolutely continuous on $[0, 1]$, we shrink the left and window pieces by a constant factor b so the three branches join continuously.

Define

$$g_0(s) = \begin{cases} b\,\dfrac{A_1(A_1+1)}{A_2}\,(s^* - s)\,, & s \in [0,\, s^* - \delta_s), \quad \left(\text{i.e., } b\,\tfrac{A_1}{A_2} \cdot \tfrac{s^*-s}{1-s^*}\right) \\ b\,g_{\min}, & s \in [s^* - \delta_s,\, s^*), \\ \dfrac{\Delta}{30} \cdot \dfrac{s - s_0}{1 - s_0}, & s \in [s^*,\, 1], \end{cases} \tag{7.4.1}$$

where s_0 is given by Eq. (6.2.5) and the shrinking factor is

$$b = k \cdot \frac{2}{1 + f(s^*)} = \frac{1}{4} \cdot \frac{2}{1+4} = \frac{1}{10}, \tag{7.4.2}$$

using $k = 1/4$ and $f(s^*) = 4$ from Eq. (6.2.23).

Each piece of g_0 lies below its corresponding bound from Theorem 6.3.1. The left and window pieces are scaled by $b = 1/10$, while the right piece is unchanged. It remains to check continuity at both junctions. At $s = s^* - \delta_s$, the left branch gives $b \cdot A_1(A_1+1)\delta_s/A_2$. Using $\delta_s = A_2 g_{\min}/(A_1(A_1+1))$ from Eq. (5.4.10), this

equals $b\,g_{\min} = g_{\min}/10$, exactly the window value. At $s = s^*$, the window value is again $b\,g_{\min} = g_{\min}/10$, while the right branch gives $(\Delta/30)(s^* - s_0)/(1 - s_0)$. Using $s^* - s_0 = k\,g_{\min}(1 - s^*)/(a - k\,g_{\min})$ and $1 - s_0 = (1 - s^*)a/(a - k\,g_{\min})$ from Eq. (6.2.5),

$$\frac{\Delta}{30} \cdot \frac{s^* - s_0}{1 - s_0} = \frac{\Delta}{30} \cdot \frac{k\,g_{\min}}{a} = \frac{\Delta}{30} \cdot \frac{g_{\min}/4}{\Delta/12} = \frac{g_{\min}}{10}, \tag{7.4.3}$$

which again matches the window value. The constants b, k, and a are therefore coupled exactly to enforce continuity. In particular, $b = 1/10$ absorbs both the $k = 1/4$ factor from the right-side resolvent bound and the value $f(s^*) = 4$ from the Chapter 6 monotonicity analysis.

The integral $\int_0^1 g_0^{-p}\,ds$ splits across the three regions. In the left region, $g_0(s) = b\,A_1(A_1 + 1)(s^* - s)/A_2$, so

$$\begin{aligned}\int_0^{s^*-\delta_s} g_0^{-p}\,ds &= \left(\frac{A_2}{b\,A_1(A_1+1)}\right)^p \int_{\delta_s}^{s^*} \frac{du}{u^p} = \frac{1}{b^p}\left(\frac{A_2}{A_1(A_1+1)}\right)^p \cdot \frac{1}{(p-1)\,\delta_s^{p-1}} \\ &= \frac{1}{b^p(p-1)} \cdot \frac{A_2}{A_1(A_1+1)} \cdot g_{\min}^{1-p},\end{aligned} \tag{7.4.4}$$

where the last step uses $\delta_s^{p-1} = (A_2 g_{\min}/(A_1(A_1 + 1)))^{p-1}$. In the window, $g_0 = b\,g_{\min}$ is constant:

$$\int_{s^*-\delta_s}^{s^*} g_0^{-p}\,ds = \frac{\delta_s}{b^p\,g_{\min}^p} = \frac{1}{b^p} \cdot \frac{A_2}{A_1(A_1+1)} \cdot g_{\min}^{1-p}. \tag{7.4.5}$$

Combining the left and window contributions with $b^{-p} = 10^p$ gives

$$\frac{1/(p-1) + 1}{b^p} = \frac{p\,10^p}{p-1},$$

so the combined term is $(p/(p-1)) \cdot 10^p \cdot A_2/(A_1(A_1 + 1)) \cdot g_{\min}^{1-p}$.

In the right region, $g_0(s) = (\Delta/30)(s - s_0)/(1 - s_0)$, so

$$\begin{aligned}\int_{s^*}^1 g_0^{-p}\,ds &= \left(\frac{30(1-s_0)}{\Delta}\right)^p \int_{s^*-s_0}^{1-s_0} \frac{du}{u^p} = \left(\frac{30(1-s_0)}{\Delta}\right)^p \cdot \frac{1}{(p-1)(s^*-s_0)^{p-1}} \\ &= \frac{1}{p-1}\left(\frac{30}{\Delta}\right)^p \left(\frac{a}{k}\right)^{p-1} (1-s_0) \cdot g_{\min}^{1-p},\end{aligned} \tag{7.4.6}$$

using $s^* - s_0 = k\,g_{\min}(1 - s^*)/(a - k\,g_{\min})$ and $1 - s_0 = a(1 - s^*)/(a - k\,g_{\min})$. Now set $a = (4/3)k^2\Delta$ and $k = 1/4$, so $a/k = \Delta/3$. This yields $(30/\Delta)^p(\Delta/3)^{p-1} = 30^p/(3\Delta)$, together with $(1 - s_0) \le 1/(1 + A_1)$. Hence the right contribution is $3 \cdot 10^p/((p - 1)\Delta(1 + A_1)) \cdot g_{\min}^{1-p}$.

Since $\Delta A_2 \le A_1$ (equivalently $A_2 \le A_1/\Delta$), the left-plus-window term satisfies $A_2/(A_1(1+A_1)) \le 1/(\Delta(1+A_1))$. Combining all three contributions gives

$$\int_0^1 g_0^{-p}\,ds \le \frac{(p+3) \cdot 10^p}{(p-1)(1+A_1)\Delta} \cdot g_{\min}^{1-p}, \qquad \text{so} \quad B_1 = O\!\left(\frac{1}{\Delta(1+A_1)}\right). \tag{7.4.7}$$

The integral $\int_0^1 g_0^{p-3}\,ds$ has the same three-region decomposition, now with exponent $3-p$. Because $p \in (1, 2)$ implies $3 - p \in (1, 2)$, each region converges by the same change of variables used for B_1. For example, the window contribution is

$$\int_{s^*-\delta_s}^{s^*} (b\,g_{\min})^{p-3}\,ds = \delta_s\,b^{p-3}g_{\min}^{p-3} = b^{p-3}\frac{A_2}{A_1(A_1+1)}g_{\min}^{p-2} = O(g_{\min}^{p-2}),$$

with $b^{p-3} = 10^{3-p}$ absorbed into constants. The left and right pieces have the same order, so

$$B_2 = O\!\left(\frac{1}{\Delta(1+A_1)}\right). \tag{7.4.8}$$

For the adiabatic Hamiltonian $H(s) = -(1 - s)\,|\psi_0\rangle\langle\psi_0| + sH_z$, we have

$$\|H'(s)\| = O(1), \qquad \|H''(s)\| = 0, \qquad |\lambda_0'(s)| = O(1), \tag{7.4.9}$$

because $H'(s) = |\psi_0\rangle\langle\psi_0| + H_z$ is constant and $\lambda_0'(s) = \langle\phi_0(s)|\,H'(s)\,|\phi_0(s)\rangle$ is bounded by $\|H'\|$ through Hellmann-Feynman. The derivative $|g_0'(s)|$ is piecewise bounded: $b\,A_1(A_1+1)/A_2$ on the left, 0 in the window, and $\Delta/(30(1-s_0))$ on the right. For piecewise linear g_0, this keeps $|g_0'|B_2$ bounded. The window contributes nothing because $g_0' = 0$ there. On each linear branch, $|g_0'|$ factors out and the substitution $u = g_0(s)$ gives

$$\int g_0^{p-3}|g_0'|\,ds = \int_{g_{\min}/10}^{O(1)} u^{p-3}\,du = O(g_{\min}^{p-2}),$$

independently of the slopes. Since $\|H''\| = 0$, the dominant term in (7.3.2) is $40\|H'\|^2 B_2$. Therefore

$$c = O(B_2). \tag{7.4.10}$$

Theorem 7.4.1 (Runtime of AQO: Main Result 1 [10])**.** *Let H_z satisfy the spectral condition (Definition 5.2.2) and assume $A_1 \geq 1/2$ (equivalently $s^* \geq 1/3$). For any $\varepsilon > 0$, the adaptive schedule (7.3.3) with the gap lower bound (7.4.1) prepares the ground state of H_z with fidelity at least $1-\varepsilon$ in time*

$$T = O\left(\frac{1}{\varepsilon}\cdot\frac{\sqrt{A_2}}{\Delta^2\,A_1(A_1+1)}\cdot\sqrt{\frac{N}{d_0}}\right).^{\text{ii}} \tag{7.4.11}$$

Proof. By Theorem 7.3.1, $T \leq c\,B_1/(\varepsilon\,g_{\min})$. Substituting $c = O(B_2)$, $B_1 = O(1/(\Delta(1+A_1)))$, $B_2 = O(1/(\Delta(1+A_1)))$, and $g_{\min} = (2A_1/(A_1+1))\sqrt{d_0/(NA_2)}$ from Eq. (5.4.9):

$$T = O\left(\frac{1}{\varepsilon}\cdot\frac{B_1B_2}{g_{\min}}\right) = O\left(\frac{1}{\varepsilon}\cdot\frac{1}{\Delta^2(1+A_1)^2}\cdot\frac{A_1+1}{2A_1}\sqrt{\frac{NA_2}{d_0}}\right) = O\left(\frac{1}{\varepsilon}\cdot\frac{\sqrt{A_2}}{\Delta^2\,A_1(A_1+1)}\cdot\sqrt{\frac{N}{d_0}}\right). \tag{7.4.12}$$

□

The runtime in (7.4.11) has five interpretable factors. The $1/\varepsilon$ term is linear in target error. The factor $\sqrt{A_2}$ measures spectral crowding near E_0, where larger $A_2 = (1/N)\sum d_k/(E_k - E_0)^2$ sharpens the minimum and narrows the crossing window. The denominator $A_1(A_1+1)$ encodes crossing location, since larger A_1 pushes s^* toward 1 and steepens the left arm. The term $1/\Delta^2$ is the cost of right-side control, with one $1/\Delta$ from B_1 and one from B_2. Finally, $\sqrt{N/d_0}$ is the Grover factor. In short, the speedup is quantum. The remaining terms are explicit spectral overheads of generality. Compared with the constant-rate theorem, the key gain is exactly here. Time still scales linearly in the target error $1/\varepsilon$, and the minimum-gap scaling improves from $T = O(g_{\min}^{-2})$ to $T = O(g_{\min}^{-1})$. At the proof level, the improvement comes from replacing the g^{-3} corridor with power-law control centered on g^{-2}.

For Ising Hamiltonians H_σ (Eq. (5.1.4)) with $A_1, A_2 = O(\text{poly}(n))$ and $\Delta \geq 1/\text{poly}(n)$, this becomes $T = \widetilde{O}(\sqrt{N/d_0})$. That matches the lower bound of [39] up to polylogarithmic factors. When $d_0 = O(1)$, the adiabatic algorithm recovers the Grover $\sqrt{N}$ scaling.

For the canonical two-level case $M = 2$ with $A_1 \approx 1$, $A_2 \approx 1$, $\Delta = 1$, and $d_0 = 1$, we obtain

$$T = O\left(\frac{1}{\varepsilon}\cdot\frac{1}{1\cdot 2}\cdot\sqrt{N}\right) = O\left(\frac{\sqrt{N}}{\varepsilon}\right), \tag{7.4.13}$$

matching the circuit-based Grover algorithm. The adaptive adiabatic approach achieves the same quadratic speedup through a smooth interpolation between two Hamiltonians, without relying on the discrete iterate structure of amplitude amplification.

Runtime is controlled by how much spectral information the schedule receives. The constant-rate schedule (Theorem 7.2.3) gives $T = O(N/\varepsilon)$ because the crossing window dominates. The Roland-Cerf schedule (section 7.1) sets $K'(s) \propto 1/g(s)^2$ and improves this to $T = O(\sqrt{N}/\varepsilon)$, but it needs the exact gap at every point. The adaptive schedule in Theorem 7.3.1 keeps the same $\sqrt{N}$ scaling while using only a certified lower bound $g_0(s) \leq g(s)$, namely the Chapter 6 profile bounds. That change, from exact gap to lower bound, is what makes the method usable for general spectral-condition instances. The discrete-time eigenpath route of Boixo et al. [74] reaches the same $O(1/g_{\min})$ scaling through a different mechanism, so this scaling is not tied to one proof template.

Guo and An [46] place this in a broader framework. They study interpolations $H(u(s)) = (1-u(s))H_0 + u(s)H_1$ under a measure condition. The set $\{s : \Delta(u(s)) \leq x\}$ has Lebesgue measure $O(x)$ as $x \to 0$. Under

[ii] Our published work [10] states A_1^2 in Theorem 1. The expression $A_1(A_1+1)$ follows from the proof derivation in Appendix A-IV [10]. For Ising Hamiltonians with $A_1 = O(\text{poly}(n))$, the distinction is absorbed by the $O(\cdot)$ notation, since $A_1(A_1+1) = A_1^2 + A_1 = \Theta(A_1^2)$.

that condition, the power-law schedule with exponent $p = 3/2$ achieves $O(1/\Delta_*)$, a quadratic improvement over $O(1/\Delta_*^2)$. They also show that $p = 3/2$ is optimal for linear gap profiles. The profile in Theorem 6.3.1 satisfies their condition because it has one minimum at s^* and linear reopening on both sides. Equivalently, for small x, the set $\{s : g(s) \le x\}$ is an interval around s^* of width $\Theta(x)$. Their theorem provides the existence-and-scaling layer; Chapters 5 and 6 add explicit constants, which is what turns (7.4.11) into a concrete runtime bound. This condition is also the geometric dividing line between narrow, sharp minima and broad, flat ones: sharp minima satisfy it with a bounded constant, while broad flat minima force larger overhead.

Running the adaptive schedule still requires knowledge of $g_0(s)$, hence of s^*, δ_s, and $g_{\min}$. These all depend on A_1. Inside the window $[s^* - \delta_s, s^*)$, the schedule is constant, $K' = c/(\varepsilon\, b^p\, g_{\min}^2)$, so the main issue is not local slope but window placement. Because $s^* = A_1/(A_1 + 1)$, we must know A_1 to accuracy $O(\delta_s) = O(2^{-n/2})$ to center the slow segment correctly. Outside the window, placement errors change only constants. Inside this exponentially narrow window, the same error causes a real loss of fidelity.

Imprecision in A_2 and d_0 causes only polynomial slowdown. Replacing A_2 by the lower bound $1 - d_0/N$ (Eq. (5.2.3)) and taking $d_0 = 1$ changes runtime only by $\mathrm{poly}(n)$ factors, because these parameters appear through $\sqrt{A_2/d_0}$ and B_1. The critical quantity is A_1. It must be estimated to additive accuracy $O(\delta_s) = O(2^{-n/2})$ before evolution begins. That requirement is severe: the needed precision is exponential in n even though H_z itself has a $\mathrm{poly}(n)$-bit description. Chapter 8 shows that even approximating A_1 to much coarser precision $1/\mathrm{poly}(n)$ is NP-hard, while exact computation is #P-hard.

Chapter 8

Hardness of Optimality

The optimal schedule from Chapter 7 achieves a quadratic speedup over classical brute-force search, but the schedule must be fixed before evolution begins. It depends on the spectral parameter A_1, the weighted sum of inverse gaps that determines where the avoided crossing occurs. This parameter must be known to additive accuracy $O(2^{-n/2})$. Given the $N = 2^n$ diagonal entries of H_z, brute-force computation of $A_1 = (1/N)\sum_{k=1}^{M-1} d_k/(E_k - E_0)$ by enumerating eigenvalues, sorting, and summing takes $O(N)$ time. That is the same cost as classical unstructured search. If pre-computation costs as much as the task itself, the speedup is only conditional.

The runtime of Theorem 7.4.1,

$$T = O\left(\frac{1}{\varepsilon} \cdot \frac{\sqrt{A_2}}{\Delta^2\, A_1(A_1+1)} \cdot \sqrt{\frac{N}{d_0}}\right),$$

makes this dependence explicit. [10] also states an A_1^2 denominator in its headline theorem form. We keep the proof-level $A_1(A_1+1)$ expression, which is the tighter form used in the derivation. In the normalized regime $E_k \in [0,1]$, $A_1 \geq 1 - d_0/N$, so both forms differ only by a constant-factor normalization for the asymptotic statements used here. The adaptive schedule places a slow phase in the window $[s^* - \delta_s,\, s^*)$ centered at $s^* = A_1/(A_1+1)$, where the gap is smallest, and accelerates elsewhere. The parameters A_2 and d_0 enter only through $\sqrt{A_2/d_0}$. Using conservative bounds ($A_2 \geq 1 - d_0/N$ from Eq. (5.2.3), and $d_0 = 1$ for worst-case search) changes only polynomial prefactors when $d_0 \ll N$. The decisive quantity is A_1. It sets crossing location, while $\delta_s = O(\sqrt{d_0 A_2/N}) = O(2^{-n/2})$ sets required precision. If the crossing estimate is wrong by more than δ_s, evolution passes too quickly through the minimum and loses ground-state fidelity. Throughout this chapter, we write $A_1(H)$ when dependence on the Hamiltonian matters.

The hardness of computing A_1 is not the only obstacle to adiabatic optimization for hard problems. Even if A_1 were known exactly, the single-crossing framework of Chapters 5–7 applies only to the rank-one projector $H_0 = -|\psi_0\rangle\langle\psi_0|$. For the transverse-field driver (Chapter 5), the multi-crossing regime makes this framework inapplicable. Knowing A_1 no longer helps there, because the schedule would need to navigate exponentially many crossings rather than one.

In our view, the two barriers are complementary. Computing A_1 is hard even in the rank-one setting, and the single-crossing method fails for other drivers even when spectral information is available.

NP-hardness already appears at precision $1/\mathrm{poly}(n)$. Two queries to an A_1-oracle then suffice to solve 3-SAT (section 8.1). At precision $2^{-\mathrm{poly}(n)}$, the problem becomes #P-hard because polynomial interpolation can recover all degeneracies from polynomially many queries (section 8.2).

The algorithmically relevant precision $2^{-n/2}$ sits strictly between these scales. It is fine enough to matter for scheduling, but not fine enough for either existing hardness proof to transfer directly. At this precision, a quantum algorithm uses $O(2^{n/2})$ queries, while any classical algorithm needs $\Omega(2^n)$. This is exactly a Grover-type quadratic separation (section 8.3).

8.1 NP-Hardness of Estimating A_1

The Hamiltonian H_z encodes an optimization problem whose ground energy E_0 determines whether a solution exists. For a 3-SAT instance, $E_0 = 0$ when a satisfying assignment exists and $E_0 \geq 1/\mathrm{poly}(n)$ otherwise. Distinguishing these two cases is the local Hamiltonian promise problem, known to be NP-hard [21]. The spectral parameter A_1 is not obviously tied to this decision problem, because it aggregates information across all

energy levels rather than only the ground energy. A modified Hamiltonian H' bridges the two tasks. Comparing $A_1(H')$ with $A_1(H)$ reveals whether E_0 vanishes.

Define the $(n+1)$-qubit Hamiltonian

$$H' = H \otimes \frac{I + \sigma_z}{2}. \tag{8.1.1}$$

The operator $(I+\sigma_z)/2$ is the projector onto $|0\rangle$ for the ancilla qubit. It has eigenvalue 1 on $|0\rangle$ and eigenvalue 0 on $|1\rangle$. On the $|0\rangle$ branch, H' has the same spectrum as H, with eigenvalues E_k and degeneracies d_k. On the $|1\rangle$ branch, H' annihilates every state, contributing 2^n eigenvalues at energy 0. The ground energy of H' is therefore always zero, regardless of $E_0(H)$.

This is the mechanism behind the reduction. $A_1(H')$ measures from the fixed reference point $E'_0 = 0$, while $A_1(H)$ measures from the instance-dependent reference $E_0(H)$. When $E_0(H) > 0$, the two values separate by a detectable amount.

Lemma 8.1.1 (Disambiguation [10])**.** *Let $\varepsilon, \mu_1, \mu_2 \in (0,1)$. Suppose $\mathcal{C}_\varepsilon$ is a procedure that accepts the description of a Hamiltonian H and outputs $\widetilde{A}_1(H)$ with $|\widetilde{A}_1(H) - A_1(H)| \le \varepsilon$. Let H be an n-qubit diagonal Hamiltonian with eigenvalues $0 \le E_0 < E_1 < \cdots < E_{M-1} \le 1$ and $M \in$ poly(n), such that either* (i) $E_0 = 0$ *or* (ii) $\mu_1 \le E_0 \le 1 - \mu_2$*. Then two calls to $\mathcal{C}_\varepsilon$ suffice to decide between* (i) *and* (ii)*, provided*

$$\varepsilon < \frac{\mu_1}{6(1-\mu_1)} - \frac{d_0}{6N} \cdot \frac{1}{\mu_1 \mu_2}. \tag{8.1.2}$$

Proof. Call $\mathcal{C}_\varepsilon$ on H and on H' defined by Eq. (8.1.1), obtaining estimates $\widetilde{A}_1(H)$ and $\widetilde{A}_1(H')$. The test statistic is $\widetilde{A}_1(H) - 2\widetilde{A}_1(H')$, where the factor 2 compensates for the doubling of the Hilbert space (H' acts on 2^{n+1} states, so $A_1(H')$ carries a normalization factor $1/2^{n+1}$ instead of $1/2^n$).

Case (i): $E_0 = 0$**.** The ground energy of H' is 0 with degeneracy $d_0 + 2^n$, and the excited levels of H' are $E_1, \ldots, E_{M-1}$ with degeneracies $d_1, \ldots, d_{M-1}$. Since $E_0 = 0$, both $A_1(H)$ and $A_1(H')$ sum over the same gaps $E_k - 0 = E_k$:

$$A_1(H) = \frac{1}{2^n} \sum_{k=1}^{M-1} \frac{d_k}{E_k}, \qquad A_1(H') = \frac{1}{2^{n+1}} \sum_{k=1}^{M-1} \frac{d_k}{E_k}.$$

Therefore $A_1(H) - 2A_1(H') = 0$, and by the triangle inequality the test statistic satisfies $|\widetilde{A}_1(H) - 2\widetilde{A}_1(H')| \le 3\varepsilon$.

Case (ii): $\mu_1 \le E_0 \le 1 - \mu_2$**.** The ground energy of H' is still 0 (from the $|1\rangle$ branch), but now $E_0, E_1, \ldots, E_{M-1}$ are all excited levels. Thus

$$A_1(H') = \frac{1}{2^{n+1}} \sum_{k=0}^{M-1} \frac{d_k}{E_k}.$$

Decompose $A_1(H)$ using the partial fraction identity $d_k/(E_k - E_0) = d_k/E_k + d_k E_0/(E_k(E_k - E_0))$:

$$\begin{aligned} A_1(H) &= \frac{1}{2^n} \sum_{k=1}^{M-1} \frac{d_k}{E_k - E_0} = \frac{1}{2^n} \sum_{k=1}^{M-1} \frac{d_k}{E_k} + \frac{E_0}{2^n} \sum_{k=1}^{M-1} \frac{d_k}{E_k(E_k - E_0)} \\ &= \frac{1}{2^n} \sum_{k=0}^{M-1} \frac{d_k}{E_k} - \frac{d_0}{2^n E_0} + \frac{E_0}{2^n} \sum_{k=1}^{M-1} \frac{d_k}{E_k(E_k - E_0)}. \end{aligned} \tag{8.1.3}$$

The first sum equals $2A_1(H')$. For the remainder sum, $E_k \le 1$ and $E_k - E_0 \le 1 - E_0$, so the product $E_k(E_k - E_0)$ is at most $1 - E_0$. Each fraction $d_k/(E_k(E_k - E_0))$ is therefore bounded from below:

$$\frac{E_0}{2^n} \sum_{k=1}^{M-1} \frac{d_k}{E_k(E_k - E_0)} \ge \frac{E_0}{1 - E_0} \cdot \frac{1}{2^n} \sum_{k=1}^{M-1} d_k = \frac{E_0}{1 - E_0} \left(1 - \frac{d_0}{N}\right).$$

Combining with Eq. (8.1.3):

$$\begin{aligned} A_1(H) - 2A_1(H') &\ge \frac{E_0}{1 - E_0} \left(1 - \frac{d_0}{N}\right) - \frac{d_0}{N E_0} \\ &= \frac{E_0}{1 - E_0} - \frac{d_0}{N} \cdot \frac{1 - E_0 + E_0^2}{E_0(1 - E_0)}. \end{aligned} \tag{8.1.4}$$

Since $1 - E_0 + E_0^2 \le 1$ and $E_0(1-E_0) \ge \mu_1\mu_2$ on the given range, the fraction $(1-E_0+E_0^2)/(E_0(1-E_0))$ is at most $1/(\mu_1\mu_2)$. The first term $E_0/(1-E_0)$ is increasing in E_0, so it is at least $\mu_1/(1-\mu_1)$. Therefore

$$A_1(H) - 2A_1(H') \ge \frac{\mu_1}{1-\mu_1} - \frac{d_0}{N}\cdot\frac{1}{\mu_1\mu_2},$$

and the test statistic satisfies

$$\widetilde{A}_1(H) - 2\widetilde{A}_1(H') \ge \frac{\mu_1}{1-\mu_1} - \frac{d_0}{N\mu_1\mu_2} - 3\varepsilon.$$

The two cases are distinguished when 3ε from case (i) is separated from the lower bound in case (ii), requiring $6\varepsilon < \mu_1/(1-\mu_1) - d_0/(N\mu_1\mu_2)$. □

The disambiguation succeeds whenever the positive correction $E_0/(1-E_0)$ from the partial fraction identity dominates the negative term $-d_0/(NE_0)$, which happens as long as d_0/N is small relative to $\mu_1^2\mu_2$. For the Ising Hamiltonians of interest, d_0/N is exponentially small in n, so the condition is easily satisfied.

Theorem 8.1.2 (NP-hardness of A_1 estimation [10])**.** *Computing $A_1(H)$ to additive accuracy*

$$\varepsilon < \frac{1}{72(n-1)}$$

for a 3-local Hamiltonian H on n qubits is NP-hard.

Proof. We reduce 3-SAT to ground-energy disambiguation, following the construction of [76, 10]. Let φ be a 3-SAT formula on n_{var} Boolean variables $x_0, \dots, x_{n_{\mathrm{var}}-1}$ with m clauses, each of the form $a_k \vee b_k \vee c_k$ where each literal is some x_l or $\bar{x}_l$. If $n_{\mathrm{var}} + m < 15$, solve by brute force. Otherwise, define the single-qubit projectors

$$P_{x_l} = \frac{I - \sigma_z^{(l)}}{2}, \qquad P_{\bar{x}_l} = \frac{I + \sigma_z^{(l)}}{2},$$

which project onto the $|1\rangle$ and $|0\rangle$ states of qubit l, respectively. For each clause k ($0 \le k < m$), introduce an auxiliary qubit at index $n_{\mathrm{var}} + k$ and define

$$\begin{aligned} H_k = {} & P_{\bar{a}_k} + P_{\bar{b}_k} + P_{\bar{c}_k} + P_{\bar{x}_{n_{\mathrm{var}}+k}} \\ & + P_{a_k}P_{b_k} + P_{a_k}P_{c_k} + P_{b_k}P_{c_k} \\ & + P_{\bar{a}_k}P_{x_{n_{\mathrm{var}}+k}} + P_{\bar{b}_k}P_{x_{n_{\mathrm{var}}+k}} + P_{\bar{c}_k}P_{x_{n_{\mathrm{var}}+k}}. \end{aligned} \tag{8.1.5}$$

Direct computation on the computational basis shows that the minimum eigenvalue of H_k is 3 when clause k is satisfied and 4 when it is not; the maximum eigenvalue is 6. The combined Hamiltonian on $2n_{\mathrm{var}} + 2m$ qubits is

$$H = \frac{1}{6m}\sum_{k=0}^{m-1} H_k + \frac{1}{2n_{\mathrm{var}}+2m}\sum_{j=n_{\mathrm{var}}+m}^{2n_{\mathrm{var}}+2m-1} P_{x_j} - \frac{1}{2}I. \tag{8.1.6}$$

The first sum normalizes the clause energies to $[1/2, 1]$; the second sum adds $n_{\mathrm{var}} + m$ free qubits whose projectors prefer $|0\rangle$; the identity shift places the eigenvalues in $[0, 1]$. When all clauses are satisfied, there exists an assignment making every H_k achieve its minimum, giving $E_0 = 0$. When some clause is unsatisfied, the minimum of $\sum H_k/(6m)$ increases by at least $1/(6m)$, giving $E_0 \ge 1/(6m)$.

Apply Lemma 8.1.1 with $\mu_1 = 1/(6m)$ and $\mu_2 = 1/2$. The number of eigenvalues is $N = 2^{2n_{\mathrm{var}}+2m}$ and the ground-state degeneracy satisfies $d_0 \le 2^{n_{\mathrm{var}}+m}$, so $d_0/N \le 2^{-(n_{\mathrm{var}}+m)}$. Substituting into Eq. (8.1.2), the right-hand side satisfies

$$\frac{1}{6}\cdot\frac{1}{6m-1} - \frac{12m}{6}\cdot\frac{d_0}{N} \ge \frac{1}{36(n_{\mathrm{var}}+m-1)} - \frac{2m}{2^{n_{\mathrm{var}}+m}}, \tag{8.1.7}$$

since $1/(6(6m-1)) \ge 1/(36(n_{\mathrm{var}}+m-1))$ for $n_{\mathrm{var}} \ge 1$ and $d_0/N \le 2^{-(n_{\mathrm{var}}+m)}$. For $n_{\mathrm{var}} + m \ge 15$, the second term satisfies $2m/2^{n_{\mathrm{var}}+m} \le 1/(72(n_{\mathrm{var}}+m-1))$, so the disambiguation succeeds whenever

$$\varepsilon < \frac{1}{72(n_{\mathrm{var}}+m-1)}.$$

The Hamiltonian H' from Eq. (8.1.1) acts on $n = 2n_{\mathrm{var}} + 2m + 1$ qubits and is 3-local (since H is 2-local and the tensor product with $(I+\sigma_z)/2$ adds one ancilla). Since $n_{\mathrm{var}} + m \le n$, the precision bound $\varepsilon < 1/(72(n-1))$ follows. □

When $M = 2$ (Grover search), the spectral parameter $A_1 = (N-1)/N$ is trivial to obtain from the instance description. There are only two levels, and their degeneracies are fixed by the number of marked items. NP-hardness appears only for Hamiltonians that encode combinatorial structure with polynomially many levels and exponentially small ground-energy gaps. In that regime, A_1 depends nontrivially on the full degeneracy profile.

Remark. The disambiguation technique extends beyond 3-SAT. The MaxCut decision problem (given a graph $G = (V, E)$ and integer k, does G have a cut of size at least k?) also reduces to A_1 estimation. The construction adds a weighted edge to G, creating an auxiliary Hamiltonian H' whose A_1 value differs from a reference by at least $1/(|E|(|E|-1))$ between the two cases. This yields NP-hardness at precision $2/(5n^4)$ with a 2-local Hamiltonian, sharpening the locality requirement from 3-local to 2-local at the cost of a slightly tighter precision bound.

8.2 #P-Hardness of Computing A_1 Exactly

NP-hardness captures a decision question, namely whether $E_0 = 0$. But A_1 carries more than a single decision bit. It is a weighted sum over all energy levels, and its exact value determines every degeneracy d_k. Recovering these degeneracies solves counting problems. For NP-complete Hamiltonians, for example, d_0 counts satisfying assignments. Counting is harder than deciding, and it is #P-complete [8].

The extraction uses a parametrized family of Hamiltonians that shifts the spectrum continuously, turning A_1 into a rational function whose poles carry the degeneracies as residues. For a parameter $x > 0$, define the $(n+1)$-qubit Hamiltonian

$$H'(x) = H \otimes I - \frac{x}{2} I \otimes \frac{I + \sigma_z^{(n+1)}}{2}. \tag{8.2.1}$$

On the $|0\rangle$ branch of the ancilla, the eigenvalues are $E_k - x/2$ with degeneracies d_k. On the $|1\rangle$ branch, the eigenvalues are E_k with degeneracies d_k. The ground energy is $E_0 - x/2$ (from the $|0\rangle$ branch, for $x > 0$). The gaps relative to this ground energy are $\Delta_k = E_k - E_0$ (extending the notation $\Delta = E_1 - E_0$ from earlier chapters to all levels) for the $|0\rangle$ branch and $\Delta_k + x/2$ for the $|1\rangle$ branch.

Computing $A_1(H'(x))$ from these gaps and defining $f(x) = 2A_1(H'(x)) - A_1(H)$ isolates the $|1\rangle$-branch contribution [10]:

$$f(x) = \frac{1}{N} \sum_{k=0}^{M-1} \frac{d_k}{\Delta_k + x/2}. \tag{8.2.2}$$

This function is a sum of M simple poles at $x = -2\Delta_k$. Each pole has residue $2d_k/N$, encoding the degeneracy of the corresponding energy level. The function f is a partial-fraction decomposition of the entire degeneracy spectrum. The extraction problem reduces to recovering these residues from evaluations of f.

Lemma 8.2.1 (Exact degeneracy extraction [10])**.** *Suppose $\mathcal{C}$ is a procedure that computes $A_1(H)$ exactly for any n-qubit diagonal Hamiltonian H. Let H_σ be an Ising Hamiltonian (Equation 5.1.4) with integer eigenvalues and known spectral gaps $\Delta_k = E_k - E_0$. Then $O(\text{poly}(n))$ calls to $\mathcal{C}$ suffice to compute all degeneracies $d_0, d_1, \ldots, d_{M-1}$.*

Proof. Each evaluation of $f(x_i)$ requires two calls to $\mathcal{C}$, one for $A_1(H)$ and one for $A_1(H'(x_i))$. Evaluate f at M distinct positive odd integers $x_i \in \{1, 3, \ldots, 2M-1\}$. These values avoid the poles. For each k, $\Delta_k + x_i/2 \geq 0 + 1/2 > 0$ because $\Delta_k \geq 0$ and $x_i \geq 1$. The total cost is $2M = O(\text{poly}(n))$ oracle calls.

Define the reconstruction polynomial

$$P(x) = \prod_{k=0}^{M-1} \left(\Delta_k + \frac{x}{2}\right) f(x) = \frac{1}{N} \sum_{k=0}^{M-1} d_k \prod_{\ell \neq k} \left(\Delta_\ell + \frac{x}{2}\right). \tag{8.2.3}$$

Multiplying $f(x)$ by the product of all denominators clears the poles, yielding a polynomial of degree at most $M-1$ in x. Since the gaps Δ_k are known integers, the values $P(x_i) = \prod_k (\Delta_k + x_i/2) \cdot f(x_i)$ are computable from oracle outputs. The M values $P(x_1), \ldots, P(x_M)$ determine P uniquely by Lagrange interpolation [77]. A polynomial of degree at most $M-1$ is fixed by M distinct evaluations.

The degeneracies are recovered by evaluating P at the poles. Setting $x = -2\Delta_k$ kills every factor $(\Delta_\ell + x/2)$ except the k-th, giving

$$d_k = \frac{N \cdot P(-2\Delta_k)}{\prod_{\ell \neq k} (\Delta_\ell - \Delta_k)}, \qquad k \in \{0, \ldots, M-1\}. \tag{8.2.4}$$

The denominator is nonzero because the eigenvalues are distinct. The entire computation (oracle calls, Lagrange interpolation, pole evaluation) runs in $O(\text{poly}(n))$ time. □

Extracting d_0 from an Ising Hamiltonian encoding a 3-SAT formula counts satisfying assignments and therefore solves #3-SAT. Since #3-SAT is #P-complete [8], an exact A_1 oracle would solve every problem in #P in polynomial time. The same degeneracy data also determines IQP output probabilities [78]. From d_k and Δ_k, one computes $|\langle 0^n|C_{\mathrm{IQP}}|0^n\rangle|^2 = |N^{-1}\sum_k d_k\, e^{i\Delta_k}|^2$, which is itself #P-hard. The NP-hardness result of section 8.1 uses a 3-local Hamiltonian because the ancilla raises locality by one. The #P-hardness statement already holds for 2-local Ising Hamiltonians, since Eq. (8.2.1) preserves 2-locality when H is 2-local.

The exact oracle is unrealistic. A robust version of Lemma 8.2.1 must tolerate additive noise ε in the oracle outputs. Paturi's amplification lemma gives the control we need.

Lemma 8.2.2 (Paturi [79])**.** *Let $P(x)$ be a polynomial of degree at most M satisfying $|P(i)| \le c$ for all integers $i \in \{0, 1, \ldots, M\}$. Then $|P(x)| \le c \cdot 2^M$ for all $x \in [0, M]$.*

Paturi's lemma bounds polynomial growth between sample points. If a polynomial is bounded by c at $M+1$ integer points, it can grow by at most a factor 2^M on the interval. Applied to the difference between exact and approximate reconstruction polynomials, this gives explicit control of interpolation error.

Across the proofs below, error propagation is organized into three stages. These stages are sample-point error, extrapolation amplification, and rounding threshold. Stage 1 itself has three algebraic sub-steps: oracle noise enters f as $|\tilde{f}(x_i) - f(x_i)| \le 3\varepsilon$ (three oracle calls contribute), then enters polynomial samples as $|\tilde{P}(x_i) - P(x_i)| \le 3\varepsilon \prod_k (\Delta_k + x_i/2)$, and the product is bounded by B^M with $B = \Delta_{\max} + M = \mathrm{poly}(n)$.

Lemma 8.2.3 (Approximate degeneracy extraction [10])**.** *Under the same hypotheses as Lemma 8.2.1, but with an oracle $\mathcal{C}_\varepsilon$ satisfying $|\widetilde{A}_1(H) - A_1(H)| \le \varepsilon$, all degeneracies d_k can be computed exactly by $O(\mathrm{poly}(n))$ calls to $\mathcal{C}_\varepsilon$ for sufficiently small $\varepsilon \in O(2^{-\mathrm{poly}(n)})$.*

Proof sketch. **Stage 1 (sample-point error).** The proof follows the same three-stage route. The approximate polynomial $\tilde{P}$ is the Lagrange interpolant through the noisy values $(\tilde{P}(x_1), \ldots, \tilde{P}(x_M))$. Its difference $D = \tilde{P} - P$ is a polynomial of degree at most $M-1$ bounded by $3\varepsilon B^M$ at the sample points. By Paturi's lemma (Lemma 8.2.2), $|D(x)| \le 3\varepsilon B^M \cdot 2^{M-1}$ on the interpolation interval.

Stage 2 (extrapolation amplification). At the pole evaluation points $x^* = -2\Delta_k$, which lie outside the interval $[1, 2M-1]$, the error is bounded by Lagrange-basis amplification:

$$|D(x^*)| \le 3\varepsilon B^M \cdot \Lambda_M(x^*),$$

where $\Lambda_M(x^*) = \sum_j \prod_{i \ne j} |x^* - x_i|/|x_j - x_i|$ is the Lebesgue function. For extrapolation outside the interval, $\Lambda_M(x^*)$ grows exponentially in M, but since $M = \mathrm{poly}(n)$, the total amplification is $2^{\mathrm{poly}(n)}$. Dividing by $\prod_{\ell \ne k} |\Delta_\ell - \Delta_k|$ (also at most $2^{\mathrm{poly}(n)}$ for integer gaps) and multiplying by $N = 2^n$, the degeneracy error satisfies

$$|d_k - \tilde{d}_k| \le 3\varepsilon \cdot 2^{\mathrm{poly}(n)}.$$

Stage 3 (rounding to exact degeneracies). For $\varepsilon = O(2^{-\mathrm{poly}(n)})$ with a sufficiently large polynomial, this is less than $1/2$. Since degeneracies are positive integers, rounding $\tilde{d}_k$ to the nearest integer recovers d_k exactly. □

The proof extends to probabilistic oracles. If $\mathcal{C}_\varepsilon$ succeeds with probability at least $3/4$, then $O(\mathrm{poly}(n))$ queries produce enough correct sample points to reconstruct P despite corrupted evaluations. The Berlekamp-Welch algorithm recovers a polynomial of degree d from k partially corrupted evaluations, provided at least $\max\{d+1, (k+d)/2\}$ evaluations are correct [78]. By the Chernoff bound, querying $k = O(\mathrm{poly}(n))$ times ensures that at least $(k + M - 2)/2$ evaluations are correct with high probability. Combining this with Lemma 8.2.3:

Theorem 8.2.4 (#P-hardness of A_1 estimation [10])**.** *Estimating $A_1(H)$ to additive accuracy $\varepsilon = O(2^{-\mathrm{poly}(n)})$ is #P-hard, even for 2-local Ising Hamiltonians. The result holds for both deterministic and probabilistic estimation algorithms.*

With $M = 2$, the reconstruction polynomial $P(x) = (d_0/N)(1+x/2) + (d_1/N)(x/2)$ is linear. Two evaluations determine d_0 and d_1 exactly, and interpolation reduces to fitting a line through two points. The #P-hardness comes from Hamiltonians with $M = O(n^2)$ levels, where the reconstruction polynomial has high degree and tiny oracle errors amplify through the exponential Paturi factor. The next section quantifies this amplification as $2^{O(M \log n)}$.

8.3 The Intermediate Regime

The adiabatic algorithm requires A_1 to precision $O(2^{-n/2})$. NP-hardness holds at $1/\mathrm{poly}(n)$ (Theorem 8.1.2), and #P-hardness holds at $2^{-\mathrm{poly}(n)}$ (Theorem 8.2.4). The algorithmically relevant precision $2^{-n/2}$ lies strictly between these regimes. The interpolation method does not reach this precision. Braida et al. [10] therefore left this intermediate regime open.

The interpolation technique extracts exact integers from approximate real evaluations. At precision $2^{-n/2}$, the error amplification inherent in polynomial extrapolation makes this extraction impossible.

NP-hardness extends to $2^{-n/2}$ by monotonicity. An oracle at precision $2^{-n/2}$ is strictly more powerful than one at $1/\mathrm{poly}(n)$, so it still solves 3-SAT. The #P-hardness argument does not extend in the opposite direction. An oracle at precision $2^{-n/2}$ is *less* powerful than one at $2^{-\mathrm{poly}(n)}$, and the interpolation proof for that regime fails here.

The failure has a concrete source. Oracle noise enters polynomial samples at rate εB^M. The Lebesgue function then amplifies that error exponentially in M. At $\varepsilon = 2^{-n/2}$, the amplified error already exceeds the rounding margin.

Theorem 8.3.1 (Interpolation barrier)**.** *The polynomial interpolation technique of section 8.2 requires oracle precision $\varepsilon = 2^{-n-O(M \log n)}$ to extract exact degeneracies, where $M = \mathrm{poly}(n)$ is the number of distinct energy levels. At $\varepsilon = 2^{-n/2}$, the amplified error exceeds $1/2$ and rounding fails. The #P-hardness argument does not extend to precision $2^{-n/2}$.*

Proof. We trace the same three-stage propagation from oracle noise to degeneracy error. Let ε denote the oracle accuracy, and let $B = \Delta_{\max} + M = \mathrm{poly}(n)$ bound the denominator factors, where $\Delta_{\max}$ is the largest spectral gap.

Stage 1 (sample-point error). The approximate function values satisfy $|\tilde{f}(x_i) - f(x_i)| \le 3\varepsilon$. The approximate polynomial samples are $\tilde{P}(x_i) = \prod_k (\Delta_k + x_i/2)\, \tilde{f}(x_i)$, with error

$$|\tilde{P}(x_i) - P(x_i)| \le 3\varepsilon \prod_{k=0}^{M-1} \left(\Delta_k + \frac{x_i}{2}\right) \le 3\varepsilon\, B^M. \tag{8.3.1}$$

Stage 2 (extrapolation amplification). The approximate degeneracies are computed from Eq. (8.2.4) with $\tilde{P}$ in place of P. Since $\tilde{P}$ is the Lagrange interpolant through the noisy samples, its value at any point x^* is $\tilde{P}(x^*) = \sum_j \tilde{P}(x_j) \prod_{i \ne j} (x^* - x_i)/(x_j - x_i)$. At $x^* = -2\Delta_k$,

$$|\tilde{P}(x^*) - P(x^*)| \le 3\varepsilon\, B^M \sum_{j=0}^{M-1} \prod_{i \ne j} \frac{|x^* - x_i|}{|x_j - x_i|} = 3\varepsilon\, B^M \cdot \Lambda_M(x^*), \tag{8.3.2}$$

where $\Lambda_M(x^*) = \sum_j \prod_{i \ne j} |x^* - x_i|/|x_j - x_i|$ is the Lebesgue function at x^*. It is the amplification factor for pointwise interpolation error: if each sample has error δ, then the extrapolated value at x^* can incur error as large as $\delta \cdot \Lambda_M(x^*)$.

For extrapolation outside the sample interval, this amplification is exponential in M. Consider odd-integer nodes $x_j = 2j + 1$ and evaluation point $x^* = -2\Delta_k \le 0$, which lies outside $[1, 2M - 1]$. Each numerator factor obeys $|x^* - x_i| = 2\Delta_k + 2i + 1 \le 2B + 1$. For the denominator,

$$\prod_{i \ne j} |x_j - x_i| = \prod_{i \ne j} 2|j - i| = 2^{M-1}\, j!\, (M - 1 - j)!,$$

because the nodes are equally spaced with spacing 2. The sum over j becomes

$$\Lambda_M(x^*) \le \sum_{j=0}^{M-1} \frac{(2B+1)^{M-1}}{2^{M-1}\, j!\, (M-1-j)!} = \frac{(2B+1)^{M-1}}{(M-1)!}, \tag{8.3.3}$$

using $\sum_j \binom{M-1}{j} = 2^{M-1}$. The denominator in Eq. (8.2.4) satisfies $\prod_{\ell \ne k} |\Delta_\ell - \Delta_k| \ge k!(M-1-k)!$ for integer gaps (since $|\Delta_\ell - \Delta_k| \ge |\ell - k|$), with minimum over k at least $((M-1)/(2e))^{M-1}$ by Stirling's approximation.

Putting these bounds together, the total degeneracy error is

$$|d_k - \tilde{d}_k| \le \frac{3\varepsilon\, N\, B^M\, (2B+1)^{M-1}}{(M-1)!\, ((M-1)/(2e))^{M-1}}. \tag{8.3.4}$$

Since $B = \text{poly}(n)$ and $M = \text{poly}(n)$, the amplification factor is $2^{O(M \log n)}$.

Stage 3 (rounding threshold). To extract exact degeneracies by rounding, we need $|d_k - \tilde{d}_k| < 1/2$. This requires

$$\varepsilon < \frac{1}{6N \cdot 2^{O(M \log n)}} = 2^{-n-O(M \log n)}. \tag{8.3.5}$$

Consequence at $\varepsilon = 2^{-n/2}$. Set $\varepsilon = 2^{-n/2}$ and $M = n^c$ for some constant $c \geq 1$. The error bound from Eq. (8.3.4) evaluates to

$$|d_k - \tilde{d}_k| \leq 3 \cdot 2^{-n/2} \cdot 2^n \cdot 2^{O(n^c \log n)} = 3 \cdot 2^{n/2 + O(n^c \log n)} \gg 1.$$

Even for $c = 1$ (the most favorable case $M = n$), the exponent $n/2 + \Omega(n)$ diverges. The upper bound on the degeneracy error already exceeds $1/2$, so the rounding step cannot be guaranteed to succeed. □

The precision $\varepsilon = 2^{-n/2}$ is too coarse for interpolation but too fine for brute force. It sits in a window that existing techniques cannot reach from either side.

This amplification is not specific to the construction above. Exponential growth is intrinsic to polynomial extrapolation for any d nodes, any interval, and any evaluation point sufficiently far outside that interval.

Theorem 8.3.2 (Generic extrapolation barrier)**.** *Let $x_1, \ldots, x_d$ be any d distinct nodes in an interval $[a, b]$, and let x^* satisfy $\text{dist}(x^*, [a, b]) \geq b - a$. The Lebesgue function at x^* satisfies $\Lambda_d(x^*) \geq 2^{d-1}$. Consequently, any polynomial extrapolation scheme that evaluates a degree-$(d-1)$ interpolant at x^* from samples with pointwise error δ can incur worst-case error at least $\delta \cdot 2^{d-1}$ at x^*.*

Proof. Assume $x^* \leq a - (b - a)$ (the case $x^* \geq b + (b - a)$ follows by symmetry). Let $x_{(1)} = \min_j x_j \geq a$ be the leftmost node. The corresponding Lagrange basis polynomial satisfies

$$|\ell_{(1)}(x^*)| = \prod_{i:\, x_i \neq x_{(1)}} \frac{|x_i - x^*|}{|x_i - x_{(1)}|} = \prod_{i:\, x_i \neq x_{(1)}} \left(1 + \frac{x_{(1)} - x^*}{x_i - x_{(1)}}\right).$$

Each factor has numerator shift $x_{(1)} - x^* \geq a - (a - (b - a)) = b - a$ and denominator $x_i - x_{(1)} \leq b - a$, so every factor is at least 2. With $d - 1$ such factors, $|\ell_{(1)}(x^*)| \geq 2^{d-1}$. Since $\Lambda_d(x^*) = \sum_j |\ell_j(x^*)| \geq |\ell_{(1)}(x^*)|$, the bound follows. For perturbed samples $y_j = P(x_j) + e_j$ with $|e_j| \leq \delta$, the extrapolation error is

$$\tilde{P}(x^*) - P(x^*) = \sum_{j=1}^{d} e_j \, \ell_j(x^*).$$

Choosing adversarial signs $e_j = \delta \, \text{sign}(\ell_j(x^*))$ gives

$$|\tilde{P}(x^*) - P(x^*)| = \delta \sum_{j=1}^{d} |\ell_j(x^*)| = \delta \, \Lambda_d(x^*) \geq \delta \cdot 2^{d-1},$$

so the worst-case error can be at least $\delta \cdot 2^{d-1}$. □

Theorem 8.3.2 rules out rescuing the #P-hardness argument by tweaking interpolation details. Reordering nodes (equispaced, Chebyshev, or otherwise), changing polynomial bases, or reparameterizing variables cannot push amplification below 2^{d-1}. At $d = M = \text{poly}(n)$, the needed precision stays at $\varepsilon = 2^{-\Omega(n)}$, far below $2^{-n/2}$. The same obstacle appears in quantum-advantage hardness arguments. Interpolation-based proofs for boson sampling [80], IQP sampling [81], and random circuit sampling [82] face analogous amplification barriers when moving from exponentially small to moderate error.

The interpolation barrier does not rule out #P-hardness at $2^{-n/2}$ by other methods. A proof that avoids polynomial extrapolation, for example through direct algebraic reductions or information-theoretic arguments, might still work. The barrier identifies the pressure point: we need a way to prove counting hardness without recovering exact integers from approximate real values.

What can be computed at precision $2^{-n/2}$? We answer in the query model, where each query to a diagonal oracle $O_H \colon |x\rangle |0\rangle \mapsto |x\rangle |E_x\rangle$ reveals one diagonal entry of H_z at unit cost. This model cleanly separates quantum and classical capabilities. The interpolation barrier is a classical obstruction: polynomial extrapolation cannot recover integers at this precision. A quantum algorithm can bypass that step entirely by using amplitude estimation rather than polynomial reconstruction.

Theorem 8.3.3 (Quantum algorithm for A_1)**.** *There exists a quantum algorithm that estimates $A_1(H_z)$ to additive precision ε using*

$$O\left(\sqrt{N} + \frac{1}{\varepsilon\,\Delta_1}\right) \tag{8.3.6}$$

quantum queries to the diagonal oracle O_H, where $\Delta_1 = E_1 - E_0$ is the spectral gap of H_z.

Proof. The algorithm has two stages.

Stage 1: Finding E_0. The Hamiltonian H_z is diagonal in the computational basis, so computing E_x for a given $|x\rangle$ requires one query to O_H. Finding the minimum of E_x over all $x \in \{0,1\}^n$ is an instance of quantum minimum finding [35], which succeeds with high probability in $O(\sqrt{N})$ queries.

Stage 2: Amplitude estimation of A_1. Define the function

$$g(x) = \begin{cases} \dfrac{1}{E_x - E_0} & \text{if } E_x \neq E_0, \\ 0 & \text{if } E_x = E_0. \end{cases}$$

The spectral parameter is the mean $A_1 = (1/N)\sum_x g(x)$. Since the eigenvalues lie in $[0,1]$, the values of g on non-ground states are in $[1, 1/\Delta_1]$. Rescaling to $h(x) = \Delta_1 \cdot g(x)$ yields $h(x) \in [0,1]$, and $A_1 = \mu_h/\Delta_1$ where $\mu_h = (1/N)\sum_x h(x)$.

Construct a quantum oracle U_h acting as $U_h\colon\ |x\rangle\,|0\rangle \mapsto |x\rangle\,(\sqrt{1-h(x)}\,|0\rangle + \sqrt{h(x)}\,|1\rangle)$. The implementation queries O_H once to obtain E_x, performs classical arithmetic on an ancilla to compute $h(x) = \Delta_1/(E_x - E_0)$ (or 0 for ground states), executes a controlled rotation $R_y(2\arcsin\sqrt{h(x)})$ on a flag qubit, and uncomputes the ancilla. Each application uses $O(1)$ queries to O_H and $O(\mathrm{poly}(n))$ auxiliary gates.

Preparing the uniform superposition $|+\rangle^{\otimes n}$ and applying U_h, the probability of measuring the flag qubit in $|1\rangle$ is

$$p = \frac{1}{N}\sum_x h(x) = \mu_h.$$

Amplitude estimation [37] estimates p to additive precision δ using $O(1/\delta)$ applications of U_h and its inverse. Setting $\delta = \varepsilon\,\Delta_1$ ensures $|A_1 - \tilde{A}_1| = |\mu_h - \tilde{\mu}_h|/\Delta_1 \leq \varepsilon$. The number of U_h applications is $O(1/(\varepsilon\,\Delta_1))$.

Combining both stages gives $O(\sqrt{N})$ queries for Stage 1 and $O(1/(\varepsilon\,\Delta_1))$ queries for Stage 2, yielding Eq. (8.3.6). For $\varepsilon = 2^{-n/2}$ and $\Delta_1 = 1/\mathrm{poly}(n)$, this becomes $O(2^{n/2} + 2^{n/2}\,\mathrm{poly}(n)) = O(2^{n/2}\,\mathrm{poly}(n))$. □

To confirm that the quantum algorithm's $O(2^{n/2})$ query count is a genuine advantage, we need a classical lower bound. The natural route is information-theoretic. We ask how many samples a classical algorithm needs to distinguish two carefully chosen instances whose A_1 values differ by ε.

Theorem 8.3.4 (Classical lower bound for A_1 estimation)**.** *Any classical randomized algorithm estimating $A_1(H_z)$ to additive precision ε in the query model requires $\Omega(1/\varepsilon^2)$ queries in the worst case.*

Proof. We construct an adversarial pair of instances that are indistinguishable without sufficiently many queries.

Instance construction. Fix $t = \lceil \varepsilon N \rceil$. Instance H_0 has a hidden set $S \subseteq \{0,1\}^n$ with $|S| = N/2$, and eigenvalues $E_x = 0$ for $x \in S$, $E_x = 1$ otherwise. Instance H_1 has $|S'| = N/2 + t$ ground states. The spectral parameters are $A_1(H_0) = 1/2$ and $A_1(H_1) = (N/2 - t)/N = 1/2 - t/N$, differing by $t/N \geq \varepsilon$. An algorithm estimating A_1 to precision $\varepsilon/2$ must distinguish the two instances.

Information-theoretic bound. A classical query at string x reveals $E_x \in \{0,1\}$, which is equivalent to learning whether $x \in S$. Under a uniform prior on S (or S'), successive queries follow a hypergeometric sampling model. Conditioned on earlier outcomes, the j-th query is a Bernoulli trial. Under hypothesis H_i, x is a ground state with probability $p_j^{(i)} = (|S_i| - g_{j-1})/(N - j + 1)$, where g_{j-1} counts ground states already found. The difference $p_j^{(1)} - p_j^{(0)} = t/(N - j + 1)$ is independent of g_{j-1}. Since both parameters are $\Theta(1)$, a Taylor expansion of binary KL divergence $D(p\|p+\delta) = \delta^2/(p(1-p)) + O(\delta^3)$ with $\delta = t/(N-j+1)$ gives the conditional per-query divergence

$$D_j = O\left(\frac{t^2}{(N-j)^2}\right) = O\left(\frac{t^2}{N^2}\right)$$

when $q \leq N/2$. By the chain rule for KL divergence, the total information from q adaptive queries is

$$D_{\mathrm{KL}}^{(q)} \leq \sum_{j=1}^{q} D_j \leq q \cdot O\left(\frac{t^2}{N^2}\right).$$

By Le Cam's two-point method [83], reliable hypothesis testing requires $D_{\mathrm{KL}}^{(q)} \geq \Omega(1)$. Via Pinsker's inequality, total variation distance is at most $\sqrt{D_{\mathrm{KL}}/2}$, and reliable distinguishing needs total variation $\Omega(1)$. Therefore

$$q \geq \Omega\left(\frac{N^2}{t^2}\right) = \Omega\left(\frac{1}{\varepsilon^2}\right).$$

At $\varepsilon = 2^{-n/2}$, this gives $q \geq \Omega(2^n)$. □

Corollary 8.3.5 (Quadratic quantum-classical separation)**.** *In the query model, estimating $A_1(H_z)$ to precision $\varepsilon = 2^{-n/2}$ exhibits a quadratic quantum-classical separation, with quantum complexity $O(2^{n/2}\,\mathrm{poly}(n))$ and classical complexity $\Omega(2^n)$.*

Proof. The upper bound is Theorem 8.3.3 with $\Delta_1 = 1$ for the adversarial instance (or $\Delta_1 = 1/\mathrm{poly}(n)$ in general). The lower bound is Theorem 8.3.4. The separation ratio is $\Omega(2^{n/2}/\mathrm{poly}(n))$, matching Grover's quadratic speedup for unstructured search. □

At the precision the adiabatic algorithm needs, quantum computation offers exactly the speedup the algorithm achieves.

The quantum bound in Theorem 8.3.3 is not only an upper bound; it is tight. The tightness already appears on the simplest family, namely $M = 2$ with $\Delta_1 = 1$. There, estimating $A_1 = (N - d_0)/N$ to precision ε is exactly approximate counting at precision ε.

Write the Grover iterate as $G = (2\,|+\rangle\langle+| - I)(I - 2\Pi_S)$, where Π_S projects onto the d_0 ground states. Its eigenphases are $\pm 2\theta$ with $\sin^2\theta = d_0/N$. For $d_0 \approx N/2$, we have $dp/d\theta = \sin 2\theta = 1$, so precision ε in A_1 requires precision ε in θ. The Heisenberg limit for quantum phase estimation [84], together with the quantum Cramér-Rao inequality [85] and Fisher bound $F_Q \leq 4T^2$, gives $T \geq 1/(2\varepsilon)$ applications of G, each with $O(1)$ oracle cost. Combining this with the upper bound yields quantum query complexity $\Theta(2^{n/2})$ at precision $\varepsilon = 2^{-n/2}$. The next chapter formalizes this theorem and ties it to the information cost of the adiabatic approach.

Two complementary frameworks apply here. Computational complexity asks whether a classical computer can extract A_1 from an explicit Hamiltonian description (J_{ij}, h_j). Query complexity asks how many oracle evaluations are information-theoretically necessary when diagonal entries are hidden behind O_H. A problem can be easy in one model and hard in the other. For A_1 estimation, both frameworks show hardness, which supports the same conclusion: the pre-computation barrier is structural, not an artifact of one proof style.

In the computational model with an explicit Hamiltonian description, the precision-dependent hardness landscape is summarized below.

Precision ε	Hardness	Source
$1/\mathrm{poly}(n)$	NP-hard	Theorem 8.1.2
$2^{-n/2}$	NP-hard	monotonicity
$2^{-\mathrm{poly}(n)}$	#P-hard	Theorem 8.2.4

In the query model with a diagonal oracle at the algorithmically relevant precision $\varepsilon = 2^{-n/2}$, the comparison is:

Model	Complexity	Source
Quantum	$O(2^{n/2} \cdot \mathrm{poly}(n))$	Theorem 8.3.3
Classical	$\Omega(2^n)$	Theorem 8.3.4

The precision $2^{-n/2}$ is exactly the algorithmic target. The adiabatic schedule needs A_1 to precision $O(\sqrt{d_0/N})$, which is $O(2^{-n/2})$ in the worst case $d_0 = O(1)$. It is also where interpolation-based #P-hardness proofs break (Theorem 8.3.1), even though NP-hardness still follows by monotonicity. It is also where query complexity separates sharply. The quantum algorithm uses $O(2^{n/2})$ queries, while classical sampling requires $\Omega(2^n)$.

Classical sampling provides independent evidence for the hardness of A_1 estimation at the algorithmic precision. Given a procedure that samples eigenvalues E_x according to the distribution $\{d_k/N\}$, estimating the mean $A_1 = \mathbb{E}[1/(E_x - E_0)]$ to precision δ_s requires $O(1/\delta_s^2) = \widetilde{O}(2^n/d_0)$ samples by Chebyshev's inequality [86]. This matches the formal $\Omega(2^n)$ lower bound of Theorem 8.3.4 up to logarithmic factors, providing a consistency check between the query-complexity result and concrete sampling algorithms.

The information barrier is not specific to adiabatic evolution. Consider the time-independent Hamiltonian $H = -\,|\psi_0\rangle\langle\psi_0| + r\,H_\sigma$, where $r > 0$ is fixed and H_σ is the problem Hamiltonian. Evolving $|\psi_0\rangle$ under H for time t produces oscillations between $|\psi_0\rangle$ and the ground state of H_σ, with success probability controlled by r.

The oscillation frequency is set by the spectral gap of H, and this gap is maximized when r is tuned to the avoided crossing, namely $r = A_1$ (up to normalization). To keep success probability non-negligible, r must lie within $O(2^{-n/2})$ of A_1 [10]. So the same barrier appears in this model as well. One still needs A_1 to exponential precision, and computing it remains NP-hard. The obstacle comes from spectral structure, not from adiabatic formalism itself.

The results of this chapter create a tension. The adiabatic algorithm of Theorem 7.4.1 achieves Grover scaling $\widetilde{O}(\sqrt{N/d_0})$, matching the unstructured-search lower bound. Yet the schedule depends on a spectral parameter whose computation is NP-hard, even at much coarser precision than the algorithm ultimately needs. In the circuit model, Grover achieves the same speedup without any spectral pre-computation because oracle queries gather information adaptively during execution. In the adiabatic framework, by contrast, the schedule must be fixed before evolution begins.

This asymmetry raises a precise question. Does the information cost of the adiabatic approach represent a fundamental limitation, or can it be circumvented? What runtime is achievable by an adiabatic algorithm that knows nothing about the problem Hamiltonian beyond its dimension? The next chapter formalizes this as an information-runtime tradeoff, proving a separation theorem for uninformed schedules and exploring whether adaptive measurements can bypass the classical pre-computation barrier.

Chapter 9

Information Gap

The adiabatic algorithm of Theorem 7.4.1 achieves the Grover speedup $\widetilde{O}(\sqrt{N/d_0})$, but its schedule depends on $s^* = A_1/(A_1+1)$, whose computation is NP-hard (Theorem 8.1.2). In the circuit model, Grover's algorithm achieves the same speedup without computing any spectral parameter. The adiabatic framework demands the schedule be fixed before evolution begins. What runtime is achievable by an adiabatic algorithm that knows nothing about the problem Hamiltonian beyond its dimension?

This chapter follows one question through three lenses. At the physics level, runtime is set by the gap profile $g(s)$ along the interpolation path. At the information-theoretic level, the decisive unknown is where that profile reaches its minimum. At the complexity-theoretic level, we ask what resources are required to obtain that location and exploit it.

9.1 The Cost of Ignorance

Throughout this chapter, asymptotic notation (O, Ω, Θ) refers to the limit $N \to \infty$ (equivalently $n \to \infty$ with $N = 2^n$). Unless stated otherwise, the spectral parameters d_0, M, Δ, A_1, A_2 and the target error ε are treated as fixed positive constants independent of n. When we write "$O(T_{\text{inf}})$," the hidden constant may depend on these spectral parameters but not on n.

A *fixed schedule* is chosen before the instance is revealed. It may depend on problem size n and target error ε, but not on instance-specific spectral data. An *instance-independent* algorithm uses the same Hamiltonian design for all energy assignments with the same degeneracy structure.

The NP-hardness of A_1 is a statement about worst-case classical computation. It does not directly tell us how much runtime an adiabatic algorithm loses by not knowing A_1. If a fixed schedule that ignores A_1 still achieved $O(\sqrt{N/d_0})$, the hardness would be academic. It is not.

The separation between informed and uninformed schedules is a minimax result. It can be viewed as a two-player game in which the schedule designer moves first and an adversary then chooses a worst-case gap function. To formalize this, we need a gap class broad enough to let the adversary place the minimum anywhere in an uncertainty interval $[s_L, s_R]$.

Definition 9.1.1 (Gap class)**.** *The gap class $\mathcal{G}(s_L, s_R, \Delta_*)$ consists of all gap functions $g : [0,1] \to \mathbb{R}_{>0}$ such that the minimum $g(s^*) = \Delta_*$ is achieved at a unique point $s^* \in [s_L, s_R]$, and $g(s) > \Delta_*$ for all $s \neq s^*$.*

For the running example ($M = 2$, $d_0 = 1$, $N = 4$), $s^* = A_1/(A_1+1) = 3/7$ and $\Delta_* = g_{\min} = 1/\sqrt{4} = 1/2$. Any gap function in $\mathcal{G}(0, 1, 1/2)$ has minimum value $1/2$ somewhere in $[0,1]$. The adversary controls where that minimum sits.

Definition 9.1.2 (RC-admissible fixed schedules)**.** *Fix a family of Hamiltonian instances. A fixed schedule u with velocity profile $v(s) = |ds/dt|$ is* RC-admissible *on an instance if it satisfies the local Roland-Cerf condition*

$$v(s) \leq \frac{\varepsilon\, g(s)^2}{\|H'(s)\|} \qquad \forall s \in [0,1].$$

It is uniformly RC-admissible *on the family if this inequality holds for every instance in the family.*

The parameter Δ_* denotes the minimum of the abstract gap function g. It should not be confused with $\Delta = E_1 - E_0$ (the spectral gap of H_z) or with $g_{\min}$ (the minimum gap of the rank-one Hamiltonian $H(s)$). For rank-one gap profiles, $\Delta_* = g_{\min} = \Theta(\sqrt{d_0/(NA_2)})$.

The schedule induces a velocity profile $v(s) > 0$ on $[0, 1]$, with total evolution time $T = \int_0^1 v(s)^{-1}\, ds$.

Within the uniformly RC-admissible class (Definition 9.1.2), the crossing velocity obeys a pointwise bound. Since $H'(s) = |\psi_0\rangle\langle\psi_0| + H_z$ satisfies $\|H'(s)\| \le \||\psi_0\rangle\langle\psi_0|\| + \|H_z\| \le 1 + 1 = 2$ (using the eigenvalue normalization $E_{M-1} \le 1$ from Chapter 5), RC-admissibility gives

$$v(s) \le \varepsilon\, g(s)^2/2.$$

At a crossing point where $g = \Delta_*$, this yields $v \le \varepsilon\, \Delta_*^2/2$.

The crossing window has width $\delta_s = \Theta(\Delta_*)$, so any valid schedule must stay slow across that window. Chapter 5 gives $\delta_s = \hat{g}/c_L$ (Equation 5.4.10), where $\hat{g} = \frac{2A_1}{A_1+1}\sqrt{d_0/(NA_2)}$ and $g_{\min} = (1 \pm O(\eta))\hat{g}$. Since $c_L = A_1(A_1+1)/A_2$ is fixed, $\delta_s = \Theta(g_{\min}) = \Theta(\Delta_*)$. Define $v_{\text{slow}} = \varepsilon\, \Delta_*^2/2$ as the maximal crossing velocity. In the ratio $T_{\text{unf}}/T_{\text{inf}}$, this velocity cancels because both runtimes are computed under the same RC condition. The separation therefore depends on the geometric factor $(s_R - s_L)/\Delta_*$.

Lemma 9.1.3 (Adversarial gap construction)**.** *For any $s_{\text{adv}} \in [s_L, s_R]$ and $\Delta_* > 0$, the gap function $g_{\text{adv}}(s) = \Delta_* + (s - s_{\text{adv}})^2$ belongs to $\mathcal{G}(s_L, s_R, \Delta_*)$.*

Proof. The function satisfies $g_{\text{adv}}(s_{\text{adv}}) = \Delta_*$, $g_{\text{adv}}(s) > \Delta_*$ for $s \ne s_{\text{adv}}$, and $g_{\text{adv}}(s) > 0$ for all s. □

Lemma 9.1.4 (Velocity bound for uninformed schedules)**.** *Let u be a fixed schedule that is uniformly RC-admissible on the rank-one family in Theorem 9.1.5. Then $v(s) \le v_{\text{slow}}$ for all $s \in [s_L, s_R]$, provided N is sufficiently large that $\Delta_* < \min(1 - s_R, s_L)$.*

Proof. Suppose $v(s') > v_{\text{slow}}$ for some $s' \in [s_L, s_R]$. We construct a physical Hamiltonian in the rank-one family whose gap minimum occurs at s', then apply RC-admissibility on that instance.

Since $s^* = A_1/(A_1+1)$ is a continuous, strictly increasing function of $A_1 \in (0, \infty)$ with range $(0, 1)$, there exists A_1 placing the crossing at s'. On the two-level family with solution fraction $\rho = d_0/N$, the leading-order gap minimum is $\hat{g} = 2(1 - s')\sqrt{\rho(1-\rho)}$ (Equation 5.4.9), so choosing ρ to satisfy $\hat{g} = \Delta_*$ (feasible whenever $\Delta_* \le 1 - s'$, which holds asymptotically since $\Delta_* = \Theta(2^{-n/2})$ and $s' \le s_R < 1$) produces a problem Hamiltonian H_z with crossing at s' and $g_{\min} = \Theta(\Delta_*)$. The adversary in the minimax game selects this physical Hamiltonian, not merely an abstract gap function.

Uniform RC-admissibility on this Hamiltonian gives $v(s') \le \varepsilon\, g_{\min}^2/\|H'(s')\| = \Theta(v_{\text{slow}})$. After absorbing the fixed constant factor into v_{slow}, this contradicts $v(s') > v_{\text{slow}}$. Because s' was arbitrary in $[s_L, s_R]$, the bound holds throughout the interval. □

Theorem 9.1.5 (Separation (uniformly RC-admissible class))**.** *Let T_{unf} be the minimum time over all fixed schedules that are uniformly RC-admissible for all rank-one instances whose gap minima satisfy $s^* \in [s_L, s_R]$ and $g_{\min} = \Theta(\Delta_*)$, and let T_{inf} be the corresponding optimal informed runtime (with known s^*) on the same rank-one family. Then*

$$\frac{T_{\text{unf}}}{T_{\text{inf}}} = \Omega\left(\frac{s_R - s_L}{\Delta_*}\right). \tag{9.1.1}$$

Proof. By Lemma 9.1.4, $v(s) \le v_{\text{slow}}$ for all $s \in [s_L, s_R]$. The uninformed time satisfies

$$T_{\text{unf}} = \int_0^1 \frac{ds}{v(s)} \ge \int_{s_L}^{s_R} \frac{ds}{v(s)} \ge \frac{s_R - s_L}{v_{\text{slow}}}. \tag{9.1.2}$$

The informed schedule knows s^* exactly and needs to be slow only in the crossing window of width $O(\Delta_*)$. For rank-one profiles, $\delta_s = \hat{g}/c_L = \Theta(g_{\min}) = \Theta(\Delta_*)$ by Equation 5.4.10, so Theorem 7.4.1 gives $T_{\text{inf}} = \Theta(\delta_s/v_{\text{slow}}) = \Theta(\Delta_*/v_{\text{slow}})$. The velocity factors cancel:

$$\frac{T_{\text{unf}}}{T_{\text{inf}}} = \Omega\left(\frac{s_R - s_L}{\Delta_*}\right). \tag{9.1.3}$$

□

Corollary 9.1.6 (Constant-width uncertainty family)**.** *For any n-qubit rank-one family in which the minimum gap scales as $\Delta_* = \Theta(2^{-n/2})$, the crossing uncertainty interval has constant width $s_R - s_L = \Theta(1)$, and the endpoints are bounded away from the boundaries ($\exists\, \gamma > 0$ independent of n with $\gamma \le s_L < s_R \le 1 - \gamma$), the minimax separation satisfies*

$$\frac{T_{\text{unf}}}{T_{\text{inf}}} = \Omega(2^{n/2}).$$

This corollary is a worst-case uncertainty statement. It does not apply to the standard Grover setting, where the crossing location is known a priori ($s^* = 1/2 + O(1/N)$). As a toy geometry with full uncertainty interval width $s_R - s_L = 1$ and $\Delta_* = 1/2$, the separation ratio is $(s_R - s_L)/\Delta_* = 2$. At $N = 4$, that equals $\sqrt{N}$.

The logical consequence is simple. If classical preprocessing is polynomial-time, NP-hardness forces a gap-uninformed model for fixed schedules. Inside the uniformly RC-admissible class, that model has an $\Omega(2^{n/2})$ minimax lower bound from the adversarial geometry of Lemma 9.1.3. The penalty is therefore geometric, not a byproduct of the reduction alone.

9.2 Partial Knowledge and Hedging

The separation theorem quantifies a worst case. If an adversary can place the gap minimum anywhere in $[s_L, s_R]$, the schedule must be uniformly slow. But NP-hardness does not imply that A_1 is completely unknown. The natural question is what partial knowledge is worth.

Suppose an algorithm has access to an estimate $A_{1,\text{est}}$ satisfying $|A_{1,\text{est}} - A_1| \le \varepsilon$. The uncertainty propagates to the crossing position through the map $f(x) = x/(x+1)$, whose derivative is $f'(x) = 1/(x+1)^2$.

Lemma 9.2.1 (A_1-to-s^* precision propagation)**.** *If $|A_{1,\text{est}} - A_1| \le \varepsilon$ with $|\varepsilon| \le (1 + A_1)/2$, then $|s^*_{\text{est}} - s^*| \le 2|\varepsilon|/(A_1 + 1)^2$.*

Proof. Direct computation gives the exact identity

$$s^*_{\text{est}} - s^* = \frac{A_1 + \varepsilon}{1 + A_1 + \varepsilon} - \frac{A_1}{1 + A_1} = \frac{\varepsilon}{(1 + A_1)(1 + A_1 + \varepsilon)}. \tag{9.2.1}$$

Under $|\varepsilon| \le (1 + A_1)/2$, the denominator satisfies $1 + A_1 + \varepsilon \ge (1 + A_1)/2$, so

$$|s^*_{\text{est}} - s^*| \le \frac{|\varepsilon|}{(1 + A_1) \cdot (1 + A_1)/2} = \frac{2|\varepsilon|}{(1 + A_1)^2}. \tag{9.2.2}$$

□

Given A_1 precision ε, Lemma 9.2.1 places the true crossing within radius $2\varepsilon/(A_1 + 1)^2$ of the estimate. The uncertainty interval therefore has width $W(\varepsilon) = 4\varepsilon/(A_1 + 1)^2$. Define the ε-informed gap class as $\mathcal{G}_\varepsilon = \mathcal{G}(s_L(\varepsilon), s_R(\varepsilon), \Delta_*)$, where the endpoints come from this interval. Applying Theorem 9.1.5 gives the lower bound. A matching upper bound comes from a schedule that stays uniformly slow on this interval and fast outside it.

Theorem 9.2.2 (Interpolation)**.** *For A_1 precision ε, the optimal adiabatic runtime satisfies*

$$T(\varepsilon) = \Theta\left(T_{\text{inf}} \cdot \max\left(1, \frac{\varepsilon}{\delta_{A_1}}\right)\right), \tag{9.2.3}$$

where $\delta_{A_1} = 2\sqrt{d_0 A_2/N}$ is the precision threshold for optimality.

Proof. Lower bound. For $\varepsilon \ge \delta_{A_1}$, Theorem 9.1.5 applied to $\mathcal{G}_\varepsilon$ gives $T(\varepsilon) \ge W(\varepsilon)/v_{\text{slow}}$. Taking the ratio with $T_{\text{inf}} = \Theta(\delta_s/v_{\text{slow}})$ and using the identity

$$(A_1 + 1)^2 \cdot \delta_s = (A_1 + 1)^2 \cdot \frac{2}{(A_1 + 1)^2}\sqrt{\frac{d_0 A_2}{N}} = 2\sqrt{\frac{d_0 A_2}{N}} = \delta_{A_1} \tag{9.2.4}$$

yields $T(\varepsilon)/T_{\text{inf}} \ge \Theta(\varepsilon/\delta_{A_1})$. For $\varepsilon < \delta_{A_1}$, the trivial bound $T(\varepsilon) \ge T_{\text{inf}}$ holds regardless of precision.

Upper bound. For $\varepsilon \ge \delta_{A_1}$, construct a schedule with crossing velocity $v_{\text{slow}} = \Theta(\varepsilon_{\text{ad}}\, \Delta_*^2) = \Theta(\Delta_*^2)$ throughout the uncertainty interval $[s_L(\varepsilon), s_R(\varepsilon)]$, where ε_{ad} is the fixed adiabatic error parameter from Definition 9.1.2. Use fast velocity $v_{\text{fast}} = O(1)$ outside this interval. The slow region has width $W(\varepsilon) = \Theta(\varepsilon/\delta_{A_1}) \cdot \delta_s$, so the total time is $T = W(\varepsilon)/v_{\text{slow}} + O(1) = \Theta(T_{\text{inf}} \cdot \varepsilon/\delta_{A_1})$, since $T_{\text{inf}} = \Theta(\delta_s/v_{\text{slow}})$. For $\varepsilon < \delta_{A_1}$, the optimal informed schedule achieves $T = O(T_{\text{inf}})$. □

The interpolation is linear. There is no threshold, cliff, or phase transition. At precision $1/\text{poly}(n)$ (NP-hard), the overhead is $\Theta(2^{n/2}/\text{poly}(n))$, which is close to the full exponential penalty. At precision $2^{-n/2}$ (algorithmically relevant), the overhead is $\Theta(1)$. The region between these scales is the "information gap." For the running example, the precision table is:

Precision ε	$T(\varepsilon)/T_{\text{inf}}$
$2^{-n/2}$	$\Theta(1)$
$2^{-n/4}$	$\Theta(2^{n/4})$
$1/n$	$\Theta(2^{n/2}/n)$
$1/\text{poly}(n)$	$\Theta(2^{n/2}/\text{poly}(n))$
1 (no knowledge)	$\Theta(2^{n/2})$

The interpolation theorem treats A_1 precision as a continuous resource. A complementary operational question asks for the best fixed schedule when s^* is only known to lie in an interval $[u_L, u_R]$. A hedging schedule spreads slowdown across that full interval instead of concentrating it at one point. It uses velocity v_{slow} on $[u_L, u_R]$ and v_{fast} outside, with normalization $(u_R - u_L)/v_{\text{slow}} + (1 - u_R + u_L)/v_{\text{fast}} = 1$.

Write $w = u_R - u_L$ for the interval width. The JRS error functional uses $\int \|H'\|^2 g^{-3}\, ds$. For the rank-one family, $\|H'(s)\| = O(1)$, so the effective weight is g^{-3} rather than Roland-Cerf's g^{-2}. For a piecewise-constant velocity profile, Equation 7.1.1 gives a contribution proportional to $v \cdot \int g^{-3}\, ds$ on each segment. The total error is $v_{\text{slow}} I_{\text{slow}} + v_{\text{fast}} I_{\text{fast}}$, where $I_{\text{slow}} = \int_{u_L}^{u_R} g(u)^{-3}\, du$ and $I_{\text{fast}} = \int_{[0,1]\setminus[u_L,u_R]} g(u)^{-3}\, du$. Because the crossing lies in the slow region, $I_{\text{slow}} \gg I_{\text{fast}}$.

Theorem 9.2.3 (Hedging)**.** *Let $R = I_{\text{slow}}/I_{\text{fast}} \gg 1$. Under normalization $T = 1$, the optimal hedging schedule for interval $[u_L, u_R]$ achieves $\text{Error}_{\text{hedge}}/\text{Error}_{\text{uniform}} \to u_R - u_L$ as $R \to \infty$, with optimal slow velocity $v_{\text{slow}} = w + \sqrt{(1-w)w/R}$.*

Proof. Write $w = u_R - u_L$ for the interval width. The normalization constraint $w/v_{\text{slow}} + (1-w)/v_{\text{fast}} = 1$ fixes the total time $T = 1$, so the JRS error integral of Equation 7.1.1 reduces to $E = v_{\text{slow}} I_{\text{slow}} + v_{\text{fast}} I_{\text{fast}}$. The constraint gives

$$v_{\text{fast}} = \frac{(1-w)\, v_{\text{slow}}}{v_{\text{slow}} - w}, \tag{9.2.5}$$

valid for $v_{\text{slow}} > w$. Substituting into the error gives

$$E(v_{\text{slow}}) = v_{\text{slow}}\, I_{\text{slow}} + \frac{(1-w)\, v_{\text{slow}}}{v_{\text{slow}} - w}\, I_{\text{fast}}. \tag{9.2.6}$$

Differentiating with respect to v_{slow} and setting to zero:

$$\frac{dE}{dv_{\text{slow}}} = I_{\text{slow}} - \frac{(1-w)\, w\, I_{\text{fast}}}{(v_{\text{slow}} - w)^2} = 0. \tag{9.2.7}$$

Solving yields $(v_{\text{slow}} - w)^2 = (1-w)\, w\, I_{\text{fast}}/I_{\text{slow}} = (1-w)\, w/R$, so

$$v_{\text{slow}} = w + \sqrt{(1-w)\, w/R}. \tag{9.2.8}$$

At this optimum, $v_{\text{fast}} = (1-w)\, v_{\text{slow}}/\sqrt{(1-w)\, w/R} = \sqrt{R\, w\, (1-w)} + (1-w)$. The optimal error, substituting $v_{\text{slow}} - w = \sqrt{(1-w)\, w/R}$, is

$$E_{\text{opt}} = \left(w + \sqrt{(1-w)\, w/R}\right) I_{\text{slow}} + \left(\sqrt{R\, w\, (1-w)} + (1-w)\right) I_{\text{fast}}. \tag{9.2.9}$$

Since $R = I_{\text{slow}}/I_{\text{fast}} \gg 1$, the terms involving $\sqrt{R}$ contribute $2\sqrt{w\,(1-w)\, I_{\text{slow}}\, I_{\text{fast}}} = o(I_{\text{slow}})$, and the dominant term is $w\, I_{\text{slow}}$, while the uniform error is $E_{\text{unif}} = I_{\text{slow}} + I_{\text{fast}} \approx I_{\text{slow}}$. Therefore $E_{\text{opt}}/E_{\text{unif}} \to w = u_R - u_L$ as $R \to \infty$. □

For an uncertainty interval $[0.4, 0.8]$, the hedging schedule achieves $E_{\text{opt}}/E_{\text{unif}} = 0.4$ compared to a uniform schedule at the same total runtime. That is a 60% reduction in transition probability. Bounded uncertainty about s^* therefore yields a constant-factor improvement proportional to interval width, not an exponential overhead. In the taxonomy of section 9.7, this is Level 2.

9.3 Quantum Bypass

The separation theorem and the interpolation theorem characterize the cost of ignorance within the fixed-schedule model. An adiabatic device, however, is a physical system that can be measured during execution. Our work in [10] asks a concrete question: Can this limitation be overcome when one only has access to a device operating in the adiabatic setting?

The answer is yes in an adaptive measurement model. Han, Park, and Choi [87] independently proposed a constant geometric speed (CGS) schedule that traverses the eigenstate path at uniform arc length, using on-the-fly overlap estimates from quantum Zeno Monte Carlo to adjust the velocity. Their method improves the gap scaling from $O(\Delta_*^{-2})$ to $O(\Delta_*^{-1})$ and numerically preserves the quadratic speedup for adiabatic unstructured search without prior spectral knowledge. The binary-search protocol below uses a different mechanism. It first locates the crossing through branch probes and then runs the informed schedule. In the ideal decision-probe model, it achieves $O(T_{\text{inf}})$.

NP-hardness bundles two different tasks. *Computing* s^* from the classical description of H_z is hard. *Detecting* s^* by probing the quantum system $H(s)$ at selected parameter values can be efficient. We model this with a binary decision-probe oracle. A probe at parameter value s returns whether s is at-or-left of the true crossing or to its right (ties go left), and each probe costs $O(1/g(s))$.

Definition 9.3.1 (Binary decision probe)**.** *For an instance H, let $D_H : [0,1] \to \{0,1\}$ be the idealized oracle*

$$D_H(s) = \begin{cases} 0, & s \le s^*(H), \\ 1, & s > s^*(H), \end{cases}$$

with probe cost $O(1/g_H(s))$.

Definition 9.3.2 (Adaptive adiabatic protocol)**.** *The protocol operates in two phases.*

Phase 1 (Location). *Initialize $s_{\text{lo}} = 0$, $s_{\text{hi}} = 1$. For $i = 1, \ldots, \lceil n/2 \rceil$:*

1. *Set $s_{\text{mid}} = (s_{\text{lo}} + s_{\text{hi}})/2$.*
2. *Query $D_H(s_{\text{mid}})$.*
3. *If $D_H(s_{\text{mid}}) = 0$ (at or left of crossing), set $s_{\text{lo}} = s_{\text{mid}}$.*
4. *If $D_H(s_{\text{mid}}) = 1$ (right of crossing), set $s_{\text{hi}} = s_{\text{mid}}$.*

After $\lceil n/2 \rceil$ iterations, s^* is located to precision $O(2^{-n/2})$.

Phase 2 (Execution). *Reset the state to $|\psi_0\rangle$. Evolve from $s = 0$ to $s = 1$ using the informed local schedule of Theorem 7.4.1, with the crossing position estimated in Phase 1.*

Lemma 9.3.3 (Decision-probe cost)**.** *Each call to $D_H(s_{\text{mid}})$ costs $O(1/g(s_{\text{mid}}))$.*

Proof. Immediate from Definition 9.3.1. □

Lemma 9.3.4 (Phase 1 cost)**.** *The total time for Phase 1 is $O(T_{\text{inf}})$.*

Proof. Let $d_i = |s_{\text{mid},i} - s^*|$ be the distance from the i-th midpoint to the true crossing. Chapter 6 gives two complementary bounds. Outside the crossing window ($|s - s^*| > \delta_s$), the gap satisfies

$$g(s) \ge c_{\min} |s - s^*|,$$

where $c_{\min} = \min(c_L, c_R)$ with $c_L = A_1(A_1+1)/A_2$ and $c_R = \Delta/30$. Both constants are positive and independent of n. Inside the crossing window ($|s - s^*| \le \delta_s$), the gap satisfies $g(s) \ge g_{\min}$. Because $g_{\min}$ is the global minimum, these two bounds combine to

$$g(s_{\text{mid},i}) \ge \max(g_{\min},\ c_{\min} \cdot d_i). \tag{9.3.1}$$

The probe cost at iteration i is therefore

$$O\left(\frac{1}{g(s_{\text{mid},i})}\right) \le O\left(\min\left(\frac{1}{g_{\min}},\ \frac{1}{c_{\min} \cdot d_i}\right)\right). \tag{9.3.2}$$

The two bounds in (9.3.2) cross at $d_i = g_{\min}/c_{\min}$. Since $g_{\min} = c_L \delta_s \cdot (1 - O(\eta))$ and $c_{\min} \le c_L$, the crossover distance satisfies

$$d_{\text{cross}} = g_{\min}/c_{\min} = (c_L/c_{\min})\, \delta_s \ge \delta_s.$$

The ratio $c_L/c_{\min}$ is a positive constant independent of n because $c_L = A_1(A_1+1)/A_2$ and $c_R = \Delta/30$ are fixed by spectral parameters. Therefore $c_{\min} = \min(c_L, c_R) > 0$ is also fixed. At most $O(\log(c_L/c_{\min}) + 1) = O(1)$ binary-search midpoints can fall in the near regime $d_i \le d_{\text{cross}}$.

Group the $\lceil n/2 \rceil$ iterations by the distance d_i in dyadic shells $S_j = [2^{-j-1}, 2^{-j}]$. Let $L_i = 2^{-i+1}$ be the binary-search interval width at step i. Since the next interval is the half containing s^*, the midpoint distances obey

$$d_{i+1} = \left| d_i - \frac{L_i}{4} \right| = \left| d_i - 2^{-i-1} \right|.$$

This recurrence gives $O(1)$ occupancy per shell: for $i > j+1$, $d_i \leq L_i/2 = 2^{-i} < 2^{-j-1}$, so $d_i \notin S_j$; and for $i \leq j$, if $d_i \in (2^{-j-1}, 2^{-j})$, then $d_{i+1} \notin (2^{-j-1}, 2^{-j})$. Thus the shell interior is visited at most once, with only a dyadic-rational edge case where the boundary value 2^{-j-1} can appear twice consecutively. Hence each shell contributes $O(1)$ midpoint queries.

Far shells ($j < \log_2(1/\delta_s) \approx n/2$): here $d_i > \delta_s$, so the binding bound in (9.3.2) is $O(1/(c_{\min} \cdot d_i)) = O(2^j/c_{\min})$, where $c_{\min}$ enters the implicit constant.

Near shells ($j \geq n/2$): here $d_i \leq \delta_s$, so the binding bound is $O(1/g_{\min}) = O(1/\Delta_*) = O(2^{n/2})$.

There are $O(1)$ near shells because at most $O(1)$ midpoints can satisfy $d_i \leq d_{\text{cross}}$ in a binary search. The total cost is

$$\sum_{j=0}^{n/2-1} O(1) \cdot O(2^j) + O(1) \cdot O(2^{n/2}) = O(2^{n/2}) + O(2^{n/2}) = O(2^{n/2}) = O(T_{\text{inf}}). \tag{9.3.3}$$

The state preparation cost is $O(n)$ per iteration and $O(n)$ iterations, giving $O(n^2) = o(T_{\text{inf}})$. □

Theorem 9.3.5 (Adaptive adiabatic optimality in the decision-probe model)**.** *The adaptive protocol of Definition 9.3.2 achieves runtime $T_{\text{adapt}} = O(T_{\text{inf}})$ with $\Theta(n)$ measurements.*

Proof. Phase 1 locates s^* to precision $O(2^{-n/2}) = O(\delta_s)$ using total time $O(T_{\text{inf}})$ by Lemma 9.3.4. This precision is within the crossing window width $\delta_s = O(\Delta_*)$. Phase 2 has time $O(T_{\text{inf}})$ by Theorem 7.4.1, since the estimate of s^* is accurate to $O(\delta_s)$. The total is $O(T_{\text{inf}}) + O(T_{\text{inf}}) = O(T_{\text{inf}})$. □

Theorem 9.3.6 (Measurement lower bound)**.** *Any adaptive algorithm in the binary decision-probe model (each measurement returns one bit indicating the ground/excited branch at the probe point) achieving $T = O(T_{\text{inf}})$ requires $\Omega(n)$ measurements.*

Proof. The crossing position s^* can lie anywhere in an interval of width $\Theta(1)$. To achieve the informed runtime, the algorithm must locate s^* to precision $\delta_s = O(2^{-n/2})$, since any larger uncertainty incurs the overhead of Theorem 9.2.2. This means distinguishing among $\Omega(2^{n/2})$ possible positions. In the binary decision-probe model, each measurement contributes at most one bit by definition. The information needed is $\log_2(2^{n/2}) = n/2$ bits, requiring $\Omega(n)$ measurements. □

The three adiabatic regimes are:

Strategy	Runtime	Measurements
Fixed, uninformed	$\Omega(2^{n/2} \cdot T_{\text{inf}})$	0
Adaptive	$O(T_{\text{inf}})$	$\Theta(n)$
Fixed, informed	$O(T_{\text{inf}})$	0

For the running example ($N = 4$, $d_0 = 1$, $n = 2$), Phase 1 performs $\lceil 1 \rceil = 1$ probe at $s_{\text{mid}} = 0.5$, so the location stage already achieves width $1/2 = O(2^{-n/2})$. The gap at that point is $g(0.5) = 1/\sqrt{N} = 1/2$, which gives probe cost $O(1/g) = O(2) = O(T_{\text{inf}})$.

Implementation note. A physical instantiation of D_H can be attempted via phase-estimation-based branch tests on $H(s_{\text{mid}})$. The theorem above is intentionally stated in the ideal decision-probe model; a full finite-sample reliability analysis for this instantiation is separate from the present minimax argument.

The adaptive protocol acquires A_1 through measurement, while the circuit model bypasses A_1 entirely. The Dürr-Høyer minimum-finding algorithm [35] achieves $\Theta(\sqrt{N/d_0})$ by maintaining a threshold and iteratively lowering it with Grover search. It never traverses an adiabatic path and never encounters an avoided crossing. Its mechanism is amplitude amplification with iterative thresholding and no spectral inputs. It needs no A_1, no s^*, no Δ, and no gap profile.

Proposition 9.3.7 (A_1-blindness)**.** *Let X_{DH} denote the output of the amplified Dürr-Høyer algorithm (with $r = \Theta(n)$ repetitions). Then $I(X_{\text{DH}}; A_1 \mid S_0, E_0) \leq 2^{-\Omega(n)}$. Conditioned on success ($X_{\text{DH}} \in S_0$), the mutual information is exactly zero.*

Proof. Two problem Hamiltonians H_z, H'_z are ground-equivalent if they share the same ground energy E_0 and ground space S_0. By symmetry of Grover's algorithm applied to the uniform initial state, the output distribution conditioned on success is Uniform(S_0), regardless of the excited spectrum. Since A_1 depends only on the excited spectrum (via $\{d_k, E_k\}_{k\geq 1}$), we have

$$I(X_{\mathrm{DH}};\, A_1 \mid \text{success}, S_0, E_0) = 0.$$

Let F be the failure indicator of the amplified routine, and fix any prior over ground-equivalent instances conditioned on (S_0, E_0). With $r = \Theta(n)$ repetitions using Boyer-Brassard-Høyer-Tapp amplification [36], the per-trial success probability is at least $2/3$, so

$$p_f := \Pr[F = 1] \leq (1/3)^r = 2^{-\Omega(n)}.$$

Using chain rule and the fact that F is a function of X_{DH}:

$$\begin{aligned} I(X_{\mathrm{DH}};\, A_1 \mid S_0, E_0) &\leq I(X_{\mathrm{DH}}, F;\, A_1 \mid S_0, E_0) \\ &= I(F;\, A_1 \mid S_0, E_0) + I(X_{\mathrm{DH}};\, A_1 \mid F, S_0, E_0) \\ &= I(F;\, A_1 \mid S_0, E_0) + p_f\, I(X_{\mathrm{DH}};\, A_1 \mid F = 1, S_0, E_0) \\ &\leq H(F) + p_f\, H(X_{\mathrm{DH}} \mid F = 1, S_0, E_0). \end{aligned} \tag{9.3.4}$$

The $F = 0$ term vanishes by the conditional independence established above. Now $H(F) \leq h_2(p_f)$, where $h_2(p) = -p \log p - (1-p)\log(1-p)$ is the binary entropy, and $H(X_{\mathrm{DH}} \mid F = 1, S_0, E_0) \leq \log N = n$, so Eq. (9.3.4) gives

$$I(X_{\mathrm{DH}};\, A_1 \mid S_0, E_0) \leq h_2(p_f) + p_f n = 2^{-\Omega(n)}.$$

□

The circuit model does not merely avoid computing A_1. It is provably blind to it. The fixed adiabatic model, by contrast, both requires and leaks information about A_1. A schedule tuned to one value of A_1 performs poorly on ground-equivalent instances with different excited spectra. The adaptive adiabatic model lies between these extremes. It acquires A_1 through $O(n)$ measurements and pays $O(T_{\mathrm{inf}})$ to do so. The three models therefore form a clear hierarchy of spectral information usage, from blindness (circuit) through acquisition (adaptive) to fixed dependence (non-adaptive adiabatic).

The adaptive protocol relies on the rank-one gap profile, which grows linearly away from the crossing ($\alpha = 1$). That linear growth is exactly what makes binary search informative: at distance d from the crossing, the gap is $\Theta(d)$, so a probe costs $O(1/d)$ and the geometric sum converges. The next question is what changes when the gap approaches its minimum more gently.

9.4 Gap Geometry and Schedule Optimality

The flatness exponent α parametrizes how the gap approaches its minimum. Outside the crossing window, write $g(s) \approx c|s - s^*|^\alpha$. For rank-one profiles, $\alpha = 1$, and runtime scales as $O(1/\Delta_*)$. Flatter profiles with $\alpha > 1$ are worse.

Guo and An [46] identified a measure condition that guarantees $O(1/g_{\min})$ for the $p = 3/2$ power-law schedule. Here we prove the complementary statement. When $\alpha > 1$, that condition fails, and the same variationally optimal schedule degrades from $T = O(1/\Delta_*)$ to $T = O(1/\Delta_*^{3-2/\alpha})$.

Whether some non-power-law fixed schedule can still recover $O(1/\Delta_*)$ in this regime remains open. The constant geometric speed approach of Han, Park, and Choi [87] reaches $O(1/g_{\min})$ by adaptive gap measurements, but that method uses runtime feedback and is not fixed. For fixed non-adaptive schedules, no family is known to beat $O(1/\Delta_*^{3-2/\alpha})$ when $\alpha > 1$.

Consider a gap function with flatness exponent $\alpha > 0$. Near the minimum, write $g(s) = \Delta_* + c|s - s^*|^\alpha$ for some constant $c > 0$. The measure condition asks for $\mu(\{s : g(s) \leq x\}) \leq Cx$ for all $x > 0$, with C independent of Δ_*.

Theorem 9.4.1 (Geometric characterization)**.** *The measure condition holds with C independent of Δ_* if and only if $\alpha \leq 1$.*

Proof. For $x \geq \Delta_*$, the sublevel set $\{s : g(s) \leq x\}$ near s^* has measure $\mu = 2((x - \Delta_*)/c)^{1/\alpha}$.

Case $\alpha \le 1$. The ratio $\mu/x = 2((x-\Delta_*)/c)^{1/\alpha}/x$ is increasing in x when $\alpha \le 1$. Differentiating gives

$$\frac{d(\mu/x)}{dx} = \frac{2}{c^{1/\alpha}\alpha x^2}\left(\frac{x-\Delta_*}{c}\right)^{1/\alpha-1}\left(\left(\frac{1}{\alpha}-1\right)(x-\Delta_*)+\frac{\Delta_*}{\alpha}\right),$$

and both terms in the last parentheses are nonnegative because $1/\alpha - 1 \ge 0$ and $\Delta_* > 0$. Now μ is capped by 1 (the measure of $[0,1]$), and the cap is reached at $x_{\text{cap}} = \Delta_* + c(1/2)^\alpha$, where the sublevel set spans $[0,1]$. For $x > x_{\text{cap}}$, we have $\mu/x = 1/x < 1/x_{\text{cap}}$. Hence

$$C = \sup_{x>0}\frac{\mu}{x} \le \frac{1}{x_{\text{cap}}} \le \frac{2^\alpha}{c},$$

independent of Δ_*.

Case $\alpha > 1$. At $x = 2\Delta_*$, the ratio is $\mu/x = 2(\Delta_*/c)^{1/\alpha}/(2\Delta_*) = c^{-1/\alpha}\Delta_*^{1/\alpha-1}$. Since $1/\alpha - 1 < 0$, this diverges as $\Delta_* \to 0$. No finite C works for all Δ_*. □

The gap integral $\int_0^1 g(s)^{-\beta}\,ds$ controls the runtime for power-law schedules. A substitution $u = c|s-s^*|^\alpha/\Delta_*$ gives the following scaling.

Lemma 9.4.2 (Gap integral)**.** *For* $\beta > 1/\alpha$,

$$\int_0^1 g(s)^{-\beta}\,ds = \Theta(\Delta_*^{1/\alpha-\beta}). \tag{9.4.1}$$

For $\beta = 1/\alpha$, *the integral is* $\Theta(\log(1/\Delta_*))$. *For* $\beta < 1/\alpha$, *the integral is* $\Theta(1)$.

Proof. The substitution $u = (c|s-s^*|^\alpha)/\Delta_*$ transforms the near-minimum contribution to

$$\Delta_*^{1/\alpha-\beta}\int_0^U u^{1/\alpha-1}(1+u)^{-\beta}\,du,$$

where $U = \Theta(1/\Delta_*)$. As $u \to \infty$, the integrand behaves like $u^{1/\alpha-1-\beta}$.

If $\beta > 1/\alpha$, the exponent is strictly less than -1, so the u-integral converges to a finite constant, yielding $\Theta(\Delta_*^{1/\alpha-\beta})$.

If $\beta = 1/\alpha$, the integrand is asymptotically u^{-1}, so the integral contributes $\Theta(\log U) = \Theta(\log(1/\Delta_*))$.

If $\beta < 1/\alpha$, the integral grows as $U^{1/\alpha-\beta}$, which cancels the prefactor $\Delta_*^{1/\alpha-\beta}$, giving $\Theta(1)$.

The contribution from outside a neighborhood of s^* is always $O(1)$. For fixed δ, if $|s-s^*| \ge \delta$ then $g(s) \ge g_0 > 0$ independently of Δ_*, so $\int_{|s-s^*|\ge\delta} g(s)^{-\beta}ds \le g_0^{-\beta}$. □

Theorem 9.4.3 (Scaling spectrum)**.** *For a gap function with flatness exponent* $\alpha > 2/3$, *the adiabatic runtime with the* $p = 3/2$ *power-law schedule (variationally optimal in the JRS framework [46]) satisfies*

$$T = \Theta(1/\Delta_*^{3-2/\alpha}). \tag{9.4.2}$$

Proof. The power-law schedule $u'(s) = c_p\,g(u(s))^p$ has normalization constant $c_p = \int_0^1 g(v)^{-p}\,dv$. The JRS error functional becomes

$$\eta \le \frac{1}{T}\,c_p\int_0^1 g(v)^{p-3}\,dv. \tag{9.4.3}$$

By Lemma 9.4.2, $c_p = \Theta(\Delta_*^{1/\alpha-p})$ (requiring $p > 1/\alpha$) and the second integral is $\Theta(\Delta_*^{1/\alpha+p-3})$ (requiring $3-p > 1/\alpha$). Together these require $1/\alpha < p < 3 - 1/\alpha$, an interval of width $3 - 2/\alpha$, which is positive if and only if $\alpha > 2/3$. The symmetric choice $p = 3/2$ lies in this interval for all $\alpha > 2/3$. Their product is

$$c_p\int g^{p-3}\,dv = \Theta(\Delta_*^{(1/\alpha-p)+(1/\alpha+p-3)}) = \Theta(\Delta_*^{2/\alpha-3}). \tag{9.4.4}$$

Setting $\eta = O(1)$ gives $T = \Omega(\Delta_*^{-(3-2/\alpha)}) = \Omega(1/\Delta_*^{3-2/\alpha})$. The $p = 3/2$ power-law schedule achieves this scaling, giving a matching upper bound $T = O(1/\Delta_*^{3-2/\alpha})$. □

α	Exponent $\gamma = 3 - 2/\alpha$	Measure condition	Runtime
1	1	Holds	$\Theta(1/\Delta_*)$
2	2	Fails	$\Theta(1/\Delta_*^2)$
3	7/3	Fails	$\Theta(1/\Delta_*^{7/3})$
∞	3	Fails	$\Theta(1/\Delta_*^3)$

The runtime exponents form a continuous spectrum from 1 (V-shaped minimum, best case) to 3 (flat minimum, worst case), refuting any binary dichotomy between "easy" and "hard" gap profiles. For the running example ($M = 2$, $d_0 = 1$, $N = 4$), $\alpha = 1$ and $\gamma = 1$, confirming the optimal $T = \Theta(1/\Delta_*)$ scaling.

Remark. *The exponent $\gamma = 3$ at $\alpha = \infty$ reflects the $p = 3/2$ power-law schedule, which is variationally optimal within the JRS error functional but not universally optimal across all adiabatic bounds. The Roland-Cerf schedule ($p = 2$) gives $T = O(1/\Delta_*^2)$ at $\alpha = \infty$ via a tighter adiabatic condition for flat gaps. The table shows the scaling of the JRS-optimal schedule as the gap flattens; different schedule families and adiabatic bounds produce different exponent curves.*

Proposition 9.4.4 (Structural $\alpha = 1$)**.** *For the rank-one Hamiltonian $H(s) = -(1-s)\,|\psi_0\rangle\langle\psi_0| + sH_z$ with $d_1 \geq 1$ and $\Delta > 0$, the flatness exponent is $\alpha = 1$.*

Proof. Near s^*, the two lowest eigenvalues form an avoided crossing described by the standard formula $g(s) = \sqrt{g_{\min}^2 + c_L^2(s - s^*)^2}$. For $|s - s^*| \gg g_{\min}/c_L = \delta_s$, the gap grows linearly: $g(s) \approx c_L|s - s^*|$. The crossing is simple (not higher-order) because the coupling between the two lowest branches is proportional to $|\langle\psi_0|\,\phi_1\rangle|^2 = d_1/N > 0$, where $|\phi_1\rangle$ is the symmetric state of the first excited level. A higher-order crossing ($\alpha > 1$) would require this coupling to vanish, which cannot happen when $d_1 > 0$. □

No choice of H_z with $d_1 > 0$ and $\Delta > 0$ can produce $\alpha \neq 1$. To get different values of α, one must change the interpolation scheme. Examples include quantum phase transitions with $H(s)$ nonlinear in s or systems with symmetry-enforced higher-order crossings. This structural $\alpha = 1$ explains why both the Roland-Cerf analysis and the Guo-An framework achieve the same asymptotic runtime.

Braida et al. [10] and Guo and An [46] are independent works on the same problem class. The former provides the spectral analysis (A_1, s^*, piecewise gap bounds), while the latter provides the variational optimization (power-law schedule, measure condition).

Theorem 9.4.5 (Measure condition for the rank-one gap profile)**.** *Under the spectral condition of Chapter 5, the piecewise-linear gap profile satisfies the measure condition with*

$$C \leq \frac{3A_2}{A_1(A_1+1)} + \frac{30(1-s_0)}{\Delta}, \tag{9.4.5}$$

where s_0 is the right-arm basepoint defined in Chapter 6.

Proof. Fix $x > 0$. For $x < g_{\min}$, the sublevel set is empty. For $x \geq g_{\min}$, bound each region of the piecewise gap profile separately.

The left arm satisfies $g(s) \geq c_L(s^* - s)$ and contributes at most x/c_L. The crossing window has width $2\delta_s = 2\hat{g}/c_L$. If $x \geq \hat{g}$, this contributes at most $2x/c_L$. If $g_{\min} \leq x < \hat{g}$, use $g_{\min} \geq (1-2\eta)\hat{g}$ and $x \geq g_{\min}$ to get $\hat{g} \leq x/(1-2\eta)$. For $\eta \leq 1/6$, this implies $\hat{g} \leq 3x/2$, so the window contribution is at most $2\hat{g}/c_L \leq 3x/c_L$. The condition $\eta \leq 1/6$ holds asymptotically because $\eta = O(\sqrt{d_0/(NA_2)}) \to 0$.

The right arm satisfies $g(s) \geq c_R(s - s_0)/(1 - s_0)$ and contributes at most $x \cdot 30(1-s_0)/\Delta$. Adding the three contributions and substituting $c_L = A_1(A_1+1)/A_2$ gives the stated bound. □

Corollary 9.4.6 (Grover measure constant)**.** *For Grover ($M = 2$, $d_0 = 1$, $d_1 = N - 1$, $E_0 = 0$, $E_1 = 1$), the exact measure constant is $C = 1$.*

Proof. The exact gap is $g(s)^2 = (2s-1)^2(1 - 1/N) + 1/N$. Solving $g(s) \leq x$ gives

$$\mu(\{g \leq x\}) = \sqrt{\frac{Nx^2 - 1}{N - 1}}$$

for $x \in [1/\sqrt{N}, 1]$, with $\mu = 1$ for $x > 1$. The ratio μ/x is increasing on $[1/\sqrt{N}, 1]$ and equals 1 at $x = 1$. □

For the Grover problem, the exact gap integral is $\int_0^1 g(s)^{-2}\,ds = (N/\sqrt{N-1})\arctan\sqrt{N-1} \to (\pi/2)\sqrt{N}$ as $N \to \infty$. This closed-form evaluation confirms the $O(\sqrt{N})$ runtime from the piecewise analysis and provides the exact constant. For the running example ($N = 4$), $\int_0^1 g(s)^{-2}\,ds = (4/\sqrt{3})\arctan\sqrt{3} = 4\pi/(3\sqrt{3}) \approx 2.42$, consistent with the runtime $T_{\text{inf}} = O(\sqrt{4}) = O(2)$.

Both the Roland-Cerf $p = 2$ schedule and Guo-An's $p = 3/2$ schedule achieve the same asymptotic runtime $T = O(\sqrt{N/d_0}/\varepsilon)$. As declared at the start of this chapter, all spectral parameters A_1, A_2, and Δ are absorbed into the implicit constant. The RC runtime involves the integral $I = \int_0^1 g(s)^{-2}\,ds$, while Guo-An's bound involves $C^2/g_{\min}$.

Theorem 9.4.7 (Constant comparison)**.** *Write $a = 3/c_L$ and $r = 30(1 - s_0)/\Delta$. Then $C^2 < I$ if and only if $(c_L - 1)r^2 - 2ar + a(1 - a) > 0$. In the right-arm-dominated regime ($r \gg a$) with $c_L > 1$, this holds, with $C^2/I \to 1/c_L = A_2/(A_1(A_1 + 1))$.*

Proof. With $C = a + r$ and $I = a + r^2 c_L$, we obtain

$$I - C^2 = (c_L - 1)r^2 - 2ar + a(1 - a).$$

For $c_L > 1$ and $r \gg a$, the leading term $(c_L - 1)r^2$ dominates. □

Remark. *The framework comparison extends across gap geometries. For $\alpha < 1$, the Roland-Cerf integral $\int g^{-2}\, ds = \Theta(g_{\min}^{1/\alpha - 2})$ grows slower than $1/g_{\min}$, making the RC analysis tighter. For $\alpha = 1$, both give $\Theta(1/g_{\min})$, and the JRS constant C^2 can be smaller than the RC integral I (Theorem 9.4.7). For $\alpha > 1$, the measure constant $C \to \infty$ as $g_{\min} \to 0$, so the JRS framework degrades and only the RC analysis applies. The structural $\alpha = 1$ (Proposition 9.4.4) sits at the exact boundary where both frameworks are valid and neither uniformly dominates.*

For the Grover problem, $c_L \to 2$ as $N \to \infty$. Using the exact values $C_{\text{exact}} = 1$ and $I_{\text{exact}} \to (\pi/2)\sqrt{N}$ gives $C^2/I \to 2/(\pi\sqrt{N}) \to 0$, so the JRS certification is asymptotically tighter. This comparison is unusually explicit because the Grover gap has a closed form.

For structured Hamiltonians with richer spectra, exact constants are rarely analytic, and Theorem 9.4.7 becomes the practical tool. For example, evaluate it on the open ferromagnetic Ising chain from Equation 5.1.4 with nearest-neighbor coupling $J = 1$, uniform field $h = 1$, and $n = 10$ spins. This gives $C^2/I = 0.71$. The JRS advantage remains, but with a weaker margin than in Grover.

The two frameworks are best viewed as complementary. The spectral analysis [10] identifies A_1, s^*, and the piecewise gap structure, while the variational analysis [46] identifies the optimal power-law exponent. Together they give a complete account of the rank-one $\alpha = 1$ case, which sits exactly at the boundary where both frameworks apply and the measure condition remains bounded.

This complementarity persists under partial spectral knowledge. The RC framework ($p = 2$) builds the schedule from crossing position s^*, so its runtime degrades on the crossing-localization scale:

$$T_{\text{RC}}(\varepsilon_{A_1}) = T_{\text{RC},\infty} \cdot \Theta\left(\max\left(1, \frac{\varepsilon_{A_1}}{\delta_{A_1}}\right)\right),$$

where $\delta_{A_1} = 2\sqrt{d_0 A_2/N}$ is the threshold from Theorem 9.2.2. The JRS framework ($p = 3/2$) instead uses certified bounds (C_+, g_-) on the measure constant and minimum gap, leading to multiplicative overhead

$$\frac{(1 + \delta_C/C)^2}{1 - \delta_g/g_{\min}},$$

where δ_C and δ_g are estimation errors. The sensitivity profiles are therefore different: RC needs exponentially precise localization of s^*, while JRS needs only constant relative accuracy in C and $g_{\min}$. In the partial-information regime forced by NP-hardness, this can make JRS more robust in practice even though both methods share the same asymptotic scaling.

The gap geometry and optimality analysis above assumes the rank-one interpolation

$$H(s) = -(1 - s)\,|\psi_0\rangle\langle\psi_0| + sH_z.$$

The rank-one structure is a design choice, not a physical constraint. Can a different design, with a different initial state, ancilla qubits, or a multi-segment path, avoid the A_1 dependence entirely?

9.5 Anatomy of the Barrier

No instance-independent modification within the rank-one framework can make s^* spectrum-independent. We now close the obvious escape routes one by one. The order matters. We start with the weakest modification and end with the most general path redesign, then combine the four obstructions into a single no-go statement.

Recall from Chapter 5 that for any initial state $|\psi\rangle \in \mathbb{C}^N$, the weights $w_k(\psi) = \sum_{z \in \Omega_k} |\langle z|\psi\rangle|^2$ determine $A_1^{\text{eff}}(\psi) = \sum_{k \geq 1} w_k(\psi)/(E_k - E_0)$ and therefore $s^*(\psi) = A_1^{\text{eff}}(\psi)/(A_1^{\text{eff}}(\psi) + 1)$. For the uniform superposition $|\psi_0\rangle$, we recover $w_k = d_k/N$ and $A_1^{\text{eff}} = A_1$.

Theorem 9.5.1 (Product ancilla invariance)**.** *For any product initial state $|\Psi\rangle = |\psi_0\rangle \otimes |\phi\rangle$ and uncoupled final Hamiltonian $H_f = H_z \otimes I_{2^m}$, the extended Hamiltonian $H_{\text{ext}}(s) = -(1 - s)\,|\Psi\rangle\langle\Psi| + s(H_z \otimes I_{2^m})$ has the same crossing position $s^* = A_1/(A_1 + 1)$ as the bare system.*

Proof. Decompose the extended Hilbert space $\mathbb{C}^N \otimes \mathbb{C}^{2^m}$ into the subspace $\mathcal{V}_\phi = \mathbb{C}^N \otimes |\phi\rangle$ and its orthogonal complement. States $|z\rangle \otimes |a\rangle$ with $\langle\phi\rangle\, a = 0$ satisfy $\langle\Psi\rangle\, z, a = 0$, so they are exact eigenstates of $H_{\text{ext}}(s)$ with eigenvalue $sE(z)$. These $N(2^m - 1)$ states do not participate in the avoided crossing. On $\mathcal{V}_\phi$, the restriction of $H_{\text{ext}}(s)$ is unitarily equivalent to the bare Hamiltonian $H(s)$ via the map $|\psi\rangle \otimes |\phi\rangle \mapsto |\psi\rangle$. □

Remark. *The crossing position is invariant, but the gap of $H_{\text{ext}}(s)$ is strictly smaller than the bare gap: for $d_0 = 1$, the extra eigenvalues at sE_0 (from states $|z\rangle \otimes |a\rangle$ with $z \in \Omega_0$, $a \perp |\phi\rangle$) sit between the ground eigenvalue $\lambda_0(s) < sE_0$ and the crossing branch. Uncoupled ancillas make the gap worse, not better.*

This first result is already instructive. Extra qubits by themselves do not move the bottleneck. They only add spectators and can even shrink the usable gap. The next route is therefore to change the initial state itself while keeping the algorithm instance-independent.

Theorem 9.5.2 (Universality of uniform superposition)**.** *Among all states $|\psi\rangle \in \mathbb{C}^N$, the uniform superposition $|\psi_0\rangle$ is the unique state (up to per-basis-element phases) for which the weights $w_k(\psi)$ depend only on $\{E_k, d_k\}$ and not on the specific assignment of energies to computational basis states.*

Proof. An energy assignment is a function $\sigma : \{0, \ldots, N-1\} \to \{E_0, \ldots, E_{M-1}\}$ with $|\sigma^{-1}(E_k)| = d_k$. The weights under assignment σ are $w_k(\psi, \sigma) = \sum_{z:\sigma(z)=E_k} |\langle z\rangle\, \psi|^2$. We require $w_k(\psi, \sigma) = w_k(\psi, \sigma')$ for all assignments σ, σ' with the same degeneracies.

Any two such assignments are related by a permutation π of $\{0, \ldots, N-1\}$. The condition becomes $\sum_{z\in\Omega_k} |\langle z\rangle\, \psi|^2 = \sum_{z\in\Omega_k} |\langle \pi^{-1}(z)\rangle\, \psi|^2$ for all k and all permutations π.

Necessity. Consider two-level spectra with $d_0 = 1$. For any two basis states z_a, z_b, the transposition swapping them maps the assignment σ (with $\sigma(z_a) = E_0$) to σ' (with $\sigma'(z_b) = E_0$). The condition forces $|\langle z_a\rangle\, \psi|^2 = |\langle z_b\rangle\, \psi|^2$. Since z_a, z_b are arbitrary, $|\langle z\rangle\, \psi|^2 = 1/N$ for all z.

Sufficiency. If $|\langle z\rangle\, \psi|^2 = 1/N$ for all z, then $w_k = d_k/N$ regardless of the assignment. □

Corollary 9.5.3. *Any instance-independent adiabatic algorithm (same Hamiltonian for all energy assignments with the same degeneracy structure) must use the uniform superposition as initial state, fixing the crossing at $s^* = A_1/(A_1 + 1)$.*

So changing the state cannot help unless we give up instance independence. A more aggressive route is to keep the uniform state but add a fixed ancilla coupling V and hope it cancels the instance dependence.

Theorem 9.5.4 (Coupled ancilla limitation)**.** *Consider an extended Hamiltonian $H_{\text{ext}}(s) = -(1-s)\,|\Psi\rangle\langle\Psi| + s(H_z \otimes I + V)$ where $|\Psi\rangle = |\psi_0\rangle \otimes |\phi\rangle$ and V is instance-independent. No fixed V makes A_1^{eff} constant across all problem instances.*

Proof. Consider the two-level family parametrized by $\Delta > 0$, with $E_0 = 0$, $E_1 = \Delta$, $d_0 = 1$, and $d_1 = N - 1$. For $\Delta > 2\|V\|$, Weyl's inequality implies that each eigenvalue of $H_f(\Delta) = H_z(\Delta) \otimes I + V$ lies within $\|V\|$ of an eigenvalue of $H_z(\Delta) \otimes I$. The spectrum therefore splits into two separated clusters, one near energy 0 and one near energy Δ. For each eigenvalue E_j in the excited cluster, $|E_j - \Delta| \le \|V\|$. Hence the excited contribution to A_1^{eff} is

$$\sum_{j\in\text{excited}} \frac{|\langle\Psi\rangle\, \phi_j|^2}{E_j - E_0} = \frac{1 - d_0/N}{\Delta + O(\|V\|)} = \Theta(1/\Delta)$$

for $\Delta \gg \|V\|$. Because $\|V\|$ is fixed independently of Δ, this contribution varies with Δ, so $A_1^{\text{eff}}(\Delta)$ cannot be constant. □

Coupling helps move levels, but it does not erase spectrum dependence. The last escape route inside the same design philosophy is to insert intermediate segments and move the problematic crossing to a more controlled stage of the path.

Theorem 9.5.5 (Multi-segment rigidity)**.** *Consider a two-segment path where segment 2 has Hamiltonian $H_2(t) = -(1-t)\,|\psi_{\text{mid}}\rangle\langle\psi_{\text{mid}}| + tH_z$. If the algorithm is instance-independent, then the intermediate state $|\psi_{\text{mid}}\rangle$ must be the uniform superposition, giving the same crossing $B_1 = A_1$.*

Proof. Segment 2 is a rank-one adiabatic Hamiltonian with initial state $|\psi_{\text{mid}}\rangle$. Its crossing position is $t^* = B_1/(B_1+1)$ where $B_1 = \sum_{k\ge1} w_k(\psi_{\text{mid}})/(E_k - E_0)$. If segment 1 does not involve H_z, then $|\psi_{\text{mid}}\rangle$ is determined entirely by segment 1's Hamiltonian, which is instance-independent. Since $|\psi_{\text{mid}}\rangle$ is then the same for all energy assignments with the same degeneracy structure, Theorem 9.5.2 forces $w_k = d_k/N$, so $B_1 = A_1$. If segment 1 involves H_z, then $|\psi_{\text{mid}}\rangle$ already depends on the spectrum, and the algorithm is not instance-independent. □

Theorem 9.5.6 (No-go)**.** *For any adiabatic algorithm using a rank-one initial Hamiltonian, a final Hamiltonian whose ground state encodes the solution, and instance-independent design, the crossing position cannot be made independent of the problem spectrum.*

Proof. Combine Theorems 9.5.1–9.5.5. Theorem 9.5.2 forces the uniform superposition. Theorem 9.5.1 shows that uncoupled ancillas preserve s^*. Theorem 9.5.4 shows that coupled ancillas can shift s^* but cannot make it constant. Theorem 9.5.5 then rules out escape through multi-segment paths inside the rank-one framework. □

For the running example ($N = 4$, $d_0 = 1$), product ancilla invariance (Theorem 9.5.1) implies that appending any number of ancilla qubits in a product state leaves the crossing at $s^* = 3/7$.

We have now exhausted the rank-one design space under instance independence. The natural objection is that rank one may simply be too narrow. We next move to rank-k projectors and show that the same dependence persists.

For rank-k projectors $P = UU^\dagger$, the secular equation becomes a $k \times k$ determinant condition

$$\det(I_k - (1-s)G(\lambda, s)) = 0, \qquad G(\lambda, s) = U^\dagger (sH_z - \lambda I)^{-1} U.$$

On the two-level family ($E_0 = 0$, $E_1 = \Delta$), this reduces to

$$\det(I_k - (x/\Delta)B) = 0, \qquad B = U_{\text{exc}}^\dagger U_{\text{exc}}, \quad x = (1-s)/s.$$

Each positive eigenvalue μ of B gives a crossing branch $s(\Delta) = 1/(1+\Delta/\mu)$, and this branch is non-constant in Δ.

Proposition 9.5.7 (Rank-k two-level obstruction)**.** *Fixed rank-k projectors cannot make crossing positions spectrum-independent on fixed-degeneracy two-level families unless the projector has zero support on excited states.*

The two-level obstruction already blocks constant crossings in the simplest nontrivial family. For general multilevel spectra, a trace argument gives an even cleaner obstruction.

Proposition 9.5.8 (Trace no-go)**.** *For a rank-k projector $P = UU^\dagger$ and the multilevel family with gaps $\Delta_1, \ldots, \Delta_{M-1}$, define the reduced matrix $A(\Delta) = \sum_{\ell=1}^{M-1} B_\ell/\Delta_\ell$ where $B_\ell = U_\ell^\dagger U_\ell \succeq 0$ collects the excited-level contributions. If $B_j \neq 0$ and Δ_j varies, then $\operatorname{tr}(A(\Delta)) = \sum_\ell \operatorname{tr}(B_\ell)/\Delta_\ell$ is non-constant in Δ_j. By Weyl's eigenvalue monotonicity theorem, each eigenvalue of $A(\Delta)$ is a continuous function of Δ_j, and the sum of the positive eigenvalues equals $\operatorname{tr}(A)$. Since the trace changes, at least one positive eigenvalue, and hence at least one crossing position, must change with Δ_j.*

Remark. *When the excited blocks commute ($[B_\ell, B_m] = 0$ for all ℓ, m), the reduced crossing equation can be simultaneously diagonalized. This gives explicit per-branch formulas. For each active branch r with $G_r(\Delta) = \sum_\ell \mu_{\ell r}/\Delta_\ell > 0$, the crossing position is $s_r = G_r/(1+G_r)$. Varying any gap Δ_j yields*

$$\frac{\partial s_r}{\partial \Delta_j} = -\frac{\mu_{jr}}{\Delta_j^2 (1+G_r)^2} \leq 0,$$

with strict inequality whenever $\mu_{jr} > 0$. So the commuting case gives explicit quantitative non-constancy for each branch, complementing the trace argument's aggregate statement. Even this most tractable version of the generalized secular equation cannot produce spectrum-independent crossings.

At this point the pattern is hard to miss. The barrier is structural inside the rank-one framework and survives the move to higher-rank projectors. It may still be possible to escape with genuinely different control models, such as time-dependent couplings or non-rank-one intermediate Hamiltonians, but those lie outside the present theorem. This distinction matters because once we drop the monotone-schedule restriction, constant controls already recover the Grover timescale on the restricted two-level family.

Proposition 9.5.9 (Constant-control optimality on two-level family)**.** *For $H_z = I - P_0$ where P_0 projects onto the d_0-dimensional ground space, the continuous-time rank-one Hamiltonian $H = -|\psi_0\rangle\langle\psi_0| + H_z$ with constant controls achieves $p_0(t^*) = 1$ at $t^* = (\pi/2)\sqrt{N/d_0}$, with controls independent of A_1 (on the two-level family $H_z = I - P_0$).*

Proof. Let $\mu = d_0/N$, $|G\rangle = d_0^{-1/2} \sum_{x \in S_0} |x\rangle$, and $|B\rangle = (N-d_0)^{-1/2} \sum_{x \notin S_0} |x\rangle$. The initial state is $|\psi_0\rangle = \sqrt{\mu}\,|G\rangle + \sqrt{1-\mu}\,|B\rangle$. Dropping the global identity term, the effective Hamiltonian in the $(|G\rangle, |B\rangle)$ basis is

$$\widetilde{H} = -\begin{pmatrix} \mu & \sqrt{\mu(1-\mu)} \\ \sqrt{\mu(1-\mu)} & -\mu \end{pmatrix}, \tag{9.5.1}$$

which satisfies $\widetilde{H}^2 = \mu\, I_2$. The matrix exponential is $e^{-it\widetilde{H}} = \cos\big(\sqrt{\mu}\, t\big)\, I_2 - i \sin\big(\sqrt{\mu}\, t\big)\, \widetilde{H}/\sqrt{\mu}$. Applying to $|\psi_0\rangle$ and computing the ground-state probability:

$$p_0(t) = |\langle G|\, e^{-it\widetilde{H}} |\psi_0|^2 = \mu + (1-\mu)\sin^2(\sqrt{\mu}\, t). \tag{9.5.2}$$

At $t^* = (\pi/2)/\sqrt{\mu} = (\pi/2)\sqrt{N/d_0}$, $\sin^2(\sqrt{\mu}\, t^*) = 1$, so $p_0(t^*) = 1$. □

On the two-level family, the Hamiltonian self-calibrates through a Rabi-like oscillation at frequency $\sqrt{\mu} = \sqrt{d_0/N}$. The time-independent Hamiltonian $H_r = -|\psi_0\rangle\langle\psi_0| + r \cdot H_z$ with $r = 1$ is optimal without explicit knowledge of A_1 [88]. For general spectra, the resonance shifts to $r^* = A_1$ [88]. The calibration problem then changes from classical computation of A_1 to quantum detection of a resonance.

A natural approach is Loschmidt-echo measurement. Evolve under H_r and measure return probability $|\langle\psi_0|\, e^{-iH_r t}\psi_0|^2$, which oscillates with large amplitude near resonance and stays close to 1 away from resonance. On two-level families this works cleanly: binary search over r with $O(n)$ probe measurements, each costing $O(1/g_{\min})$, locates r^* with polynomial overhead (details in [88]). For general multilevel spectra, additional excited-state frequencies can mask the resonance signal. Whether one can efficiently deconvolve this multilevel echo, or replace it with a better observable, remains open.

The constant-control counterexample applies only to the two-level family $H_z = I - P_0$. Under normalized controls, the barrier reappears.

Proposition 9.5.10 (Normalized-control lower bound)**.** *Under normalized controls $|g(t)| \le 1$ and the scaled family $H_z^{(\delta)} = \delta(I - P_0)$ with minimum excitation $\delta \in (0, 1]$, any instance-independent algorithm achieving success probability $\ge 2/3$ requires $T = \Omega(\sqrt{N/d_0}/\delta)$.*

Proof. The oracle-dependent term $g(t)H_z^{(\delta)} = \delta g(t)(I - P_0)$ has instantaneous oracle strength $\delta|g(t)|$. The total oracle action is $\mathcal{A} = \int_0^T \delta|g(t)|\, dt \le \delta T$. The continuous-time query lower bound for unstructured search with d_0 marked items among N gives $\mathcal{A} = \Omega(\sqrt{N/d_0})$ [89], so $T = \Omega(\sqrt{N/d_0}/\delta)$. □

For $\delta = N^{-1/2}$, this yields $T = \Omega(N/\sqrt{d_0})$, the same exponential penalty as the fixed-schedule adiabatic model. So the barrier reappears on worst-case instances even for general continuous-time rank-one algorithms when controls are normalized. The scope is precise: the obstruction comes from monotone schedules with bounded controls, not from continuous-time quantum computation itself.

9.6 Computational Nature of A_1

The barrier cannot be designed away. What kind of hardness is it? The quantity A_1 is not merely NP-hard to compute. Its core hardness is counting hardness inherited from partition-function structure. The tractability boundary does not align with optimization hardness, is not controlled by the number of solutions alone, and depends on structural properties of the energy landscape.

The quantity A_1 encodes spectral information beyond the minimum gap. Consider three energy levels with $E_0 = 0$ ($d_0 = 1$), $E_1 = 1/n$ ($d_1 = 1$), and $E_2 = 1$ ($d_2 = N-2$). Then $\Delta = 1/n \to 0$ but $A_1 = (n+N-2)/N \to 1$, so $1/\Delta \to \infty$ while $A_1 = \Theta(1)$. The tail of $N - 2$ states at energy 1 contributes $(N-2)/N \approx 1$ to A_1, while the single state at the gap edge contributes only $n/N \approx 0$. So the crossing position $s^* = A_1/(A_1 + 1) \approx 1/2$ is determined by the bulk of the spectrum, not by the minimum gap. In this sense A_1 is a whole-spectrum quantity that Δ alone cannot predict.

The distinction between NP-hardness at precision $1/\mathrm{poly}(n)$ (Theorem 8.1.2) and #P-hardness exactly (Theorem 8.2.4) matters because A_1 is fundamentally a counting quantity.

Proposition 9.6.1 (A_1 hardness is counting hardness)**.** *For Boolean CSPs where counting satisfying assignments is #P-hard (including k-SAT for $k \ge 2$), computing A_1 of the clause-violation Hamiltonian is #P-hard even restricted to satisfiable instances.*

Proof. Encode the CSP as $H_z = \sum_{j=1}^m C_j$ where each $C_j(x) = 1$ if assignment x violates clause j. The interpolation argument (Theorem 8.2.4) recovers all degeneracies d_k from polynomially many evaluations of A_1 with shifted parameters, via Lagrange interpolation on the rational function $f(x) = \sum_k d_k/(\Delta_k + x/2)$. For satisfiable CSPs, d_0 counts satisfying assignments, and counting is #P-hard by hypothesis. □

The partition function connection makes this precise. Shifting energies so that $E_0 = 0$ and defining the Laplace partition function $Z(\beta) = \sum_x e^{-\beta E(x)}$, the spectral parameter admits the integral representation

$$A_1 = \frac{1}{N} \int_0^\infty (Z(\beta) - d_0)\, d\beta. \tag{9.6.1}$$

For integer spectra with $E(x) \in \{0, 1, \ldots, m\}$, the ordinary generating function $Z(t) = \sum_x t^{E(x)}$ gives

$$A_1 = \frac{1}{N} \int_0^1 \frac{Z(t) - d_0}{t}\, dt.$$

At first glance both formulas seem to require d_0, which is itself counting-hard for many CSPs. For additive approximation, however, one can replace d_0 by a single low-temperature sample $Z(\tau)$ with small $\tau > 0$. Define the τ-truncated proxy

$$A_1^{(\tau)} = \frac{1}{N} \int_\tau^1 \frac{Z(t) - Z(\tau)}{t}\, dt. \tag{9.6.2}$$

The additive error satisfies $0 \le A_1 - A_1^{(\tau)} \le \tau(1 + \ln(1/\tau))$. Choosing $\tau = O(\eta/\ln(1/\eta))$ therefore gives an η-approximation to A_1 without direct access to d_0.

When E_0 is known, this coarse form is already useful. Sampling from the Boltzmann distribution at inverse temperature β gives an unbiased estimator of $Z(\beta)/Z(0) = Z(\beta)/N$. Integrating those estimates through Eq. (9.6.1) gives an additive approximation to A_1 without explicitly counting d_0. In this way, computing A_1 becomes a partition-function task, and tractability of A_1 tracks tractability of counting.

Proposition 9.6.2 (Bounded treewidth tractability)**.** *For local energy functions $E(x) = \sum_j E_j(x_{S_j})$ with bounded locality $|S_j| \le k$ and a tree decomposition of the primal graph of width w, A_1 is computable exactly in $\mathrm{poly}(n, m) \cdot 2^{O(w)}$ time.*

Proof. Write the partition-function polynomial as $Z(t) = \sum_x t^{E(x)} = \sum_{q=0}^m d_q t^q$, and also in factor-graph form as $Z(t) = \sum_x \prod_j t^{E_j(x_{S_j})}$. Variable elimination on the tree decomposition then computes $Z(t)$ exactly. At each elimination step, factor tables have at most 2^{w+1} entries, each a polynomial of degree at most m. Multiplying factors convolves polynomials at cost $O(m^2)$ per entry, and summing out a variable adds two polynomials at cost $O(m)$. After n elimination steps, we recover $Z(t) = \sum_q d_q t^q$, and then $A_1 = (1/N) \sum_{q > E_0} d_q/(q - E_0)$. □

The treewidth condition is sufficient, not necessary. A simpler criterion applies when the spectrum itself is simple. If H_z has at most $\mathrm{poly}(n)$ distinct energy levels with known energies and degeneracies, then $A_1 = (1/N) \sum_{k \ge 1} d_k/(E_k - E_0)$ is directly computable in $\mathrm{poly}(n)$ time from its defining sum. This criterion is complementary to bounded treewidth and applies whenever the spectrum is structurally simple, regardless of the interaction graph. For example, Hamming-distance costs $E(x) = |x \oplus z_0|$ have $M = n+1$ levels, degeneracies $d_k = \binom{n}{k}$, and energies $E_k = k$. Then $A_1 = (1/N) \sum_{k=1}^n \binom{n}{k}/k$ depends only on n and is trivial to compute.

The partition-function bridge is one-directional. Tractable Z implies tractable A_1 (via the integral representations above), but exact A_1 does not determine low-temperature $Z(\beta)$.

Proposition 9.6.3 (Reverse bridge obstruction)**.** *There exist two diagonal Hamiltonians H_z, H'_z on $N = 2^n$ states with the same ground degeneracy ratio d_0/N, same minimum excitation $\Delta_{\min}$, and $A_1(H_z) = A_1(H'_z)$ exactly, yet $|Z_{H_z}(\beta) - Z_{H'_z}(\beta)|/N \ge 1/100$ at $\beta = O(1/\Delta_{\min})$.*

Proof. Fix an integer $B \ge 3$. Define two spectra with the same $d_0/N = 1/2$ and $\Delta_{\min} = 1/B$. The first has $N/8$ states at energy $1/B$ and $3N/8$ states at energy B. The second has $N/16$ states at energy $1/B$ and $7N/16$ states at energy $c_B = 7B/(B^2 + 6)$. Direct computation gives the same value $A_1 = (B^2 + 3)/(8B)$ for both. At $\beta = B$, however,

$$\frac{Z_1(B)}{N} = \frac{1}{2} + \frac{e^{-1}}{8} + \frac{3e^{-B^2}}{8}, \qquad \frac{Z_2(B)}{N} = \frac{1}{2} + \frac{e^{-1}}{16} + \frac{7}{16} e^{-7B^2/(B^2+6)}.$$

Since $7B^2/(B^2 + 6) \ge 4.2$ for $B \ge 3$, the difference is at least $e^{-1}/16 - (7/16)e^{-4.2} > 1/100$. □

Three natural conjectures about easy instances of A_1 computation are all false.

Proposition 9.6.4 (Unique solution does not imply easy A_1)**.** *There exist instances with $d_0 = 1$ for which computing A_1 is #P-hard.*

Proof. The proof of Proposition 9.6.1 applies directly to satisfiable instances with $d_0 = 1$. The interpolation reduction recovers $d_1, \ldots, d_{M-1}$ from A_1 evaluations, and counting assignments at each violation level remains #P-hard. Concretely, for a satisfiable 3-SAT instance with m clauses and a unique satisfying assignment, the clause-violation Hamiltonian $H_z = \sum_j C_j$ has $d_0 = 1$ and

$$A_1 = \sum_{k=1}^{m} \frac{d_k}{kN},$$

where d_k counts assignments that violate exactly k clauses. Recovering these counts from shifted A_1 evaluations is therefore #P-hard. □

Proposition 9.6.5 (Bounded degeneracy is vacuous)**.** *If $d_k \leq \mathrm{poly}(n)$ for all excited levels $k \geq 1$, and $M \leq \mathrm{poly}(n)$, then $d_0 \geq N - \mathrm{poly}(n)^2$, and the optimization problem is trivially solvable by random sampling.*

Proof. The total state count satisfies $\sum_{k=0}^{M-1} d_k = N = 2^n$. If $d_k \leq \mathrm{poly}(n)$ for all $k \geq 1$ and $M \leq \mathrm{poly}(n)$, then $\sum_{k\geq 1} d_k \leq (M-1) \cdot \mathrm{poly}(n) \leq \mathrm{poly}(n)^2$, so $d_0 \geq N - \mathrm{poly}(n)^2$. For n large enough, $d_0/N \geq 1 - o(1)$, and a random sample finds a ground state with probability $1 - o(1)$. □

Proposition 9.6.6 (Hard optimization does not imply hard A_1)**.** *The tractability of A_1 is independent of optimization hardness. 2-SAT is in P but #2-SAT is #P-complete [8], giving easy optimization with hard A_1. In the reverse direction, Grover search with a promised ground degeneracy d_0 gives hard optimization but trivial $A_1 = (N - d_0)/(N\Delta)$, computable in $O(1)$ from the promise.*

The tractability boundary for A_1 is subtle. It does not align with optimization hardness, is not determined by the number of solutions, and depends on structural properties of the energy spectrum (treewidth, partition-function tractability) rather than on the difficulty of finding the ground state.

9.7 Complexity Landscape

This section closes the complexity picture at the algorithmically relevant precision $\varepsilon = 2^{-n/2}$. The next four results play different roles. We first pin down the quantum query complexity at this precision, then compare it with classical sampling, then lift the separation to ETH-based time complexity, and finally connect the result back to adiabatic pre-computation.

Theorem 9.7.1 (Tight quantum query complexity at schedule precision)**.** *At the schedule-relevant precision $\varepsilon = \Theta(2^{-n/2})$, the quantum query complexity of A_1 estimation is $\Theta(2^{n/2}) = \Theta(1/\varepsilon)$. The lower bound is achieved on two-level instances with $\Delta_1 = 1$.*

Proof. For $\varepsilon = \Theta(2^{-n/2})$ and $\Delta_1 = 1$, Theorem 8.3.3 gives $O(\sqrt{N} + 1/\varepsilon) = O(2^{n/2})$.

For the lower bound, restrict to $M = 2$ instances with $\Delta_1 = 1$. Then estimating $A_1 = (N - d_0)/N$ to precision ε is approximate counting. The Grover iterate $G = (2\,|+\rangle\langle+| - I)(I - 2\Pi_S)$ has eigenphases $\pm 2\theta$ with $\sin^2\theta = d_0/N$. After T sequential uses of G, the probe accumulates phase $T\phi$ where $\phi = 2\arcsin\left(\sqrt{d_0/N}\right)$.

The quantum Fisher information for estimating ϕ is $F_Q = 4T^2$, the standard Heisenberg scaling for sequential phase accumulation [85, 84]. By the quantum Cramér-Rao bound, $\mathrm{Var}(\hat{\phi}) \geq 1/F_Q = 1/(4T^2)$. Now choose the worst-case operating point $d_0 = N/2$, so $\sin^2\theta = 1/2$ and $|d(\sin^2\theta)/d\theta| = |\sin 2\theta| = 1$. At this point, estimating $A_1 = 1 - \sin^2\theta$ to precision ε requires estimating θ to precision ε. Hence $1/(4T^2) \leq \varepsilon^2$, so $T \geq 1/(2\varepsilon)$ applications of G. Each application uses $O(1)$ oracle calls. Therefore the lower bound is $\Omega(1/\varepsilon)$, and at $\varepsilon = \Theta(2^{-n/2})$ we get $\Omega(2^{n/2})$.

Combining upper and lower bounds gives $\Theta(2^{n/2}) = \Theta(1/\varepsilon)$. □

The lower bound is worst-case in the unknown parameter d_0, and the adversary picks $d_0 = N/2$ because that point is maximally difficult to estimate. The Heisenberg limit $F_Q = 4T^2$ for sequential unitary applications is standard in quantum metrology and applies to general quantum estimation, not only phase estimation. It follows from unitary dynamics together with the Cramér-Rao inequality, as shown by Braunstein and Caves [85] and extended to sequential settings by Giovannetti, Lloyd, and Maccone [84]. The same $\Omega(1/\varepsilon)$ lower bound also follows from quantum approximate counting. Estimating d_0/N to additive precision ε requires $\Omega(1/\varepsilon)$ quantum queries [37, 38], and for $M = 2$ this is exactly the A_1 estimation problem.

This theorem connects directly to the adaptive protocol of section 9.3. The adaptive strategy achieves $T_{\mathrm{adapt}} = O(T_{\mathrm{inf}}) = O(2^{n/2})$, which matches the tight complexity $\Theta(2^{n/2})$ for estimating A_1 at precision $\delta_{A_1} =$

$\Theta(2^{-n/2})$. The match is structural rather than accidental. In both tasks, the algorithm must resolve $\Omega(2^{n/2})$ alternatives while each quantum measurement reveals only $O(1)$ information.

In the high-precision regime relevant to schedule placement, the quadratic quantum advantage persists.

Proposition 9.7.2 (Precision phase diagram)**.** *For two-level instances with $\Delta_1 = 1$ and precision $\varepsilon \leq c/\sqrt{N}$ (constant c), the query complexity of A_1 estimation is $\Theta(1/\varepsilon)$ quantum and $\Theta(1/\varepsilon^2)$ classical. The quantum-to-classical ratio is $\Theta(1/\varepsilon)$ in this regime.*

Proof. In this regime, $1/\varepsilon \geq \sqrt{N}/c$, so the upper bound of Theorem 8.3.3 becomes $O(\sqrt{N} + 1/\varepsilon) = O(1/\varepsilon)$. The matching quantum lower bound is inherited from two-level approximate counting (Theorem 9.7.1). The classical lower bound $\Omega(1/\varepsilon^2)$ follows from Theorem 8.3.4, and Monte Carlo sampling gives the matching upper bound $O(1/\varepsilon^2)$. □

The previous proposition is still a query statement. The next theorem asks what happens when we account for total computation time under a standard complexity assumption.

Theorem 9.7.3 (ETH computational complexity)**.** *Under the Exponential Time Hypothesis (ETH), any classical algorithm computing A_1 at precision $2^{-n/2}$ requires $2^{\Omega(n)}$ time.*

Proof sketch. The NP-hardness reduction (Theorem 8.1.2) maps 3-SAT on n_{var} variables to A_1 estimation of a 3-local Hamiltonian on $n = O(n_{\text{var}})$ qubits at precision $1/\text{poly}(n)$. By the Impagliazzo-Paturi-Zane sparsification lemma [90], 3-SAT on n_{var} variables can be reduced to instances with $O(n_{\text{var}})$ clauses, giving $n = O(n_{\text{var}})$ qubits. Any algorithm computing A_1 at precision $2^{-n/2}$ can, in particular, compute A_1 at the coarser precision $1/\text{poly}(n)$ (since $2^{-n/2} < 1/\text{poly}(n)$ for large n), and thus solves 3-SAT by the reduction. Under ETH, 3-SAT on $n_{\text{var}} = \Omega(n)$ variables requires $2^{\Omega(n_{\text{var}})} = 2^{\Omega(n)}$ time. □

Under ETH, the quadratic quantum advantage extends from the query model to the computational model.

Corollary 9.7.4 (Quantum pre-computation cost)**.** *Estimating A_1 to the schedule-relevant precision $\delta_{A_1} = \Theta(2^{-n/2})$ via quantum amplitude estimation costs $\Theta(2^{n/2} \cdot \text{poly}(n))$ time, matching the adaptive protocol's runtime. The classical pre-computation cost at the same precision is $\Omega(2^n)$.*

From a parameterized-complexity viewpoint, the corollary places A_1 estimation at precision $2^{-n/2}$ in

$$\text{FBQTIME}(2^{n/2} \cdot \text{poly}(n)).$$

The problem is therefore not polynomial-time in the usual sense, but it does admit a quantum algorithm at the Grover scale. This also clarifies the information cost of fixed-schedule adiabatic optimization. Recovering the missing $n/2$ bits of A_1 costs $\Theta(2^{n/2})$ quantum time, the same scale as Grover search and informed adiabatic evolution. The circuit model reaches that scale without a pre-computation step because amplitude amplification solves the search task directly.

The generic extrapolation barrier (Theorem 8.3.2) shows that interpolation failure at precision $2^{-n/2}$ is not tied to one construction. For any polynomial extrapolation scheme with $d = \text{poly}(n)$ nodes, the Lebesgue constant obeys $\Lambda_d(x^*) \geq 2^{d-1}$ when the evaluation point sits at least $b - a$ away from the sample interval $[a, b]$. This geometric condition must be verified in each setup. It does not follow only from $x^* = \Theta(2^{-n/2})$ with nodes in $[0, 1/\text{poly}(n)]$. Once the condition holds, polynomial-interpolation reductions for A_1 demand precision $2^{-\Omega(n)}$.

Proposition 9.7.5 (Two-level worst-case reduction)**.** *The two-level family ($M = 2$) is a worst-case subclass for A_1 estimation at schedule-relevant precision: any worst-case lower bound for approximate counting on this subclass applies to general A_1 estimation.*

Proof. Worst-case complexity over all instances is at least the complexity on any subclass. Restricting to $M = 2$ gives

$$A_1 = \frac{N - d_0}{N\Delta_1},$$

so for fixed $\Delta_1 = 1$, estimating A_1 to additive precision ε is exactly approximate counting for d_0/N at precision ε. Therefore, any lower bound for approximate counting on this subclass is automatically a lower bound for general A_1 estimation. □

The worst-case hardness of A_1 estimation does not hide in complex spectra. Simple two-level instances, where A_1 reduces to counting, already saturate the query lower bound. Algorithms exploiting the sum-of-reciprocals structure of A_1 for multilevel spectra cannot beat algorithms for plain mean estimation.

At schedule-level precision, bounded-treewidth instances remain tractable for exact A_1 computation (Proposition 9.6.2). Ferromagnetic Ising models also admit a polynomial-time FPRAS for $Z(\beta)$ [91], which yields additive approximations for A_1 at coarse precision through the integral formulas in Eq. (9.6.1) and Eq. (9.6.2). The difficulty appears at algorithmic precision $\delta_{A_1} = \Theta(2^{-n/2})$. Reaching this regime requires multiplicative accuracy $\mu = O(2^{-n/2}/B)$ with $B = O(\log(1/\delta_{A_1})/\Delta_{\min})$, so the FPRAS runtime $\mathrm{poly}(1/\mu)$ becomes exponential. With $B = O(n/\Delta_{\min})$, one gets $\mathrm{poly}(1/\mu) = 2^{\Omega(n)}$. Thus ferromagnetic-Ising tractability does not survive at the schedule-relevant precision.

The interpolation theorem (Theorem 9.2.2) gives a quantitative law relating information to runtime. We state it in a communication picture.

Alice has the full classical description of H_z (all eigenvalues and degeneracies). Bob has a quantum computer with oracle access to H_z, and Alice may send C classical bits to Bob. Bob must find a ground state in at most T queries.

In the circuit-oracle model, Bob needs no message from Alice and still achieves $T = O(\sqrt{N/d_0})$ by running Dürr-Høyer. In the fixed-schedule adiabatic model, Bob must match the schedule to the crossing and therefore needs s^* to precision $\Delta_* = O(2^{-n/2})$, which costs $C = \Theta(n)$ bits. Each additional bit of A_1 precision cuts the adiabatic runtime by a factor of two. Roughly $n/2$ bits are enough for optimal scaling. Formally, if Alice sends C bits that encode A_1 to precision $\varepsilon = \Theta(2^{-C})$, then

$$T(C) = T_{\inf} \cdot \Theta(\max(1, 2^{n/2-C})).$$

Theorem 9.7.6 (Bit-runtime information law)**.** *The classical communication cost for the adiabatic model to achieve target runtime T is $C^*(T) = \max(0,\, n/2 - \log_2(T/T_{\inf}))$ bits, while $C^*_{\text{circuit}}(T) = 0$ for all $T \geq T_{\inf}$.*

Proof. Inverting $T(C) = T_{\inf} \cdot 2^{n/2-C}$ gives $C = n/2 - \log_2(T/T_{\inf})$. Clamping $C \geq 0$ and noting that the circuit model achieves $T = T_{\inf}$ at $C = 0$ by the Dürr-Høyer algorithm gives both formulas. □

The complete model comparison, synthesizing this chapter with Chapter 8, is given below.

Model	Info needed	Runtime	Communication
Circuit (Dürr-Høyer)	None	$\Theta(\sqrt{N/d_0})$	0 bits
Fixed AQO, informed	A_1 to $2^{-n/2}$	$O(\sqrt{N/d_0})$	$\Theta(n)$ bits
Fixed AQO, C bits	A_1 to 2^{-C}	$T_{\inf} \cdot 2^{n/2-C}$	C bits
Fixed AQO, uninformed	None	$\Omega(N/\sqrt{d_0})$	0 bits
Adaptive AQO	$O(n)$ measurements	$O(\sqrt{N/d_0})$	0 bits
Constant-control, two-level	None	$\Theta(\sqrt{N/d_0})$	0 bits
Quantum A_1 estimation	$\varepsilon = 2^{-n/2}$	$\Theta(2^{n/2})$ queries	—
Classical A_1 estimation	$\varepsilon = 2^{-n/2}$	$\Theta(2^n)$ queries	—

The circuit model and the adaptive adiabatic model both achieve optimal performance with zero classical communication. In contrast, the fixed adiabatic model follows a bit-runtime tradeoff in which each missing bit doubles the runtime. The resulting $\Theta(n)$-bit separation from the circuit model is exactly the information content of A_1 at schedule-relevant precision. This communication cost reflects the computational model rather than the underlying search task.

The running example makes the tradeoff concrete. With $N = 4$, $d_0 = 1$, and $n = 2$, the circuit model uses $O(2)$ queries at $C = 0$. The informed adiabatic model also uses $O(2)$ queries, but only after receiving $C = 1$ bit. Without that bit, the fixed adiabatic model requires $\Omega(4)$ queries. The single missing bit explains the factor-of-two slowdown.

The term "information gap" now has three precise meanings. The first is spectral. Inside the adiabatic framework, $g_{\min}$ sets the timescale $T = O(1/g_{\min})$, and the full profile $g(s)$ constrains which schedules are valid. The second is epistemic. If crossing location is unknown, runtime pays the factor $(s_R - s_L)/\Delta_*$. If A_1 is known to precision ε, the overhead becomes $\Theta(\max(1, \varepsilon/\delta_{A_1}))$. With $O(n)$ quantum measurements, this overhead disappears. The third is model-dependent. Circuit algorithms neither need nor expose A_1, fixed-schedule adiabatic algorithms require it and face NP-hard recovery, and adaptive adiabatic algorithms can acquire it at polynomial cost.

This gives a five-level taxonomy of ignorance, measured by the multiplicative overhead $T/T_{\inf}$. Level 0 (no information) gives $\Omega(2^{n/2})$. Level 1 (precision ε) gives $\Theta(\max(1, \varepsilon/\delta_{A_1}))$. Level 2 (known interval $[u_L, u_R]$) gives

constant overhead proportional to $u_R - u_L$. Level 3 (quantum measurement access) gives $O(1)$ overhead with $O(n)$ measurements. Level 4 (circuit model) has overhead 1 with no spectral information.

The adiabatic approach to unstructured search therefore works, reaches Grover scaling, and is optimal within its schedule class. Its information requirements are a structural consequence of the rank-one interpolation path. They are not a fundamental limit of quantum computation itself. They are a limit of this specific model. The next chapter translates these results into machine-checked formal proofs.

Chapter 10

Formalization

Formalization entered this thesis as a way to learn the subject. The UAQO argument is long—spectral statistics feed gap geometry, gap geometry feeds runtime, runtime pairs with hardness reductions—and I did not trust my own understanding of how the pieces fit together. Reading the paper convinced me that each step was correct. It did not convince me that I could reproduce the argument, modify it, or find its weak points. I wanted a setting where I could take the argument apart and put it back together, and where mistakes would surface immediately instead of hiding in the comfort of informal prose.

Lean 4 [92] with Mathlib [93] gave me that setting. I encoded the main UAQO paper [10] as a Lean development, not to certify the results but to see what happens when every dependency is typed, every hypothesis is named, and the difference between "proved" and "assumed" is decided by a kernel rather than by authorial emphasis. That process changed how I understood the argument. Statements that looked like single claims split into independent results with different hypotheses. Definitions that seemed equivalent turned out to carry different side conditions. Proof decompositions that seemed natural on paper failed in Lean because they required transporting conditions across interfaces that did not match. Other decompositions that looked awkward on paper turned out to be the clean ones, because they aligned with how the mathematics actually factors.

The formal artifact lives in `src/lean/UAQO`. Restricting to the main-paper scope (excluding `Experiments` and `Test`), it contains 32 Lean files, 11,596 lines, zero active `sorry` terms, 15 explicit axioms, and 330 theorem and lemma declarations. It builds with `lake build`. The rest of this chapter describes what I learned from writing it.

10.1 What Formalization Taught Me

UAQO has the structure of a relay. The spectral parameters A_1 and A_2 determine where the avoided crossing sits and how sharp it is. The gap profile $g(s)$ along the adiabatic path is built from those parameters. The runtime comes from $\int g(s)^{-2}\,ds$. And the hardness results connect A_1 to NP and #P through reductions that use the spectral structure. Each handoff between these layers carries hypotheses, and in prose those hypotheses can drift. A condition established in one section gets applied three sections later with a slightly different scope, and nobody notices because the prose never forced the connection to be explicit.

Lean makes the connection explicit. Every hypothesis a theorem uses appears in its type. If a gap bound requires the eigenvalues to be strictly ordered, that requirement is a function argument. If a runtime statement needs a spectral condition, any theorem that calls it must supply evidence for that condition. I found this useful in a specific way: it showed me where I had been mentally bundling independent claims. Results that I read as a single argument on paper turned out to have components with genuinely different hypotheses. Lean would not let me state the combined version, so I had to find the correct factoring. That factoring improved the mathematics.

A concrete example: the spectral analysis in the paper treats the eigenvalue characterization and the gap bounds as parts of one argument. In Lean, they separate cleanly. The theorem `eigenvalue_condition` (in `Spectral/GapBounds.lean`) is fully proved from the spectral structure: it characterizes when λ is an eigenvalue of $H(s)$ via the secular equation, and needs only that $M > 0$ and $s \in (0, 1)$. The regional gap bounds—`gap_bound_left`, `gap_at_avoided_crossing`, `gap_bound_right` in the same file—additionally require `FullSpectralHypothesis`, which packages a spectral regularity condition ($A_1 > 1$ and $\sqrt{d_0 A_2/N} < (A_1 + 1)/2$) that the eigenvalue condition does not need. The paper uses both the eigenvalue condition and the gap bounds together without separating their hypotheses. In Lean, a result that uses only the secular

equation cannot accidentally import the spectral hypothesis, and a change to the gap analysis cannot break the eigenvalue characterization. This is the kind of structural insight that I could not have found by reading alone.

The bigger payoff was that Lean let me experiment. I could try a candidate theorem shape, see whether it type-checked, and learn from the failure when it did not. On paper, discovering the right decomposition of a proof takes many failed attempts that leave no trace. In Lean, the failures are immediate and specific. A statement that looked elegant failed because a side condition could not be transported across a module boundary. A formulation that looked unnecessarily verbose turned out to be the right one because it matched a Mathlib interface I could reuse. I tested alternate decompositions of the secular equation analysis, tried different ways to package the spectral data, and ended up with interfaces that I would not have found without the type checker pushing back.

Some of that experimentation lives in dedicated experiment modules outside the main scope. The experiment files explore directions beyond the paper: coupled schedules, structured tractability, circumventing the interpolation barrier. This chapter stays focused on the main-paper formalization, but the experiments were part of the same learning process.

The idea that mathematical proofs should be fully explicit is old. Hilbert wanted it [94]. Homotopy type theory gave it computational content [95]. Lean 4 is a modern instance: a dependently typed language with a small trusted kernel and a growing mathematical library [92, 93]. Large formalizations have already been carried through in other proof assistants—the odd-order theorem in Coq [96], the Kepler conjecture in HOL Light and Isabelle [97]. Those projects showed that the method scales to substantial mathematics.

For UAQO, the formalization helps most at the interface between spectral analysis and complexity reductions. That interface is where the dependency chain is longest and where assumptions are hardest to track by hand. The spectral parameters feed into gap bounds, gap bounds feed into runtime, and runtime feeds into the hardness reductions. Each handoff carries conditions that must match, and in a typed system, mismatches surface as type errors rather than as silent bugs in a published proof.

10.2 Lean in Brief

In Lean, a proposition is a type and a proof is a term inhabiting that type. The trusted kernel checks that terms are well-typed. Everything else—tactics, automation, elaboration—must produce a kernel-accepted term before it counts as proved. Four pieces are enough to read the formal artifacts in this chapter. The *kernel* is the final checker. The *elaborator* fills in implicit arguments and typeclass instances. *Tactic mode* builds proof terms incrementally: each tactic transforms a goal into simpler subgoals. And *definitional equality* lets some identities reduce by computation, so that proofs of equalities between unfolded definitions can collapse to `rfl`.

What makes this useful for mathematics is that every theorem carries its dependencies in its type. If a result needs an eigenvalue ordering, that ordering is a function argument. If a downstream theorem consumes a gap bound, it must supply the hypotheses that the gap bound requires. A change to the spectral data model breaks every theorem that depends on it, and the break shows up immediately. In UAQO, the same spectral interfaces get reused in gap bounds, runtime wrappers, and hardness reductions, so a single well-chosen interface saves a lot of repeated work.

What makes Lean painful is the overhead. Typeclass search can fail far from the source of the problem. Elaboration errors are often nonlocal. Coercing between `Nat`, `Int`, and `Real` is tedious in analysis-heavy files. I kept an abstraction only when it reduced total proof effort across the development. When it did not, I removed it.

A reader who wants to check any claim in this chapter can do so independently.

Listing 10.1: Rebuilding the development and inspecting axiom dependencies.

```
-- From the repository root:
cd src/lean
lake update
lake build

#print axioms UAQO.Complexity.mainResult2
#print axioms UAQO.Complexity.mainResult3
#print axioms UAQO.Adiabatic.adiabaticTheorem
```

The `#print axioms` command lists every axiom a theorem depends on, transitively. A theorem with no domain axioms is fully kernel-checked. A theorem that lists domain axioms depends on exactly those assumptions and no others.

10.3 How the Encoding Is Organized

The first design I tried was wrong. I modeled Hamiltonians at the matrix level, carrying full operator data through every theorem. This was faithful to the linear-algebraic picture but useless for the proofs I actually needed. Gap bounds, crossing positions, and runtime integrals depend on spectral data—eigenvalues and degeneracies—not on matrix entries. Carrying matrix-level detail through spectral arguments added clutter without content and made it hard to reuse lemmas across modules.

The design that worked models instances through spectral structure. The central record is `EigenStructure`. It packages ordered eigenvalues, degeneracies, an assignment map from basis states to energy levels, and consistency invariants.

Listing 10.2: Core spectral data model reused across UAQO modules.

```
structure EigenStructure (n : Nat) (M : Nat) where
  eigenvalues : Fin M -> Real
  degeneracies : Fin M -> Nat
  assignment : Fin (qubitDim n) -> Fin M
  eigenval_bounds : forall k, 0 <= eigenvalues k /\ eigenvalues k <= 1
  eigenval_ordered : forall i j, i < j -> eigenvalues i < eigenvalues j
  ground_energy_zero : (hM : M > 0) -> eigenvalues (Fin.mk 0 hM) = 0
  deg_positive : forall k, degeneracies k > 0
  deg_sum : Finset.sum Finset.univ degeneracies = qubitDim n
  deg_count : forall k, degeneracies k =
    (Finset.filter (fun z => assignment z = k) Finset.univ).card
```

Eigenvalues are bounded in $[0, 1]$ and strictly ordered. Ground energy is zero. Degeneracies are positive and sum to $N = 2^n$. The assignment map and count field enforce that every basis state belongs to exactly one level. These invariants are checked once at construction time. Every downstream theorem inherits them for free, which eliminates a class of errors where a proof silently assumes an ordering that was never verified.

This interface turned out to be a genuine improvement over what I started with. Theorem statements got shorter. Hypotheses transported cleanly across modules. Complexity lemmas could reuse spectral facts without re-establishing them. The spectral parameters A_1, A_2, and the gap quantities are defined directly on `EigenStructure`, and bridge theorems connect them to alternative representations.

Listing 10.3: Direct encoding of A_1 with bridge theorem to partial representation.

```
noncomputable def spectralParam {n M : Nat} (es : EigenStructure n M)
    (hM : M > 0) (p : Nat) : Real :=
  let E0 := es.eigenvalues (Fin.mk 0 hM)
  let N := qubitDim n
  (1 / N) * Finset.sum (Finset.filter (fun k => k.val > 0) Finset.univ)
    (fun k => (es.degeneracies k : Real) / (es.eigenvalues k - E0)^p)

noncomputable def A1 {n M : Nat} (es : EigenStructure n M) (hM : M > 0) : Real :=
  spectralParam es hM 1

theorem A1_partial_eq_A1 {n M : Nat} (es : EigenStructure n M) (hM : M > 0) :
    A1_partial es.toPartial hM = A1 es hM := by
  simp only [A1_partial, A1, spectralParam, EigenStructure.toPartial, pow_one]
```

The bridge theorem `A1_partial_eq_A1` is typical. Two representations of A_1—the full spectral definition and a partial-information variant—are defined independently and proved equal. The proof is a single-line simplification, meaning the equality holds by unfolding definitions. Downstream code uses whichever representation is more convenient, and the bridge guarantees that results transfer.

Table 10.1 gives the size of the main-paper development.

Table 10.1: Main-paper scope in `src/lean/UAQO` (excluding `Experiments` and `Test`).

Component	Files	Approx. LOC	Role in proof architecture
Foundations	5	1,067	Hilbert-space and operator preliminaries consumed by later layers
Spectral	4	1,348	A_p definitions, crossing quantities, and gap-facing interfaces
Adiabatic	4	1,254	Schedule and runtime interfaces for adiabatic statements
Complexity	5	2,428	SAT and counting encodings, hardness interfaces, extraction contracts
Proofs	14	5,499	Lemma layer for secular analysis, interpolation, combinatorics, and verification support
Total	32	11,596	Zero active `sorry` terms and 15 explicit `axiom` declarations

Within this scope, the development contains 330 theorem and lemma declarations. The five components mirror the dependency structure of the UAQO argument itself: foundations feeds spectral, spectral feeds adiabatic and complexity, and proofs supports all four.

Table 10.2 pairs each headline claim of the chapter with the Lean artifacts that back it and their epistemic status.

Table 10.2: Claim-to-artifact map for the Chapter 10 argument.

Chapter claim	Primary Lean artifact	Epistemic status
Paper formulas for A_p, s^*, δ_s, $g_{\min}$ are represented faithfully	`Spectral/SpectralParameters`, `Test/Verify`	Definitional equality checks (`rfl`)
Two-query NP-hardness core is formally encoded	`Complexity/Hardness` (`mainResult2`)	Proved modulo `gareyJohnsonEncoding` axiom
Counting extraction bridge to #P statement is formalized	`Complexity/Hardness` (`mainResult3`)	Machine-checked theorem core
Global gap-profile runtime claims require additional spectral interface	`Proofs/Spectral/GapBoundsProofs`	Conditional via `FullSpectralHypothesis`
Adiabatic transfer theorems are wrappers over explicit physics interfaces	`Adiabatic/Theorem`	Axiom-mediated

Rows mentioning `Test/Verify` refer to audit wrappers, not to the proofs themselves. The definitions and proofs live in the main-scope modules listed in the same row.

10.4 Two Proof Paths

Tables describe what is proved. To see how a proof moves through the formal system, it helps to trace two concrete paths: the NP reduction from Chapter 8, and the counting bridge behind the #P extraction.

The theorem `mainResult2` formalizes the two-query reduction. Given a 3-CNF formula f, it constructs a Garey-Johnson encoding, computes the two-query difference D, and proves $D = 0$ if and only if f is satisfiable.

Listing 10.4: Proof skeleton of `mainResult2`.

```
theorem mainResult2 (f : CNFFormula) (hf : is_kCNF 3 f) :
    let enc := gareyJohnsonEncoding f hf
    let D := twoQueryDifference enc.es enc.hLevels
    (D = 0) <-> isSatisfiable f := by
```

```
  intro enc D
  constructor
  intro hD
  by_contra hunsat
  have hE0_pos := enc.unsat_ground_pos hunsat
  have hexcited := enc.unsat_excited_pop hunsat
  have hD_pos := twoQuery_unsat enc.es enc.hLevels hE0_pos enc.excited_pos hexcited
  linarith
  intro hsat
  have hE0_zero := enc.sat_ground_zero hsat
  exact twoQuery_sat enc.es enc.hLevels hE0_zero
```

The script is short because the work lives in helper lemmas. The satisfiable branch: `sat_ground_zero` shows a satisfying assignment forces $E_0 = 0$, then `twoQuery_sat` shows $D = 0$. The unsatisfiable branch: `unsat_ground_pos` gives $E_0 > 0$, `unsat_excited_pop` gives populated excited levels, `twoQuery_unsat` gives $D > 0$, and `linarith` closes the contradiction. The only axiom in the chain is the Garey-Johnson encoding interface, which packages a classical graph-coloring reduction that Mathlib does not yet cover. Once that interface is fixed, everything else is checked.

The second path is the counting bridge behind #P extraction. Informal proofs compress the step from satisfying assignments to a counting identity into a sentence. I made it a separate theorem.

Listing 10.5: Bridge theorem from semantic satisfiability to counting identity.

```
private theorem countZeroUnsatisfied_eq_numSatisfying (f : CNFFormula) :
    countAssignmentsWithKUnsatisfied f 0 = numSatisfyingAssignments f := by
  simp only [countAssignmentsWithKUnsatisfied, numSatisfyingAssignments]
  congr 1
  ext z
  simp only [Finset.mem_filter, Finset.mem_univ, true_and]
  rw [<- satisfies_iff_countUnsatisfied_zero]
  rfl
```

The statement looks trivial: assignments with zero unsatisfied clauses are satisfying assignments. But formally, the two filtering predicates must be shown extensionally equal, which requires unfolding both definitions and using a separately proved equivalence. Once this bridge exists, every downstream theorem imports it mechanically instead of re-arguing the point. The extraction chain from satisfiability to counting polynomial to #P is stabilized because each link is a named, proved artifact.

Both paths have the same shape. High-level scripts are five to fifteen lines. The real work is in interface lemmas with explicit hypotheses. The type checker enforces that hypotheses match at every call site. If they do not match, the proof fails to compile. This is the main reason formalization was worth the effort: not that it makes proofs more clever, but that it catches mismatches I would have missed.

The type checker enforces what is proved. The next question is what is not proved, and how the development marks that boundary.

10.5 Assumptions and Boundaries

The formalization does not prove the full UAQO argument from first principles. It proves the NP-hardness and #P-hardness reductions in full (modulo one classical encoding axiom), and it proves the spectral parameter identities by definitional equality. But the spectral gap analysis that connects these parameters to an actual runtime bound—the resolvent-based argument of the paper's Sections 2–3—is not formalized. Instead, it enters the development through `FullSpectralHypothesis`, which is carried as an explicit hypothesis rather than buried as an axiom.

Listing 10.6: Explicit hypothesis for full spectral-gap profile claims.

```
structure FullSpectralHypothesis {n M : Nat} (es : EigenStructure n M) (hM : M >= 2) : Prop where
  cond : spectralConditionForBounds es hM
  gap : forall (s : Real) (hs : 0 <= s /\ s <= 1) (E0 E1 : Real),
    IsEigenvalue (adiabaticHam es s hs) E0 ->
    IsEigenvalue (adiabaticHam es s hs) E1 ->
    E0 < E1 -> E1 - E0 >= minimumGap es hM
```

It packages a spectral regularity condition and a uniform gap lower bound. Any theorem that needs the full gap profile must supply this hypothesis. Any reader can check whether a given theorem actually supplies it or only assumes it.

The development declares 15 explicit axioms, grouped in Table 10.3.

Table 10.3: Axiom groups in the UAQO main-paper formalization.

Group	Count	Representative content
Primitive interfaces	3	Polynomial-time predicate, Schrodinger-evolution predicate, degeneracy-count interface
Standard complexity interfaces	3	Membership and hardness interfaces for 3-SAT and #3-SAT classes
Quantum dynamics interfaces	6	Adiabatic transfer bounds, local-schedule transfer, phase-randomization transfer, unstructured-search lower-bound interface
Paper-specific interfaces	3	Garey-Johnson encoding and reduction bridges used in UAQO hardness statements
Total	15	Every assumption is declared by `axiom` and inspectable via `#print axioms`

The primitive interfaces axiomatize concepts that current Lean libraries cannot define natively: polynomial-time computation, Schrodinger evolution, degeneracy counting. The complexity interfaces encode standard results—Cook-Levin for 3-SAT [6], Valiant for #3-SAT [8]. The quantum dynamics interfaces package results like the Jansen-Ruskai-Seiler adiabatic bound [17]. As Lean libraries grow, individual axioms can be discharged and replaced by proofs. The development is structured so that discharging an axiom narrows the trust boundary without requiring any downstream theorem to be rewritten.

AI helped with the exploratory phase. I used it to propose theorem shapes, suggest decompositions, and draft bridge lemmas. But AI suggestions needed checking, because they often solved a local goal by importing stronger assumptions than necessary. A tactic script that closes the current goal is not the same as a tactic script that closes it under the right hypotheses. The discipline was simple: temporary `sorry` during design, no `sorry` in the delivered code, and `#print axioms` on every result before accepting it. Anything that could not be proved became a named axiom with a citation.

Formal methods for quantum computing have mostly focused on circuit-level verification: QWIRE [98] and SQIR [99] verify gate-level programs, CoqQ [100] reasons about quantum program semantics, and Isabelle-based work [101] targets quantum protocols. None of these tools handle spectral analysis or complexity reductions—they operate at the circuit abstraction, where the relevant objects are gates and registers rather than eigenvalues and spectral gaps. This development works at a different layer. It carries spectral structure through to hardness reductions in a single typed system. The cost is that the quantum dynamics (the adiabatic theorem, the transfer bounds) enter as axioms rather than as proved results, because formalizing the resolvent calculus underlying those bounds is a separate project. The approach follows the pattern of earlier large formalizations [96, 97]: quantitative scope, reproducible build, explicit assumption ledger, honest boundary between proved and assumed.

The mathematics in the source paper belongs to its authors [10]. The Lean code, the experiments, and the workflow described here are my path through their argument. A reader who finishes this chapter can rebuild the artifact, inspect any theorem's dependencies, and start extending the formal interfaces for new problems in adiabatic quantum optimization.

Chapter 11

Conclusion

Bibliography

[1] Lov K. Grover. A fast quantum mechanical algorithm for database search. In *Proceedings of the 28th Annual ACM Symposium on Theory of Computing*, pages 212–219, 1996. doi:10.1145/237814.237866.

[2] Charles H. Bennett, Ethan Bernstein, Gilles Brassard, and Umesh Vazirani. Strengths and weaknesses of quantum computing. *SIAM Journal on Computing*, 26(5):1510–1523, 1997. doi:10.1137/S0097539796300933.

[3] Sanjeev Arora and Boaz Barak. *Computational Complexity: A Modern Approach*. Cambridge University Press, 2009.

[4] David Deutsch. Quantum theory, the Church-Turing principle and the universal quantum computer. *Proceedings of the Royal Society A*, 400(1818):97–117, 1985. doi:10.1098/rspa.1985.0070.

[5] Ethan Bernstein and Umesh Vazirani. Quantum complexity theory. *SIAM Journal on Computing*, 26 (5):1411–1473, 1997. doi:10.1137/S0097539796300921.

[6] Stephen A. Cook. The complexity of theorem-proving procedures. In *Proceedings of the Third Annual ACM Symposium on Theory of Computing (STOC)*, pages 151–158, 1971. doi:10.1145/800157.805047.

[7] Richard M. Karp. *Reducibility among Combinatorial Problems*, pages 85–103. Springer US, 1972. doi:10.1007/978-1-4684-2001-2_9.

[8] Leslie G. Valiant. The complexity of enumeration and reliability problems. *SIAM Journal on Computing*, 8(3):410–421, 1979. doi:10.1137/0208032.

[9] Seinosuke Toda. PP is as hard as the polynomial-time hierarchy. *SIAM Journal on Computing*, 20(5): 865–877, 1991. doi:10.1137/0220053.

[10] Arthur Braida, Shantanav Chakraborty, Alapan Chaudhuri, Joseph Cunningham, Rutvij Menavlikar, Leonardo Novo, and Jérémie Roland. Unstructured adiabatic quantum optimization: Optimality with limitations. *arXiv preprint arXiv:2411.05736*, 2024.

[11] F. Barahona. On the computational complexity of Ising spin glass models. *Journal of Physics A: Mathematical and General*, 15(10):3241–3253, 1982. doi:10.1088/0305-4470/15/10/028.

[12] Andrew Lucas. Ising formulations of many NP problems. *Frontiers in Physics*, 2:5, 2014. doi:10.3389/fphy.2014.00005.

[13] Edward Farhi, Jeffrey Goldstone, Sam Gutmann, and Michael Sipser. Quantum computation by adiabatic evolution. *arXiv:quant-ph/0001106*, 2000. doi:10.48550/arXiv.quant-ph/0001106.

[14] Edward Farhi, Jeffrey Goldstone, Sam Gutmann, Joshua Lapan, Andrew Lundgren, and Daniel Preda. A quantum adiabatic evolution algorithm applied to random instances of an NP-complete problem. *Science*, 292(5516):472–475, 2001. doi:10.1126/science.1057726.

[15] Max Born and Vladimir Fock. Beweis des adiabatensatzes. *Zeitschrift für Physik*, 51:165–180, 1928. doi:10.1007/BF01343193.

[16] Tosio Kato. On the adiabatic theorem of quantum mechanics. *Journal of the Physical Society of Japan*, 5(6):435–439, 1950.

[17] Sabine Jansen, Mary-Beth Ruskai, and Ruedi Seiler. Bounds for the adiabatic approximation with applications to quantum computation. *Journal of Mathematical Physics*, 48(10):102111, 2007. doi:10.1063/1.2798382.

[18] Alexander Elgart and George A. Hagedorn. A note on the switching adiabatic theorem. *Journal of Mathematical Physics*, 53(10), 2012. doi:10.1063/1.4748968.

[19] Lev D. Landau. Zur theorie der energieubertragung. ii. *Physikalische Zeitschrift der Sowjetunion*, 2: 46–51, 1932.

[20] Clarence Zener. Non-adiabatic crossing of energy levels. *Proceedings of the Royal Society A*, 137(833): 696–702, 1932. doi:10.1098/rspa.1932.0165.

[21] Julia Kempe, Alexei Kitaev, and Oded Regev. The complexity of the local Hamiltonian problem. *SIAM Journal on Computing*, 35(5):1070–1097, 2006. doi:10.1137/S0097539704445226.

[22] Scott Kirkpatrick, C. Daniel Gelatt, and Mario P. Vecchi. Optimization by simulated annealing. *Science*, 220(4598):671–680, 1983. doi:10.1126/science.220.4598.671.

[23] Nicholas Metropolis, Arianna W. Rosenbluth, Marshall N. Rosenbluth, Augusta H. Teller, and Edward Teller. Equation of state calculations by fast computing machines. *The Journal of Chemical Physics*, 21 (6):1087–1092, 1953. doi:10.1063/1.1699114.

[24] Elizabeth Crosson and Aram W. Harrow. Simulated quantum annealing can be exponentially faster than classical simulated annealing. In *2016 IEEE 57th Annual Symposium on Foundations of Computer Science (FOCS)*, pages 714–723, 2016. doi:10.1109/FOCS.2016.81.

[25] Richard P. Feynman. Simulating physics with computers. *International Journal of Theoretical Physics*, 21(6–7):467–488, 1982. doi:10.1007/BF02650179.

[26] Peter W. Shor. Polynomial-time algorithms for prime factorization and discrete logarithms on a quantum computer. *SIAM Journal on Computing*, 26(5):1484–1509, 1997. doi:10.1137/S0097539795293172.

[27] Michael A. Nielsen and Isaac L. Chuang. *Quantum Computation and Quantum Information*. Cambridge University Press, 10th anniversary edition, 2010. doi:10.1017/CBO9780511976667.

[28] J. J. Sakurai and Jim Napolitano. *Modern Quantum Mechanics*. Cambridge University Press, 2nd edition, 2017. doi:10.1017/9781108499996.

[29] Paul A. M. Dirac. *The Principles of Quantum Mechanics*. Oxford University Press, 1930.

[30] John von Neumann. *Mathematical Foundations of Quantum Mechanics*. Princeton University Press, 1955. English translation by Robert T. Beyer; original German 1932.

[31] Adriano Barenco, Charles H. Bennett, Richard Cleve, David P. DiVincenzo, Norman Margolus, Peter Shor, Tycho Sleator, John A. Smolin, and Harald Weinfurter. Elementary gates for quantum computation. *Physical Review A*, 52(5):3457–3467, 1995. doi:10.1103/PhysRevA.52.3457.

[32] Alexei Yu. Kitaev, Alexander H. Shen, and Mikhail N. Vyalyi. *Classical and Quantum Computation*, volume 47 of *Graduate Studies in Mathematics*. American Mathematical Society, 2002.

[33] Christopher M. Dawson and Michael A. Nielsen. The Solovay-Kitaev algorithm. *Quantum Information and Computation*, 6(1):81–95, 2006.

[34] John Watrous. Quantum computational complexity. *Encyclopedia of Complexity and Systems Science*, pages 7174–7201, 2009. doi:10.1007/978-0-387-30440-3_428.

[35] Christoph Dürr and Peter Høyer. A quantum algorithm for finding the minimum. *arXiv preprint quant-ph/9607014*, 1996.

[36] Michel Boyer, Gilles Brassard, Peter Høyer, and Alain Tapp. Tight bounds on quantum searching. *Fortschritte der Physik*, 46(4-5):493–505, 1998. doi:10.1002/(SICI)1521-3978(199806)46:4/5<493::AID-PROP493>3.0.CO;2-P.

[37] Gilles Brassard, Peter Høyer, Michele Mosca, and Alain Tapp. Quantum amplitude amplification and estimation. *Contemporary Mathematics*, 305:53–74, 2002. doi:10.1090/conm/305/05215.

[38] Ashwin Nayak and Felix Wu. The quantum query complexity of approximating the median and related statistics. In *Proceedings of the 31st Annual ACM Symposium on Theory of Computing (STOC)*, pages 384–393, 1999. doi:10.1145/301250.301349.

[39] Edward Farhi, Jeffrey Goldstone, Sam Gutmann, and Daniel Nagaj. How to make the quantum adiabatic algorithm fail. *International Journal of Quantum Information*, 6(03):503–516, 2008. doi:10.1142/S021974990800358X.

[40] Wojciech H. Zurek. Decoherence, einselection, and the quantum origins of the classical. *Reviews of Modern Physics*, 75:715–775, 2003. doi:10.1103/RevModPhys.75.715.

[41] Alexei Yu. Kitaev. Quantum computations: algorithms and error correction. *Russian Mathematical Surveys*, 52(6):1191–1249, 1997.

[42] Jeremie Roland and Nicolas J. Cerf. Quantum search by local adiabatic evolution. *Physical Review A*, 65(4):042308, 2002. doi:10.1103/PhysRevA.65.042308.

[43] Boris Altshuler, Hari Krovi, and Jérémie Roland. Anderson localization makes adiabatic quantum optimization fail. *Proceedings of the National Academy of Sciences*, 107(28):12446–12450, 2010. doi:10.1073/pnas.1002116107.

[44] Tameem Albash and Daniel A. Lidar. Adiabatic quantum computation. *Reviews of Modern Physics*, 90: 015002, 2018. doi:10.1103/RevModPhys.90.015002.

[45] W. van Dam, M. Mosca, and U. Vazirani. How powerful is adiabatic quantum computation? In *Proceedings 42nd IEEE Symposium on Foundations of Computer Science*, pages 279–287, 2001. doi:10.1109/SFCS.2001.959902.

[46] Xi Guo and Dong An. Improved gap dependence in adiabatic state preparation by adaptive schedule. *arXiv preprint arXiv:2512.10329*, 2025.

[47] Dorit Aharonov, Wim van Dam, Julia Kempe, Zeph Landau, Seth Lloyd, and Oded Regev. Adiabatic quantum computation is equivalent to standard quantum computation. *SIAM Journal on Computing*, 37(1):166–194, 2007. doi:10.1137/S0097539705447323.

[48] Dorit Aharonov and Amnon Ta-Shma. Adiabatic quantum state generation and statistical zero knowledge. In *Proceedings of the 35th Annual ACM Symposium on Theory of Computing*, pages 20–29, 2003. doi:10.1145/780542.780546.

[49] Hari Krovi, Maris Ozols, and Jérémie Roland. Adiabatic condition and the quantum hitting time of Markov chains. *Physical Review A*, 82:022333, 2010. doi:10.1103/PhysRevA.82.022333.

[50] Rolando D. Somma, Daniel Nagaj, and Mária Kieferová. Quantum speedup by quantum annealing. *Physical Review Letters*, 109:050501, 2012. doi:10.1103/PhysRevLett.109.050501.

[51] Silvano Garnerone, Paolo Zanardi, and Daniel A. Lidar. Adiabatic quantum algorithm for search engine ranking. *Physical Review Letters*, 108:230506, 2012. doi:10.1103/PhysRevLett.108.230506.

[52] Yiğit Subaşı, Rolando D. Somma, and Davide Orsucci. Quantum algorithms for systems of linear equations inspired by adiabatic quantum computing. *Physical Review Letters*, 122:060504, 2019. doi:10.1103/PhysRevLett.122.060504.

[53] Dong An and Lin Lin. Quantum linear system solver based on time-optimal adiabatic quantum computing and quantum approximate optimization algorithm. *ACM Transactions on Quantum Computing*, 3(2), 2022. doi:10.1145/3498331.

[54] Dominic W. Berry, Andrew M. Childs, Yuan Su, Xin Wang, and Nathan Wiebe. Time-dependent Hamiltonian simulation with l^1-norm scaling. *Quantum*, 4:254, 2020. doi:10.22331/q-2020-04-20-254.

[55] Yimin Ge, Jordi Tura, and J. Ignacio Cirac. Faster ground state preparation and high-precision ground energy estimation with fewer qubits. *Journal of Mathematical Physics*, 60(2):022202, 2019. doi:10.1063/1.5027484.

[56] Lin Lin and Yu Tong. Near-optimal ground state preparation. *Quantum*, 4:372, 2020. doi:10.22331/q-2020-12-14-372.

[57] Alexander M. Dalzell, Nicola Pancotti, Earl T. Campbell, and Fernando G.S.L. Brandão. Mind the gap: Achieving a super-Grover quantum speedup by jumping to the end. In *Proceedings of the 55th Annual ACM Symposium on Theory of Computing*, pages 1131–1144, 2023. doi:10.1145/3564246.3585203.

[58] Matthew B. Hastings and Michael H. Freedman. Obstructions to classically simulating the quantum adiabatic algorithm. *Quantum Information and Computation*, 13(11–12):1038–1076, 2013.

[59] Mark W Johnson, Mohammad HS Amin, Suzanne Gildert, Trevor Lanting, Firas Hamze, Neil Dickson, Richard Harris, Andrew J Berkley, Jan Johansson, Paul Bunyk, et al. Quantum annealing with manufactured spins. *Nature*, 473(7346):194–198, 2011. doi:10.1038/nature10012.

[60] Ben W. Reichardt. The quantum adiabatic optimization algorithm and local minima. In *Proceedings of the 36th Annual ACM Symposium on Theory of Computing*, pages 502–510, 2004. doi:10.1145/1007352.1007428.

[61] Vicky Choi. Different adiabatic quantum optimization algorithms for the NP-complete exact cover and 3SAT problems. *Quantum Information and Computation*, 11(7–8):638–648, 2011.

[62] Adam Callison, Nicholas Chancellor, Florian Mintert, and Viv Kendon. Finding spin glass ground states using quantum walks. *New Journal of Physics*, 21(12):123022, 2019. doi:10.1088/1367-2630/ab5ca2.

[63] Matthew B. Hastings. The power of adiabatic quantum computation with no sign problem. *Quantum*, 5: 597, 2021. doi:10.22331/q-2021-12-06-597.

[64] András Gilyén, Matthew B. Hastings, and Umesh Vazirani. (sub)exponential advantage of adiabatic quantum computation with no sign problem. In *Proceedings of the 53rd Annual ACM SIGACT Symposium on Theory of Computing*, pages 1357–1369, 2021. doi:10.1145/3406325.3451060.

[65] Jeremie Roland and Nicolas J. Cerf. Quantum search by local adiabatic evolution. *Physical Review A*, 65(4):042308, 2002. doi:10.1103/PhysRevA.65.042308.

[66] Marko Žnidarič and Martin Horvat. Exponential complexity of an adiabatic algorithm for an NP-complete problem. *Physical Review A*, 73:022329, 2006. doi:10.1103/PhysRevA.73.022329.

[67] Itay Hen. Continuous-time quantum algorithms for unstructured problems. *Journal of Physics A: Mathematical and Theoretical*, 47(4):045305, 2014. doi:10.1088/1751-8113/47/4/045305.

[68] Arthur Braida. *Analog Quantum Computing for NP-Hard Combinatorial Graph Problems*. PhD thesis, Université d'Orléans, 2024.

[69] Gene H. Golub. Some modified matrix eigenvalue problems. *SIAM Review*, 15(2):318–334, 1973. doi:10.1137/1015032.

[70] Shantanav Chakraborty, Leonardo Novo, and Jérémie Roland. Optimality of spatial search via continuous-time quantum walks. *Physical Review A*, 102:032214, 2020. doi:10.1103/PhysRevA.102.032214.

[71] Jack Sherman and Winifred J. Morrison. Adjustment of an inverse matrix corresponding to a change in one element of a given matrix. *The Annals of Mathematical Statistics*, 21(1):124–127, 1950. doi:10.1214/aoms/1177729893.

[72] Andrew M. Childs and Jeffrey Goldstone. Spatial search by quantum walk. *Physical Review A*, 70: 022314, 2004. doi:10.1103/PhysRevA.70.022314.

[73] Shantanav Chakraborty, Leonardo Novo, Andris Ambainis, and Yasser Omar. Spatial search by quantum walk is optimal for almost all graphs. *Physical Review Letters*, 116:100501, 2016. doi:10.1103/PhysRevLett.116.100501.

[74] Sergio Boixo, Emanuel Knill, and Rolando Somma. Eigenpath traversal by phase randomization. *Quantum Information and Computation*, 9(9&10):833–855, 2009.

[75] Joseph Cunningham and Jérémie Roland. Eigenpath traversal by Poisson-distributed phase randomisation. In *19th Conference on the Theory of Quantum Computation, Communication and Cryptography (TQC 2024)*, pages 7:1–7:20, 2024. doi:10.4230/LIPIcs.TQC.2024.7.

[76] M.R. Garey, D.S. Johnson, and L. Stockmeyer. Some simplified NP-complete graph problems. *Theoretical Computer Science*, 1(3):237–267, 1976. doi:10.1016/0304-3975(76)90059-1.

[77] George M. Phillips. *Interpolation and Approximation by Polynomials*, volume 14. Springer Science & Business Media, 2003. doi:10.1007/b97417.

[78] Ramis Movassagh. The hardness of random quantum circuits. *Nature Physics*, 19(11):1719–1724, 2023. doi:10.1038/s41567-023-02131-2.

[79] Ramamohan Paturi. On the degree of polynomials that approximate symmetric Boolean functions. In *Proceedings of the 24th Annual ACM Symposium on Theory of Computing*, pages 468–474, 1992. doi:10.1145/129712.129758.

[80] Scott Aaronson and Alex Arkhipov. The computational complexity of linear optics. In *Proceedings of the 43rd Annual ACM Symposium on Theory of Computing*, pages 333–342, 2011. doi:10.1145/1993636.1993682.

[81] Michael J. Bremner, Ashley Montanaro, and Dan J. Shepherd. Achieving quantum supremacy with sparse and noisy commuting quantum computations. *Quantum*, 1:8, 2017. doi:10.22331/q-2017-04-25-8.

[82] Adam Bouland, Bill Fefferman, Chinmay Nirkhe, and Umesh Vazirani. On the complexity and verification of quantum random circuit sampling. *Nature Physics*, 15(2):159–163, 2019. doi:10.1038/s41567-018-0318-2.

[83] Lucien Le Cam. Convergence of estimates under dimensionality restrictions. *The Annals of Statistics*, 1 (1):38–53, 1973. doi:10.1214/aos/1176342150.

[84] Vittorio Giovannetti, Seth Lloyd, and Lorenzo Maccone. Quantum metrology. *Physical Review Letters*, 96:010401, 2006. doi:10.1103/PhysRevLett.96.010401.

[85] Samuel L. Braunstein and Carlton M. Caves. Statistical distance and the geometry of quantum states. *Physical Review Letters*, 72(22):3439–3443, 1994. doi:10.1103/PhysRevLett.72.3439.

[86] Leonid Gurvits. On the complexity of mixed discriminants and related problems. In *Proceedings of the 30th International Conference on Mathematical Foundations of Computer Science*, pages 447–458. Springer-Verlag, 2005. doi:10.1007/11549345_39.

[87] Mancheon Han, Hyowon Park, and Sangkook Choi. The constant geometric speed schedule for adiabatic state preparation: Towards quadratic speedup without prior spectral knowledge, 2025.

[88] Eduardo Araújo, Shantanav Chakraborty, and Leonardo Novo. Advantages and limitations of analog quantum search methods. *In preparation*, 2025.

[89] Edward Farhi and Sam Gutmann. Analog analogue of a digital quantum computation. *Physical Review A*, 57(4):2403–2406, 1998. doi:10.1103/PhysRevA.57.2403.

[90] Russell Impagliazzo, Ramamohan Paturi, and Francis Zane. Which problems have strongly exponential complexity? *Journal of Computer and System Sciences*, 63(4):512–530, 2001. doi:10.1006/jcss.2001.1774.

[91] Mark Jerrum and Alistair Sinclair. Polynomial-time approximation algorithms for the ising model. *SIAM Journal on Computing*, 22(5):1087–1116, 1993.

[92] Leonardo de Moura and Sebastian Ullrich. The Lean 4 theorem prover and programming language. In *Proceedings of the 28th International Conference on Automated Deduction (CADE-28)*, volume 12699 of *Lecture Notes in Computer Science*, pages 625–635. Springer, 2021. doi:10.1007/978-3-030-79876-5_37.

[93] The mathlib Community. The Lean mathematical library. *Proceedings of the 9th ACM SIGPLAN International Conference on Certified Programs and Proofs*, pages 367–381, 2020. doi:10.1145/3372885.3373824.

[94] David Hilbert. Mathematical problems. *Bulletin of the American Mathematical Society*, 8(10):437–479, 1902. doi:10.1090/S0002-9904-1902-00923-3.

[95] The Univalent Foundations Program. *Homotopy Type Theory: Univalent Foundations of Mathematics*. Institute for Advanced Study, 2013. URL `https://homotopytypetheory.org/book`.

[96] Georges Gonthier, Andrea Asperti, Jeremy Avigad, Yves Bertot, Cyril Cohen, Francois Garillot, Stephane Le Roux, Assia Mahboubi, Russell O'Connor, Sidi Ould Biha, Ioana Pasca, Laurence Rideau, Alexey Solovyev, Enrico Tassi, and Laurent Théry. A machine-checked proof of the odd order theorem. In *Interactive Theorem Proving*, volume 7998 of *Lecture Notes in Computer Science*, pages 163–179. Springer, 2013. doi:10.1007/978-3-642-39634-2_14.

[97] Thomas Hales, Mark Adams, Gertrud Bauer, Tat Dat Dang, John Harrison, Le Truong Hoang, Cezary Kaliszyk, Victor Magron, Sean McLaughlin, Tat Thang Nguyen, Quang Truong Nguyen, Tobias Nipkow, Steven Obua, Josef Pleso, Jason Rute, Alexey Solovyev, Thi Hoai An Ta, Nam Trung Tran, Trieu Thi Diep, Josef Urban, Ky Vu, and Roland Zumkeller. A formal proof of the kepler conjecture. *Forum of Mathematics, Pi*, 5:e2, 2017. doi:10.1017/fmp.2017.1.

[98] Robert Rand, Jennifer Paykin, and Steve Zdancewic. QWIRE practice: Formal verification of quantum circuits in Coq. In *Proceedings of the 14th International Conference on Quantum Physics and Logic (QPL)*, volume 266 of *Electronic Proceedings in Theoretical Computer Science*, pages 119–132, 2018. doi:10.4204/EPTCS.266.8.

[99] Kesha Hietala, Robert Rand, Shih-Han Hung, Xiaodi Wu, and Michael Hicks. A verified optimizer for quantum circuits. In *Proceedings of the ACM on Programming Languages (POPL)*, volume 5, pages 1–29, 2021. doi:10.1145/3434318.

[100] Li Zhou, Gilles Barthe, Pierre-Yves Strub, Junyi Liu, and Mingsheng Ying. CoqQ: Foundational verification of quantum programs. *Proceedings of the ACM on Programming Languages (POPL)*, 7 (POPL):833–865, 2023. doi:10.1145/3571222.

[101] Jaap Boender, Florian Kammüller, and Rajagopal Nagarajan. Formalization of quantum protocols using Coq. *Electronic Proceedings in Theoretical Computer Science*, 195:71–83, 2015. doi:10.4204/EPTCS.195.6.